The University of Adelaide

RESERVOIR SIMULATION STUDIES OF FORMATION DAMAGE FOR IMPROVED RECOVERY ON OIL-GAS RESERVOIRS

Australian School of Petroleum (ASP)

Master's Candidate:

Thi Kim Phuong Nguyen **1129274**

Supervisors:

Professor Pavel Bedrikovetsky (Principal supervisor)

Professor Manouchehr Haghighi (Co-supervisor)

ABSTRACT

This thesis is dedicated to the development of new technologies for sweep improvement due to plugging of highly permeable channels and layers by injected or lifted or mobilized fines particles. The following methods of improved waterflood have been proposed in the thesis:

- Injection of raw or poorly treated water with consequent homogenization of the injectivity profile due to distributed along the well skin factor.
- Injection of low salinity or fresh water resulting in lifting of reservoir fines, their migration and further capture by the rock with permeability reduction and redirection of the injected water into unswept area.
- Injection of sweet water into watered-up abandoned wells during pressure blowdown in oil and gas reservoirs with strong water support.

In the above three cases, the proposal of the new technologies was backed by detailed reservoir simulations. In all cases, the application of the proposed improved oil recovery technology, as forecasted by reservoir simulation, leads to 3-15% of incremental recovery and 2-3 times decrease of the amount of produced and injected water.

The technology of raw water injection was developed using Eclipse waterflood BlackOil simulator with modelling of injectivity decline along the well due to plugging of porous media by injected particles. A new numerical procedure describing skin growth with time in each section of long horizontal wells have been developed and implemented into BlackOil Eclipse model. Different configurations of horizontal injectors and producers have been modelled resulting in production forecast with raw waterflooding.

The technology of low salinity water injection have been developed using Eclipse reservoir modelling with polymer injection option, which can describe mobilization of fines particles, their migration, capture and subsequent permeability decline. The main physics mechanism of incremental oil recovery found is the diversion of the injected water into unswept zones due to plugging the swept zone by capture particles. The incremental recovery, as obtained by reservoir simulation, is 12%. It may also result in 2 to 3 times decrease in water injection and production.

The proposal of a new technology of small bank of fresh water injection into watered-up and abandoned production wells result in lifting of reservoir fines, their migration and plugging the path for invaded aquifer water. It results in decrease of water production and prolongation of oil or gas production from wells.

DECLARATION AND STATEMENT OF ORIGINALITY

I herewith confirm that this work contains no material which has been accepted for the award of any other degree or diploma at any university or other tertiary institution to „Thi Kim Phuong Nguyen‟ and, to the best of my knowledge and belief, this thesis/report contains no material previously published or written by another person, except where due reference has been made in the text.

I give consent to this copy of my thesis when deposited in the University Library, being made available for loan and photocopying, subject to the provisions of the Copyright Act 1968.

The author acknowledges that copyright of published works contained within this thesis (as listed below) resides with the copyright holders of those works.

I also give permission for the digital version of my thesis to be made available on the web, via the University‟s digital research repository, the Library catalogue and also through web search engines, unless permission has been granted by the University to restrict access for a period of time.

I give consent to this copy of my thesis/report, when officially submitted to the Australian School of Petroleum, to be available for loan and photocopying.

Signed Date

…… 14th October 2011

Thi Kim Phuong Nguyen

ACKNOWLEDGEMENTS

Special thanks are to Professor Pavel Bedrikovetsky (ASP) and Professor Manouchehr Haghighi for their technical and moral support throughout this project.

I also would like to express my appreciation and gratitude to the Australian School of Petroleum Engineering (ASP) for providing support to my research.

TABLE OF CONTENTS

LIST OF FIGURES

LIST OF TABLES

PUBILICATIONS

Peer-Review Journal Paper:

- Bedrikovetky, PG., **Nguyen, TKP,** Hage, A, Ciccarelli, JR, ab Wahab, M, Chang, G, de Souza, ALS, Furtado, CA 2011, 'Taking Advantage of Injectivity Decline for Improved Recovery during Waterflood with Horizontal Wells', Journal of Petroleum Science & Engineering, vol. 78, pp. 288-303.

Conference Paper:

- Zeini, A, **Nguyen, TKP**, Bedrikovetsky, P 2011, 'Taking advantage of fines-migration-induced formation damage for improved waterflooding (reservoir simulation using polymer flood option)', SPE 144009 prepared for presentation at the SPE European Formation Damage Conference, Noordwijk, The Nevetherlands, 7-10 June.

CHAPTER 1: INTRODUCTION

1.1 WATERFLOODING OVERVIEW

During oil and gas production, it has been observed that there is still a large quantity of hydrocarbon remained in the un-swept zone of the reservoir after the primary recovery stage, during which the reservoir natural energy, i.e from pressure drawdown, gas expansion or gravity drainage, is sufficient to support the oil production from the reservoir (Dake 2004). When the reservoir pressure can no long sustain an economical production, an external compatible fluid is injected into the reservoir in order to provide extra pressure support and to assist with the displacement of the oil towards the producer. The recovery factor of primary recovery stage is about 10%; while with secondary recovery, it increases by 15% to 40%. After secondary recovery process, different methods can be employed to modify the reservoirs or fluid"s characteristics to enhance the oil recovery after the reservoir"s natural energy becomes insufficient to support the production. (Civan 2000)

Waterflooding is a widely used method during secondary recovery stage as it is more cost-sufficient and simple compared to other available enhanced oil recovery (EOR) methods (Hadia et al. 2006). Water quality plays an important role in determining the effectiveness of the waterflood. During sea and produced water injection, particles retention in the pore space and plugging the flowpath is considered to have adverse effects on well quality (Civan 2000).

Injectivity damage, due to the retained particles in porous media around the wellbore and within the reservoir during sea/produced waterflooding, has been widely reported in Gulf of Mexico, the North Sea and Campos Basin in Brazil. The plugging of pore spaces leads to the formation of external cake around the injector"s wellbore and consequently the permeability decline. Yet with long horizontal injectors in heterogeneous reservoirs, moderate injectivity decline is not too detrimental due to the high initial injectivity index.

Similarly, during low salinity water injection, the occurrence of fines migration and a subsequent reduction in permeability have been observed to occur as a result of decreased water salinity (Mungan 1965; Lever & Dawe 1984; Valdya

& Fogler 1992; Civan 2007). During low salinity waterflooding, fines migration causes the reduction in the effective permeability to water in the water-swept zone, which can be used as an alternative for mobility control to improve the performance of the waterflood. Low salinity water is also often readily available and inexpensive compared to other alternatives. Hence, injection of low quality and low salinity water help to deliver a significant saving on the otherwise expensive water treatment cost in offshore projects with limited available space.

1.2 OBJECTIVES

The primary objectives of this research are to investigate the effects of raw water injection and of low salinity water injection on recovery and sweep efficiency of the reservoir. Horizontal wells configuration is used in simulation models due to its high initial injectivity index. Various horizontal wells configurations are also to be studied for their efficiency under different fluid‟s properties.

In previous honours project, it was found out that the induced injectivity damage resulted in increased sweep efficiency due to the homogenization of injectivity profile in heterogeneous reservoir (Nguyen & Hage 2009). The similar behavior is also observed during the injection of low salinity water due to fines mobilization. In heterogeneous reservoirs, the injection rate is distributed un-uniformly along the long horizontal well and water advances faster in higher permeable zone leading to the unfavorable mobility ratio. Consequently, early water breakthrough occurs at the producer and a significant un-swept reservoir volume is left behind. During raw water injection, the well quality can be determined from the induced skin damage around the injector‟s wellbore, which is from the deposition of particles in the pore space causing the injectivity decline. While, the injection of low salinity water causes formation particles detachment with consequent migration and capture to plug pore space. In both phenomenon, the plugging of pore spaces contributes to the homogenization of the injectivity profile resulting in better sweep efficiency.

Analytical models for injectivity decline during raw water injection and low salinity waterflood will be implemented into a black-oil reservoir simulator

Eclipse 100. Sensitivity analyses are conducted for both oil and gas reservoirs with different fluid"s properties in order to test the robustness of these methods.

CHAPTER 2: SWEEP INCREASE DUE TO INDUCED SKIN DAMAGE IN HORIZONTAL WELLS:

2.1 LITERATURE REVIEW:

2.1.1 SWEEP INCREASE DUE TO INJECTIVITY IN HORIZONTAL WELLS:

Horizontal wells have been used widely and effectively in a number of EOR methods, such as: waterflooding, polymer flooding or steamflooding, due to its advantages in providing greater reservoir contact to increase the injectivity of the injector and improve sweep efficiency (Joshi 1991). Joshi et al. (1993) conducted a study on horizontal application in waterflooding and found that the horizontal wells exhibiting several advantages over vertical wells with higher productivity and injectivity; hence helped to increase the ultimate recovery during EOR. In this research, various configurations of horizontal wells are investigated for their effectiveness and applicability for raw waterflooding.

2.1.2 SWEEP INCREASE FOR WATERFLOODING DUE TO INDUCED SKIN DAMAGE:

In oil bearing formations, reservoir‟s heterogeneity is a major factor controlling the sweep efficiency and consequently oil recovery factor during waterflooding. When injected into a heterogeneous reservoir, a large portion of the injected water follows the high permeability zones and forms a high conductivity channel between the injector and the producers. Ultimately, this causes the early breakthrough of low viscosity water fingers at the producer, which is undesirable for any oil development project. Another setback from this is a significant amount of injected water being recirculated back to the surface without any additional oil recovered, resulting in an uneconomical operation. (Bedrikovetsky et al. 2005).

Several Enhanced Oil Recovery (EOR) methods are based on plugging of swept areas or highly permeable zones in order to redirect the injected water into un-swept zones to improve the sweep efficiency (Lake 1989; Bedrikovetsky 1993). The possibility of raw water injection, in which the injected particles are captured in the pore space causing the permeability decline (formation damage) in the waterflooded zones, and the consequent

sweep increases have been discussed in previous literature (Khambharatana et al. 2000). The capturing of particles in the pore space also helps to reduce the residual oil in the reservoir at the end of the production (Soo & Radke 1986a & b). This phenomenon encourages the consideration of the injection of particulated/raw water for improved oil recovery. According to the study done by Herzig et al. (1970), it was determined that the amount of retained/captured particles is a monotonically increasing function of injected water volume. During raw water injection, since the majority of injected water enters the most permeable channel, a high concentration of particles will be strained and captured in the pore spaces in high permeable zones. These zones are then referred to as “damaged zones” and the plugging of pore space creates the induced skin, which helps to homogenize the injectivity profile, redirects the water flow towards the less permeable zones to improve sweep efficiency and delay the water breakthrough. Additionally, this also causes the injectivity decline as the induced skin acts as a resistance to the water flow.

The possibility of preferential plugging of swept zones by „captured“ particles was discussed for vertical injectors and found to be unsuccessful (Khambharatana et al. 1997 & 1998). Yet, a study conducted by Nunes et al. (2005) found that the induced injectivity damage zone by captured particles around the injector“s wellbore radius rarely exceeds 1-2 meters. The injected water would by-pass the damaged zone and is redirected into the more permeable zone or the high-velocity stream lines close to the injector. Since the productivity index for vertical wells is limited, the incremental sweep efficiency due to the induced formation damage is small and the reservoir simulations show a negligible sweep increase due to the induced injectivity damage in a system of vertical wells (Khambharatana et al. 1997 & 1998).

In this study, the application of poorly treated water in reservoirs with long horizontal injectors for both horizontal and vertical producers. Preferential deposition of particles „in front“ of the high-speed streamlines causes an increase of „flight“ times. High variation of streamline sizes for long horizontal wells may result in the preferential plugging of highly swept zones and in significant increase of sweep efficiency.

Figure 1 shows a displacement schematic in a horizontal two-permeability-zone reservoir with horizontal injector and producer. During raw water injection, water enters preferably in the high permeability zone. Therefore, the main portion of the injected water passes via the well sections in the highly permeable zone. So, the particles deposit mainly in the highly permeable zone which then creates an additional resistance to the water flow and slowdown the water encroachment to the producer. Thus, it helps to slow down the water front advancement towards the producers and subsequently, helps to delay the water breakthrough and increase the sweep efficiency. As illustrated in Figure 1, the continuous line represents the sweep pattern by „clean" water in a damage-free case. Whereas, the dotted line corresponds to the displacement of the raw water injection with the induced skin build-up in the high permeable zone, which helps to redirect the flow of water towards the low permeable zone to displace more oil. As a result, this would increase the incremental oil recovery as well as delay the water breakthrough, which are the two main economical factors during the oil-field development (Bedrikovetsky 2009).

FIGURE 1: SWEEP PATTERNS FOR "CLEAN" WATER AND "RAW" WATER IN TWO-PERMEABILITY-ZONE RESERVOIR (BEDRIKOVETSKY 2009)

The final conclusion of the importance of the sweep increase effect must be based on results of reservoir simulations that account for injectivity damage.

2.1.3 FORMATION DAMAGE PHENOMENON:

Formation damage phenomenon refers to the permeability impairment of petroleum-bearing formations. During raw water injection, it can be identified from the decline in well performance due to induced skin damage. There are three stages during injection of raw water:

i. Deep bed filtration, particles captured and deposited on a grain surface
ii. Internal cake build-up followed by the formation of the low permeable external filter cake around the wellbore, during which particles no longer invade into the formation;
iii. As the external filter cake reaches the critical thickness, cake erosion takes place then particles start to dislodge from the cake surface by drag force. (Civan 2000; Nabzar et al. 1996)

The deposition and capture of solid particles during water flow in porous media leads to the permeability decline and consequently the injectivity decline at the damage zone. The particles capturing processes are presented in Figure 2.

FIGURE 2: PARTICLES CAPTURING PROCESSES: DEEP BED FILTRATION AND EXTERNAL CAKE BUILD-UP (BEDRIKOVETSKY ET AL. 2005)

During raw water injection, particles penetrate the reservoir and eventually being captured in the pore spaces due to various forces acting on the particles during deep bed filtration. The high concentration of retained particles then results in induced skin damage and subsequently the permeability decline and

creates a damaged zone adjacent to the injector‟s wellbore. This leads to the injectivity decline along the wellbore depending on the induced skin damage at different zones. After some partial filling, the particles start to clog the reservoir inlet section and form an external filter cake on the reservoir inlet section. External filter cake build-up is a process in which the particles start to be retained at the interface between the wellbore and the porous medium, causing further injectivity decline. It is assumed that the transition between deep bed filtration and external cake formation is instantaneous. Both deep bed filtration and external cake build-up create an additional resistance to the water movement from injector into the reservoir; hence, causing the injectivity decline. The thickness of external cake grows with increasing volume of injected water (Bedrikovetsky et al. 2005). Then, cake erosion takes places when the external filter cake has reached its critical thickness. While in the porous medium, the injected particles are under the influence of various forces in a continuous motion, such as: drag forces, lift forces, gravity forces and friction forces, until they either get captured or transported out of the system (Figure 3). (Farshbaf Zinati et al. 2007)

FIGURE 3: FORCES ACTING ON A PARTICLE CAPTURED ON THE SURFACE OF THE HORIZONTAL EXTERNAL CAKE (FARSHBAF ZINATI ET AL. 2007)

Crossflow filtration is defined as a separation process driven by pressure difference, where the feed flow is tangential to the permeate flow. A proportion of particles, smaller than the medium pore size, pass through the medium as filtrate; while the remaining particles are retained on the other side of the porous medium. During a filtration process, the volume of filtrate can be increased before the complete blockage of pore spaces by the external cake (Altmann et al. 1996). As the crossflow drag force increases and the permeate force decreases during the external cake build-up, particles start to detach from the cake surface and fall down the borehole causing cake erosion. During cake erosion, it has been observed that well injectivity index starts to stabilize. The thicker the cake, the lower the permeate velocity and thus the lower the viscous force holding the particles to the cake surface (Farshbaf Zinati et al. 2007). During cake erosion, the drag force exceeds the friction force from the permeate force resulting in no more particles deposited onto the cake surface, resulting in the stabilization of the injectivity index. (Bedrikovetsky 2009)

The well quality of the injector can be determined from the dimensionless impedance index (J), which is the ratio between the well"s initial and its current injectivity indexes (II). Figure 4 illustrates the piece-wise relationship between the well"s impedance indexes to the pore volume injected during deep bed filtration and external cake build-up. The dimensionless time measure in pore volume injected is used in this method to show how the injectivity decline is related to the amount of injected water. During cake erosion, the impedance index remains constant. The increasing impedance index compared to that at the beginning indicates the decrease in injectivity decline of the well during raw water injection. (Sharma et al. 1997)

NOTE:
This figure is included on page 10 of the print copy of the thesis held in the University of Adelaide Library.

FIGURE 4: PIECE-WISE RELATIONSHIP BETWEEN IMPEDANCE INDEX AND TIME (PVI) DURING FORMATION DAMAGE (SHARMA ET AL., 1997)

The critical parameters when determining the injectivity damage are:

i. Filtration coefficients (λ‟): characterizes the intensity of particle capture by the formation rock.
ii. Formation damage coefficients (β): shows the reservoir‟s permeability decline due to the particle capture.
iii. Critical porosity ratio (α)
iv. Filter cake permeability (k_c) (Bedrikovetsky et al 2005).

These parameters are determined from laboratory coreflood tests and vary from well to well. The impedance slope “m” of deep bed filtration is dependent on the formation damage coefficient (β), filtration coefficient (λ‟) and the initial injected particle concentration (c^0). While during the external filter cake formation, the slope “m_c” is defined by the external cake permeability (k_c), cake porosity (θ_c), initial rock permeability (k_0) and porosity (ø) (Bedrikovetsky et al, 2005). The analytical model for deep bed filtration, external cake build-up and injectivity index decline during water flooding are shown in Appendix B along with the relevant derivations.

2.1.4 ANALYTICAL MODEL FOR IMPEDANCE INDEX FORMATION DAMAGE

i. During Deep Bed Filtration

Well injectivity index (II_t) is ratio between the flowrate to per unit of pressure drop between the injector and the reservoir. While, the dimensionless injectivity index (II) is determined as the ratio of the instantaneous injectivity index (II_t) to the initial injectivity index (II_0) before the damage. (Bedrikovetsky 2009)

$$II = \frac{II_t}{II_0} = \frac{q_{(t)}}{\Delta P_t} = \frac{q}{P_w - P_c} \tag{1}$$

Where: q: injection rate (m^3/d); P: pressure (Pa)

Then, the impedance index (J) is the reciprocal of the dimensionless injectivity index:

$$J(t) = \frac{II_{t=0}}{II_t} = \frac{q_{t=0}\Delta P_t}{\Delta P_{t=0} q_t} = \frac{\Delta P_t}{\Delta P_{t=0}} \tag{2}$$

Where: J: impedance index.

(Bedrikovetsky 2009)

NOTE:
This figure is included on page 11 of the print copy of the thesis held in the University of Adelaide Library.

FIGURE 5: IMPEDANCE INDEX DURING DEEP BED FILTRATION AND EXTERNAL FILTER CAKE BUILD-UP (BEDRIKOVETSKY 2009)

As illustrated in Figure 5, increasing impedance index indicated the decline in well"s injectivity index. Due to the penetration and capture of particles in the reservoir, the injectivity index at any point of time during the raw water injection

will be less than that compared to the initial injectivity index. The impedance index can be calculated from integrals of the dimensionless pressure drop and particles concentration: (Derivations are included in Appendix C):

$$J(T)=\frac{\Delta P}{\Delta P_0}=1+\frac{\frac{\beta\phi c^0}{2}\left(\lambda' R_c\right)^2}{\ln\left(\frac{R_c}{r_w}\right)}\left(\frac{1}{\lambda' r_w}+e^{\lambda' r_w}ei\left(\lambda' r_w\right)\right)T \qquad (3)$$

Where: R_c: reservoir drainage radius (m); r_w: well radius (m); λ': filtration coefficient (1/m); c^0: initial injected particle concentration (ppm); β: formation damage coefficient; T: dimensionless time (pvi)

Impedance index can also be expressed as a straight line equation:

$$J(T)=1+mT \qquad (4)$$

Where: m: slope during deep bed filtration

The slope "m" represents the rate at which particles being capture by the pore space during the deep bed filtration, and can be determined by:

$$m=\frac{\frac{\beta\phi c^o}{2}\left(\lambda' R_c\right)^2}{\ln\left(\frac{R_c}{r_w}\right)}\left(\frac{1}{\lambda' r_w}+e^{\lambda r_w}ei(\lambda' r_w)\right) \qquad (5)$$

ii. <u>During External Filter Cake Development:</u>

As shown in Figure 5, at transition time "t_{tr}", the reservoir inlet section is completely plugged by the injected particles. Then, the particles would start to be deposited at the cake surface and consequently lead to the build-up of an external filter cake around the wellbore. It has been assumed that the transition between deep bed filtration to external cake build up is instantaneous for the mathematical model.

The transition time (t_{tr}) is when the deposited particles concentration has filled a certain fraction of pore space at the reservoir inlet section.

$$t_{tr} = \frac{2\alpha\phi\pi r_w}{\lambda' c^0 q}$$

$$q = \frac{Q}{h} \tag{6}$$

The dimensionless time (T_{tr}) is calculated using the following formula:

$$T_{tr} = \frac{2\alpha r_w}{\lambda' c^0 R_c^2} \tag{7}$$

Where: q: injection rate per reservoir height (m^2/d); α: the retained particle concentration (ppm); ø: porosity.

The volume of particles required for external cake formation is:

$$\pi\left[r_w^2 - (r_w - h_c)^2\right](1-\phi_c) = c^0 \int_{t_{tr}}^{t} q_{(t)} dt \tag{8}$$

Where: h_c: the cake thickness (m); $ø_c$: cake porosity

Then, the thickness of the external filter cake is calculated by:

$$h_{c(t)} = \frac{c^0}{2\pi r_w (1-\phi_c)} \int_{t_{tr}}^{t} q_{(t)} dt = \frac{c^0 R_c^2 \phi (T - T_{tr})}{2 r_w (1-\phi_c)} \tag{9}$$

The dimensionless pressure drop across on external cake (ΔP_c) is:

$$\Delta P_c = \frac{k_0 k_{rwor} c^0 \phi}{2 X_w k_c (1-\phi_c)} (T - T_{tr}) \tag{10}$$

Where: k_0: reservoir initial permeability (m^2); k_{rwor}: relative permeability of water to residual oil, X_w: contour; ΔP_c: pressure drop across the filter cake (Pa)

Hence using the relationship between the impedance index (J) to the pressure drop in equation (2), the impedance index can be calculated as:

$$J(T) = 1 + mT_{tr} + \frac{k_o k_{rwor} \phi c^o}{k_c (1-\phi_c) X_w (-\ln X_w)} (T - T_{tr}) \tag{11}$$

The slope "m_c" during external cake formation can be determined as:

$$m_c = \frac{k_o k_{rwor} \phi c^o}{k_c (1-\phi_c) X_w (-\ln X_w)} \tag{12}$$

So, the impedance index for each stage of deep bed filtration and external cake build-up is:

$$J_d(T) = \begin{cases} 1 + mT & T < Ttr \\ 1 + mT_{tr} + m_c (T - T_{tr}) & T > Ttr \end{cases} \tag{13}$$

(Bedrikovetsky et al. 2002 & 2009)

Since this research focuses mainly on the effect of induced skin damage on the oil recovery, cake erosion effect is neglected.

2.1.5 DETERMINING THE INDUCED SKIN FACTOR:

The formation damage resulting from raw water injection can be determined from calculating the induced skin value around the injector‟s wellbore. This is done by incorporating the dimensionless impedance index (J) and Darcy‟s equation for both deep bed filtration (before the transition time) and external cake build-up (after transition times). (Derivations are shown in Appendix E)

$$S_{(t_D)} = \begin{cases} \ln\left(R_c / r_w\right) m t_D & 0 < t_D < t_{tr} \\ \ln\left(R_c / r_w\right)\left(m t_D + m_c\left(t - t_{tr}\right)\right) & t_{tr} < t_D < t_e \\ \ln\left(R_c / r_w\right)\left(m t_{trD} + m_c\left(t_e - t_{tr}\right)\right) & t_e < t_D \end{cases} \quad (14)$$

Where: S: skin factor; t_e: dimensionless erosional time; t_D: current dimensionless time.

When the skin factor is obtained, the profile of the skin build-up (at a particular well section) versus the dimensionless time (t_D) can be developed, which is similar to the impedance index curve as it incorporates three stages: deep bed filtration, external cake formation and cake erosion. For the purpose of this research, cake erosion phenomenon is neglected. (Bedrikovetsky et al. 2002)

2.2 COUPLED SIMULATION OF NEAR WELLBORE DAMAGE AND RESERVOIR MODELS:

There are various available reservoir simulator programs available to aid reservoir engineers in predicting the fluid flow and reservoir behaviors in the petroleum industry. In this research, the Black-oil simulator of Eclipse (E100) is used where the oil recovery is determined but the fluid-phase composition effects are not considered (Schlumberger 2007).

It has been studied and acknowledged that the near wellbore damage has significant impacts on the well performance. There have been several approaches proposed for coupling the induced damage into reservoir simulations by modeling with fine gridblocks around the wellbore relative to the full-scale reservoir models to facilitate the different fluid-flow behaviors around the near-well and in far-well regions (Ding 2010; Minssieux et al. 1998; Bedrikovetsky et al. 2006). In these approaches, a separate fine gridblock system is developed around the wellbore in order to provide better descriptions for the fluid-flow behavior to better determine the formation damage and its effect on the well‟s injectivity or productivity. However with fine/small gridblocks, reservoir simulations require very small timesteps and a significant number of iterations to acquire computational stability. It is also unrealistic during the data update process from the reservoir model to the near well bore model and vice versa, which are quite complex (Ding 2010).

For the purpose of this study, only the injector‟s performance is interested in while investigating the effect of raw water injection on the homogenization of the injectivity profile in heterogeneous reservoirs. The heterogeneities are designed as layers, which mean that the heterogeneities around the wellbore are the same to that of the reservoir. Hence, it can be assumed that the fluid-flow behavior around the wellbore is the same as that in the far-region in the reservoir.

It is proposed that the reservoir models of raw water injection are simulated to produce fluid-flow properties after a set time. These properties will then be used to calculate the near-well-flow damage (or induced skin factor from particles capture) separately using the analytical model to predict the induced injectivity damage around the wellbore, which will then be imposed onto the

reservoir models by updating the well skin factors at each open gridblock of the injector. As the injection flowrate at each open grid blocks of the injector is provided by the simulations, the near-well performance can be determined using equation (1) to (14) presented previously. Since the skin factor is the only parameter to be updated, all reservoirs‟ properties are preserved. Thus, this approach is simpler and provides consistency to improve the efficiency for the simulation process.

The coupled modeling steps are as following (Figure 6):

1. Develop a reservoir model with well specifications and designs.
2. Create an Excel program to define the well design and to calculate the induced skin for each section of the injector.
3. Timesteps for the simulation models are kept quite small to ensure the skin build-up near the wellbore resembles the real scenario as accurately as possible.
4. Simulating the model to obtain the flow properties (injection rates, pressure drop, etc.) around the wellbore at the end of each timestep
5. Transfer them to the Excel program to determine the induced skin factor around the injector‟s wellbore.
6. Update the skin factors for the reservoir model and run simulation till the next timestep.
7. Repeat step 4 to 6 for each timestep.

The timestep of 30 days was used. The smaller is the timestep, the more accurate is the calculated skin factor. The sequence of the calculations performed in Excel is:

i. Calculate the transition time (T_{tr}) between deep bed filtration to the external cake build-up (eq. 7).
ii. Calculate the slope “m” for skin build-up during the deep-bed filtration (eq. 5).
iii. Calculate the slope “m_c” for skin build-up during the external cake build-up (eq. 12).
iv. If the time $T<T_{tr}$, calculate the impedance index (J) (eq. 13).
v. Use eq. (14) to calculate the induced skin around the wellbore.

During the induced skin calculations, filtration coefficient (λ"), formation damage coefficient (β), critical porosity (α) and filter cake permeability (k_c) are kept constant.

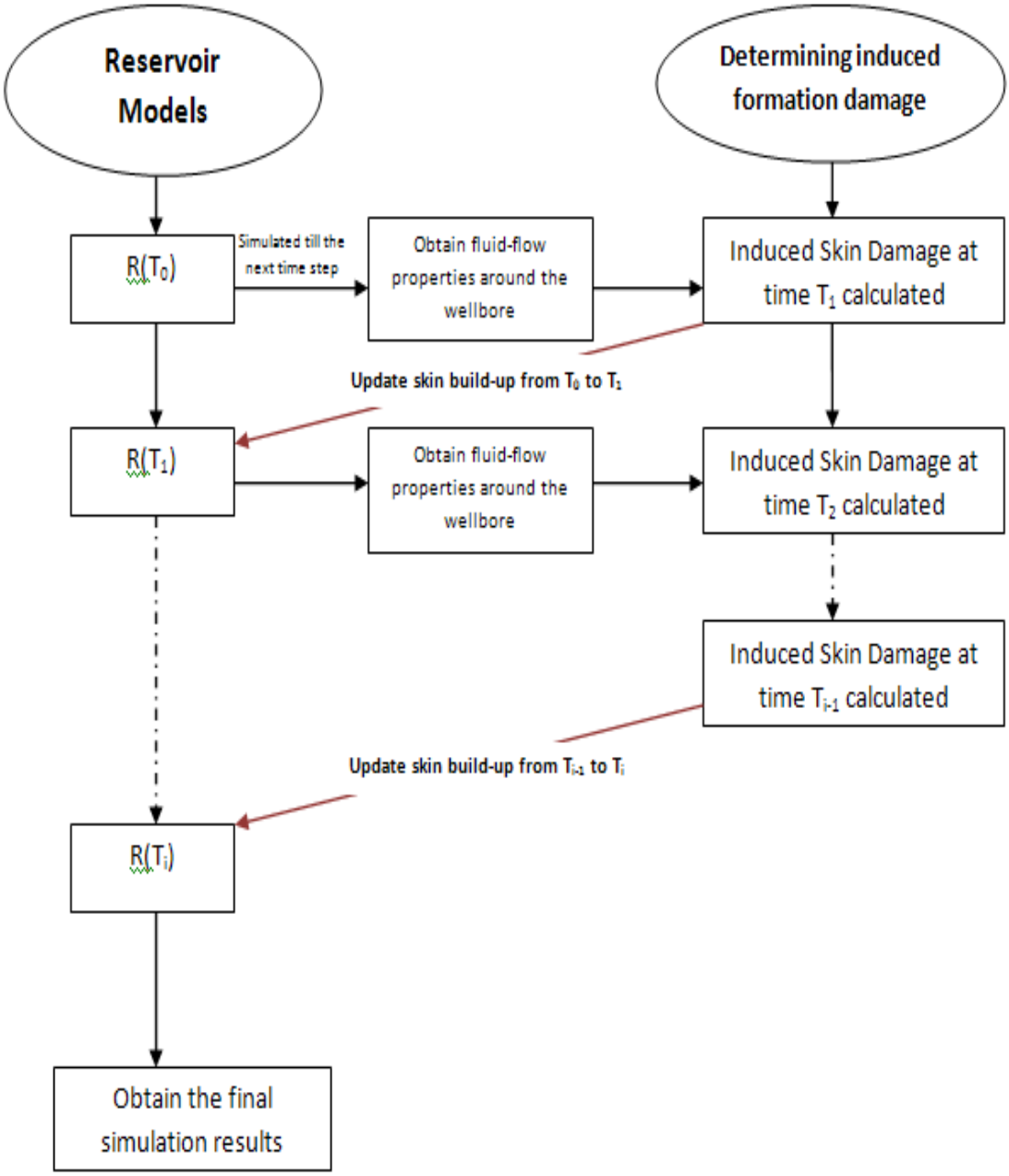

FIGURE 6: FRAMEWORK FOR COUPLE MODELING FORMATION DAMAGE INTO THE RESERVOIR MODEL

2.3 CASE STUDY AND SIMULATION MODELS:

The effects of injectivity decline on the sweep efficiency are studied for both heterogeneous and homogeneous reservoir. Sensitivity analysis is conducted on various oil viscosities to determine the robustness of this method. Descriptions for reservoir‟s characteristics and simulation models are discussed as followed.

2.3.1 PARALLEL HORIZONTAL INJECTOR AND PRODUCER IN THIN HORIZONTAL RESERVOIR WITH HIGH AND LOW PERMEABILITY ZONES (TWO-ZONE)

A reservoir model of a thin horizontal reservoir with lateral low permeability and high permeability zones and without vertical heterogeneity completed with two parallel injection and production wells is simulated (Figure 1). It is assumed that the well pressures are above bubble point pressure during the overall injection-production period, i.e. two-phase flow of immiscible fluids takes place.

The most favourable reservoir conditions of the application of waterflood with poor quality water had been studied in previous honours project by Muhammad (2008). The recovery factor after 1 pvi is plotted against permeability ratio k_l/k_h (Figure 13a) where the high permeability is 1 d, in which k_l and k_h are permeabilities of low and high permeability zones, respectively. As expected, the curve that corresponds to „clean‟ waterflooding lies below than that for poor quality waterflood. If k_l/k_h =0, oil is not recovered from the low permeability zone; sweep becomes equal for both cases of clean and poor quality water injection, which means that the incremental recovery vanishes. If k_l/k_h =1, water displaces oil uniformly in both patterns, i.e. the displacement profile is already uniform, and the damage does not contribute to the straightening of the injectivity profile. This also means that the incremental recovery in homogeneous reservoirs is zero. So, two curves intercept at two points, and one curve is above the other in the interval between the two points (Figure 13a). Therefore, there does exist a maximum point, where the incremental recovery is highest for some permeability ratio (Figure 7b). The optimal permeability ratio is 0.05 for the case under consideration. For this case, the incremental recovery reaches the value 5% after 1 pvi and 9% after 2 PVI.

a)

b)

FIGURE 7: A) RECOVERY FACTOR DURING WATERFLOOD BY CLEAN WATER AND SUSPENSION AFTER 1 PVI AS A FUNCTION OF PERMEABILITY RATIO; B) INCREMENTAL RECOVERY DURING WATERFLOOD BY "RAW" WATER IF COMPARED WITH "CLEAN" WATER INJECTION AS A FUNCTION OF THE PERMEABILITY RATIO (MUHAMMAD, 2008)

The permeability ratio of 0.1 between high and low permeable zones is chosen for this study to test the robustness of raw water injection method. The permeabilities of the two zones are 50 and 500 mD as illustrated in Figure 8.

The injection and production pressures are imposed on the wells ($r=r_w$) as boundary conditions, i.e. the distribution of rates along wells are calculated by the simulations. The default values for relative permeability and capillary pressure have been used. Both well lengths were 200 m. Oil viscosity was 1 cP. The main grid and reservoir parameters are presented in Table 1.

TABLE 1: PARAMETERS USED FOR TWO-ZONE RESERVOIR

Parameters of the geological model	Value used Two Zone Study
Node numbers for fine grids	100 x 100 x 1
Node numbers for moderate grids	50 x 50 x 1
Node numbers for coarse grids	25 x 25 x 1
The length of the reservoir (m)	1000
The width of the reservoir (m)	1000
The thickness of the reservoir (m)	10
The length of wells (m)	200 320 (sensitivity)
Initial Reservoir Pressure (Psi)	3000
Viscosity of Water (cP)	1
Viscosity of Oil (cP)	1
Initial Oil Saturation	0.8
Initial Porosity	0.3
Initial Horizontal Permeability (mD)	50 & 500
Initial Vertical Permeability (mD)	10
Injection Pressure (psi)	5000

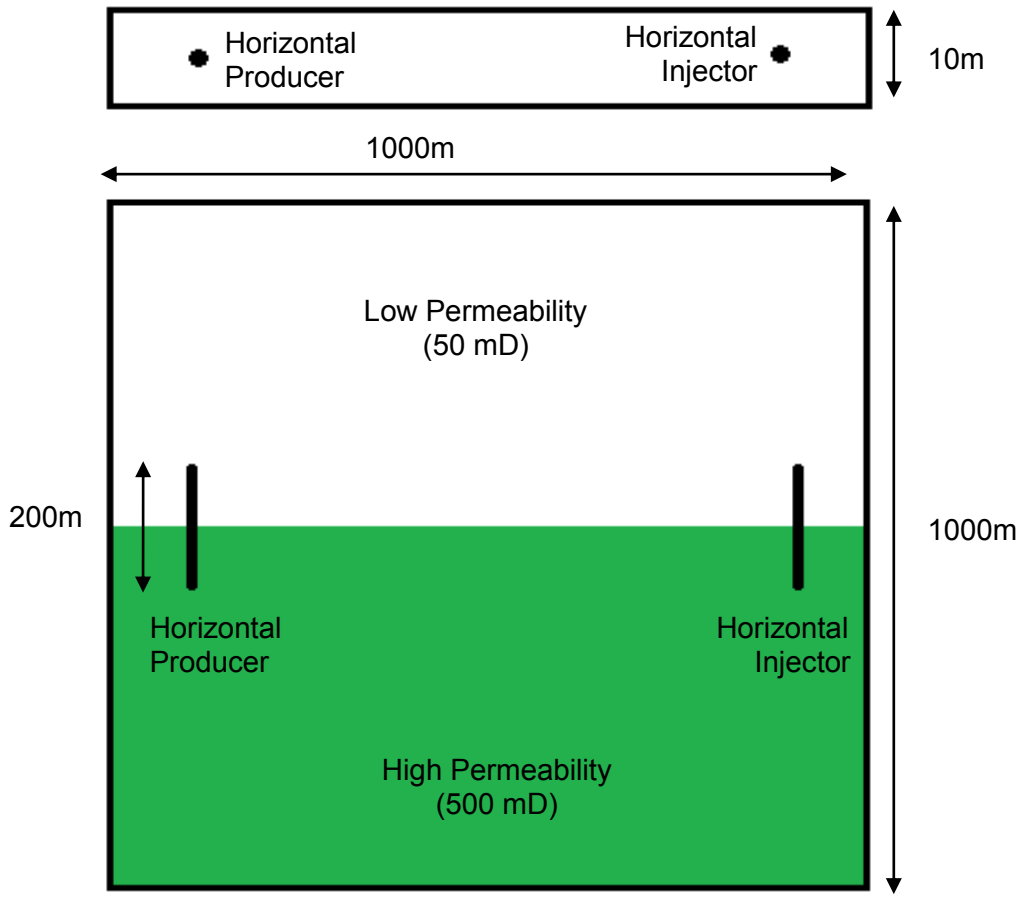

FIGURE 8: TWO ZONE RESERVOIR WITH THE HIGH PERMEABILITY SHOWN IN GREEN

Hence, horizontal permeability values of 50 and 500 mD were used for the simulations. Vertical permeabilities are kept the same for both zones to ensure that the high permeable zone remains the more dominant flow regime throughout the simulation.

The data for analytical modeling of injectivity damage are presented in Tables 2, where the usual range values of formation damage parameters were taken (Pang and Sharma 1997; Wennberg and Sharma 1997; Bedrikovetsky 2001; Moghadasi et al. 2004). Let us compare waterflood sweep with injection of clean water and poor quality water, which results in S=60 after 1 pvi. This high number is acceptable at deep water offshore waterflood projects. Souza et al. (2005) reports about 10-times injectivity decrease in giant field A (Brazil, Campos Basin), which corresponds to skin factor S=83 for well radius r_w=0.1 m and well drainage radius r_e=1000 m. Furui et al. (2003) considers skin factor up to 30-40. Bennion et al. (1996) calls skin factor up to 10 as the “low skin regime”. The authors investigate “S until 200, …which may occur in a badly

damaged overbalanced open-hole completion". The plots and dependencies in this paper are presented until S=200.

TABLE 2: DATA FOR SIMULATION OF FORMATION DAMAGE DURING WATERFLOODING IN A TWO-ZONE RESERVOIR.

Data	Skin = 11	Skin = 25	Skin = 40	Skin = 60
λ' (1/m)	1	1	1	1
α	0.2	0.2	0.2	0.2
β	150	250	300	500
ϕ	0.3	0.3	0.3	0.3
c^0 (ppm)	5	10	15	25
r_w (m)	0.14	0.14	0.14	0.14
h (m)	10	10	10	10
k_c (mD)	20	20	20	20
ϕ_c	0.2	0.2	0.2	0.2

2.3.2 *BOTTOM-UP WATER INJECTION USING HORIZONTAL WELLS (OVERLAPPING WELLS) IN HOMOGENEOUS RESERVOIR:*

The effect of injectivity profile homogenization by the skin, induced by utilizing poor quality water, for bottom-up injection in the system of horizontal injector and producer are investigate in this part of the study. The homogeneous rectangular reservoir was waterflooded by a horizontal injector below the horizontal producer (Figure 9). The geometrical placement of wells in the reservoir is symmetrical with respect to planes x= 500 m and y= 500 m. The corresponding reservoir and formation damage properties are given in Table 3 and Table 4. The constant pressures along both wells are assumed, i.e. the pressure losses due to fluid flows in well columns are neglected.

TABLE 3: PARAMETERS USED FOR OVERLAP STUDIES

Parameters of the geological model	Value used Overlap Study
Node numbers for fine grids	-
Node numbers for moderate grids	50 x 50 x 3
Node numbers for coarse grids	-
The length of the reservoir (m)	500
The width of the reservoir (m)	500
The thickness of the reservoir (m)	30
The length of wells (m)	200
Initial Reservoir Pressure (Psi)	3000
Viscosity of Water (cP)	1
Viscosity of Oil (cP)	1
Initial Oil Saturation	0.8
Initial Porosity	0.3
Initial Horizontal Permeability (mD)	50
Initial Vertical Permeability (mD)	10
Injection Pressure (psi)	5000

TABLE 4: FORMATION DAMAGE DATA FOR SIMULATION IN OVERLAP CONFIGURATION CASE STUDY

Data	Skin = 11	Skin = 25	Skin = 40	Skin = 60
λ' (1/m)	1	1	1	1
α	0.1	0.1	0.1	0.1
β	5	150	220	450
ϕ	0.3	0.3	0.3	0.3
c^0 (ppm)	5	10	10	15
r_w (m)	0.14	0.14	0.14	0.14
h (m)	1.21	1.21	1.21	1.21
k_c (mD)	20	20	20	20
ϕ_c	0.2	0.2	0.2	0.2

The speed along the shortest stream line AB in Figure 9 highly exceeds those along the stream lines between the well heels and toes (curves CD and FE, respectively) that pass the remote areas near to the rectangular vortexes. This explains the poor sweep in periphery areas (Bedrikovetsky 1993). The plugging by poor quality water occurs preferentially along the streamlines with higher speed, where the larger volumes of injected particles yield the higher particle retention concentrations. This occurrence constitutes to a natural conformance control by diverting the fluid from the zones, swept by high speed streamlines, to low speed zones which results in more uniform displacement of oil (enhanced sweep). In the case of two-zone reservoir, the effect of different speed along the streamlines was due to the heterogeneity of the reservoir, while in the bottom-up injection case it is due to the more complex geometry of stream lines.

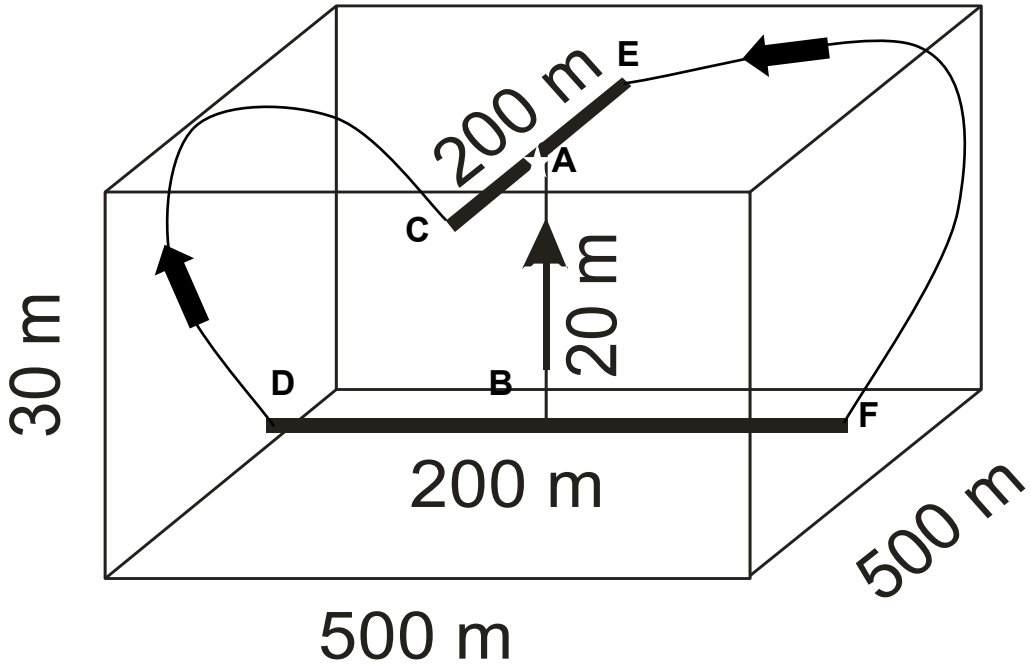

FIGURE 9: BOTTOM-UP WATER INJECTION USING HORIZONTAL WELLS

The competitive factors of the improved sweep due to the redirection of water flux into the peripheral areas and of the reduced flux due to induced skin are the same as that in the two-permeability-zone reservoir. Yet, the gravity brings the additional complexity to the displacement process. The higher is the flow velocity in the gravity stable displacement the lower is the recovery (Lake 1989; Bedrikovetsky 1993). Plugging the high speed stream lines causes the recovery increase while the flow acceleration in low speed streamlines yields the decrease of the recovery factor. The complex interaction of the above gravity effects with the skin induced factors can be revealed by 3D numerical simulation. Longer wells lengths of 320 m are also studied for overlap configuration to determine its effect on the sweep efficiency.

This study aims to investigate the effectiveness of the overlap configuration for future developments. The wells are designed to be longer in this case to provide more reservoir contact in order to obtain more accurate simulation results. Figure 10 shows the layout of the well arrangement in Eclipse interface.

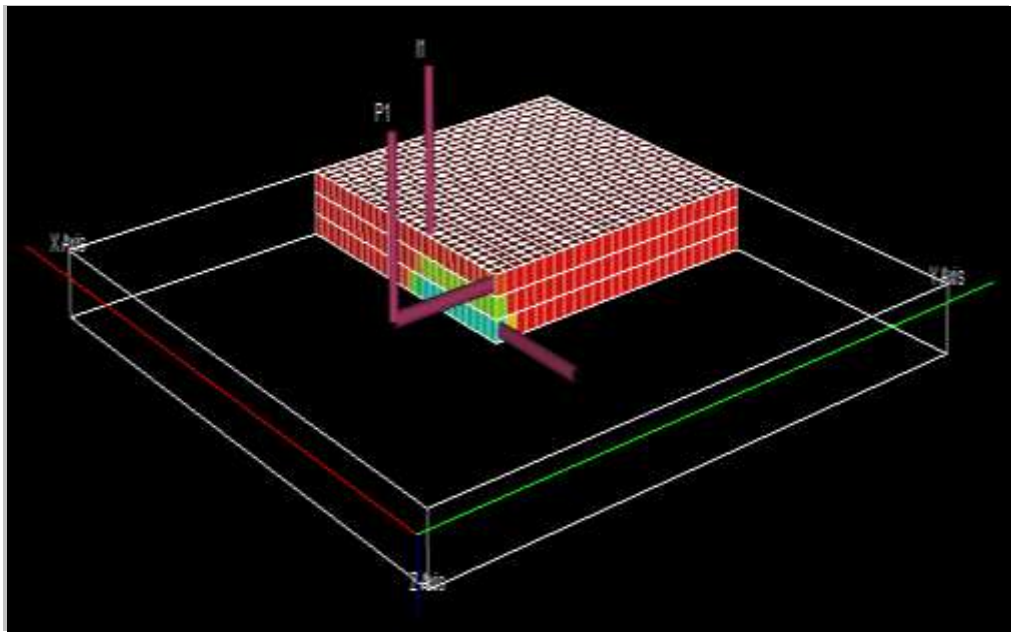

FIGURE 10: ECLIPSE VISUALIZATION FOR LAYOUT OF OVERLAPPING WELLS IN HOMOGENEOUS RESERVOIR

Sensitivity analysis is also conducted on volatile oil (viscosity of 1 cP), conventional oil (viscosity of 10 cP) and heavy oil (viscosity of 100 cP).

2.4 RESULTS

2.4.1 TWO ZONE RESERVOIR

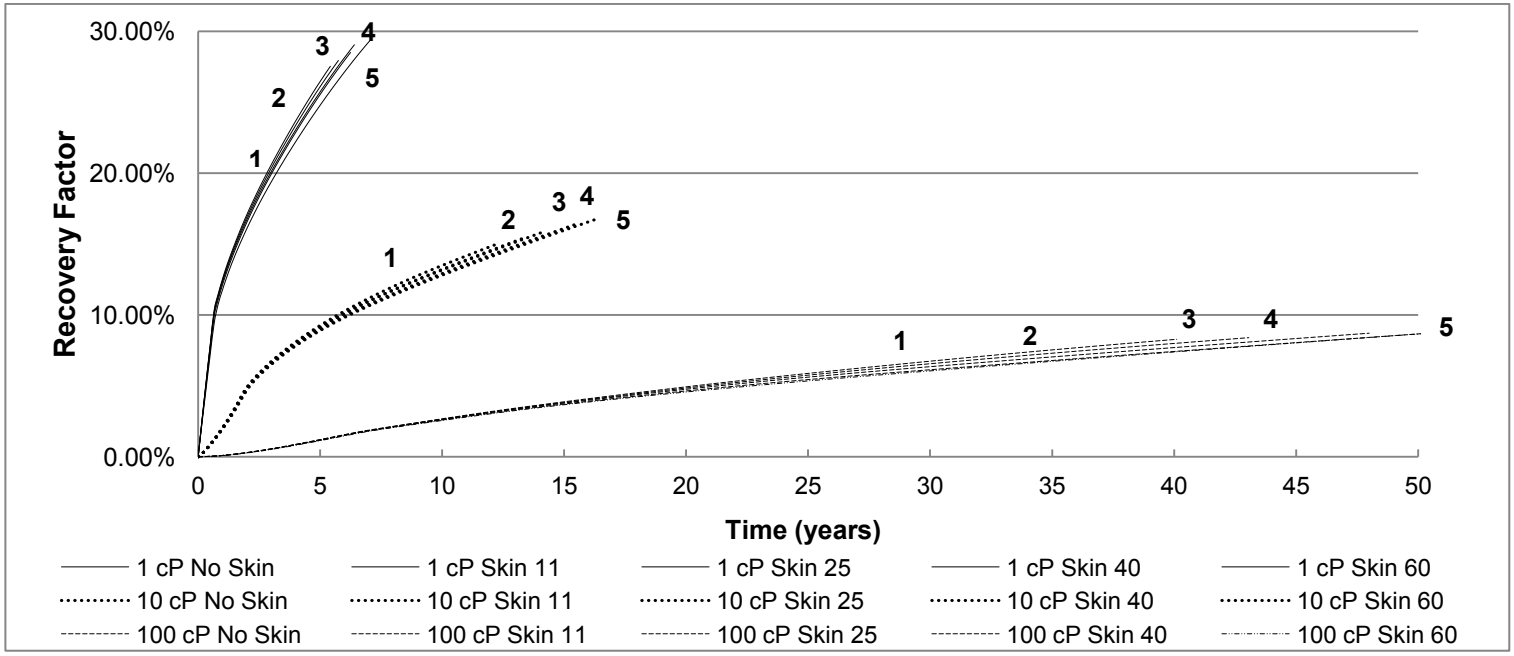

FIGURE 11: RECOVERY FACTOR VS REAL TIME (YRS) FOR INJECTION OF "CLEAN" WATER AND OF "RAW" WATER IN TWO-ZONE RESERVOIR

Curves 1, 2, 3, 4 and 5 correspond to injection of clean water and of suspensions resulting in skin factors of 11, 25, 40, 60 after 1 PVI, respectively. Solid, dotted and dashed curves correspond to oil viscosities 1 cP, 10 cP and 100 cP, respectively.

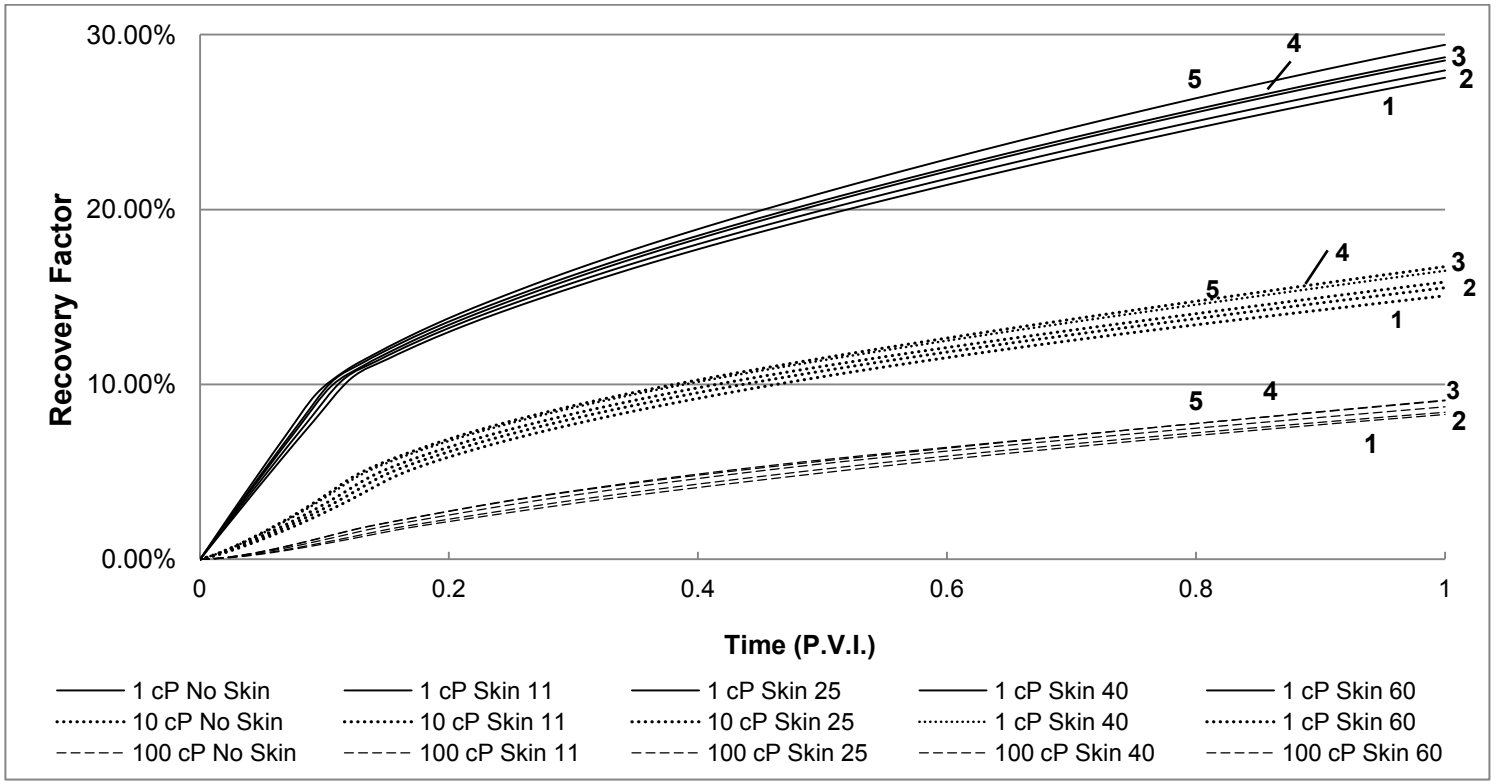

FIGURE 12: RECOVERY FACTOR VS TIME (PVI) FOR "CLEAN" AND "RAW" WATER INJECTION IN TWO-ZONE RESERVOIR

Curves 1, 2, 3, 4 and 5 correspond to injection of clean water and of suspensions resulting in skin factors 11, 25, 40 and 60 after 1 P.V.I, respectively. Solid, dotted and dashed curves correspond to oil viscosities 1 cP, 10 cP and 100 cP, respectively.

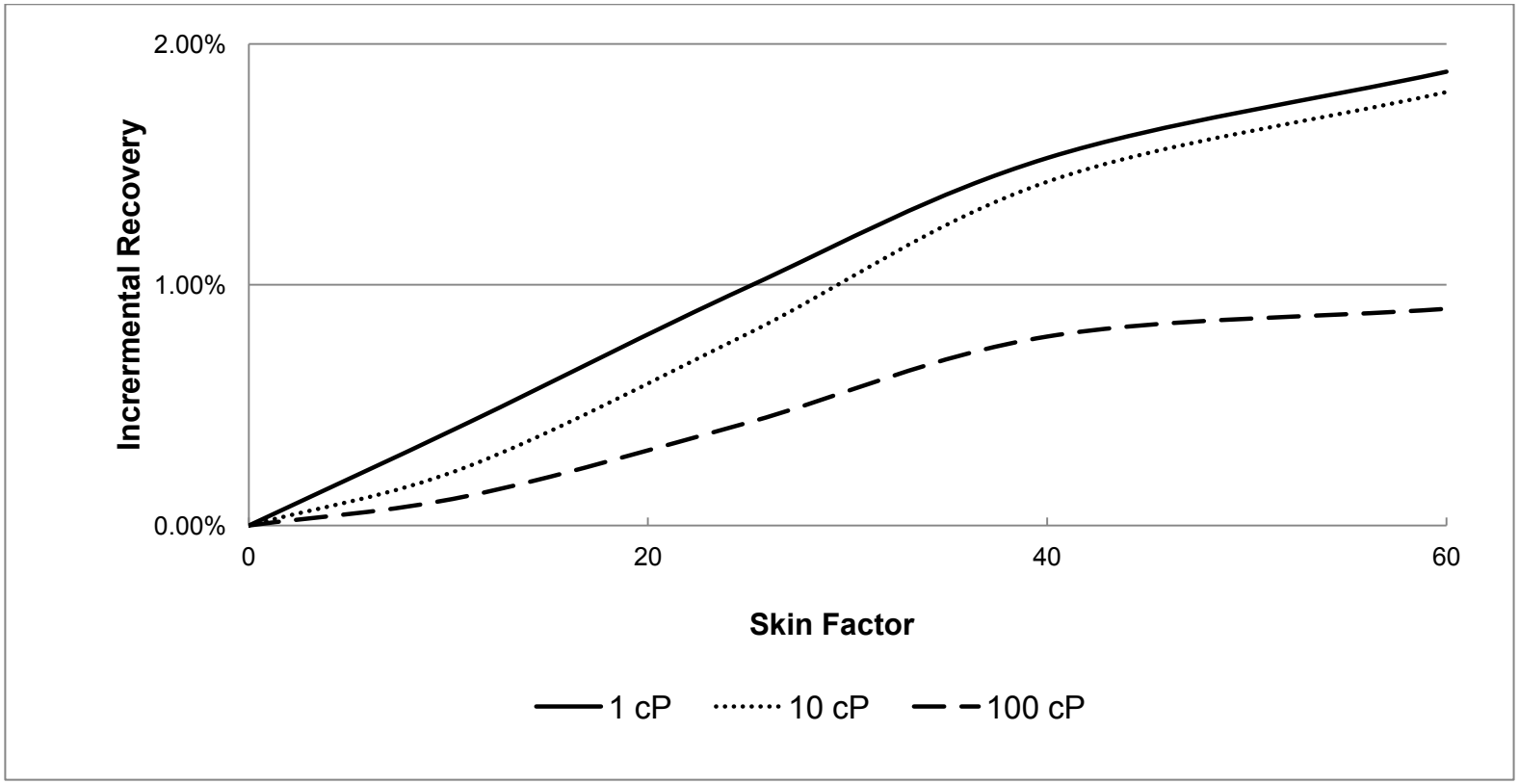

FIGURE 13: INCREMENTAL RECOVERY, BY USING "RAW" WATER INJECTION INSTEAD OF "CLEAN" WATER, VS SKIN FACTOR IN THE TWO-ZONE RESERVOIR

(both are calculated after 1 PVI). Solid, dotted and dashed curves correspond to oil viscosities 1 cP, 10 cP and 100 cP, respectively

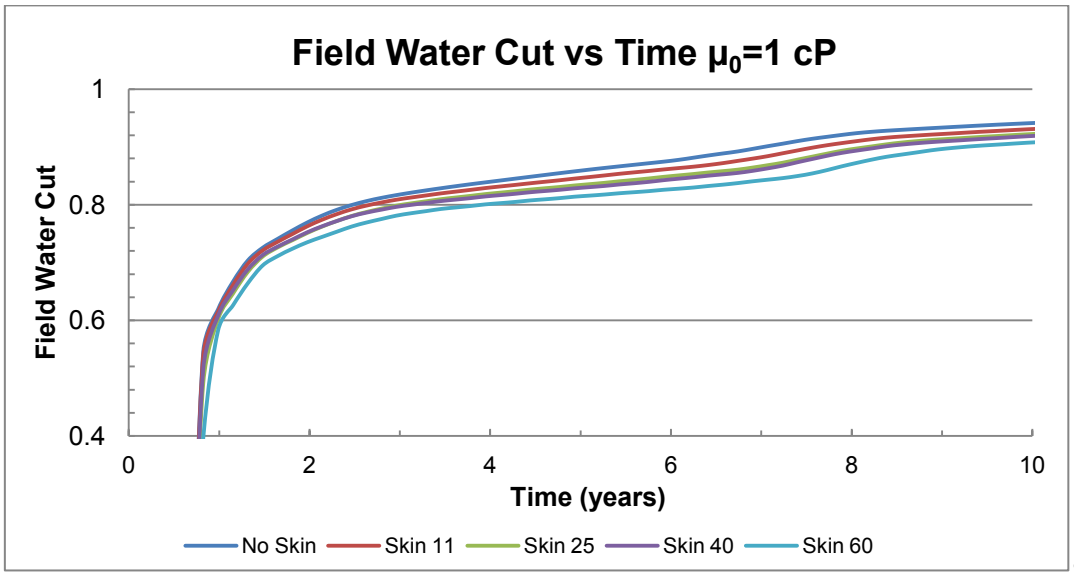

a)

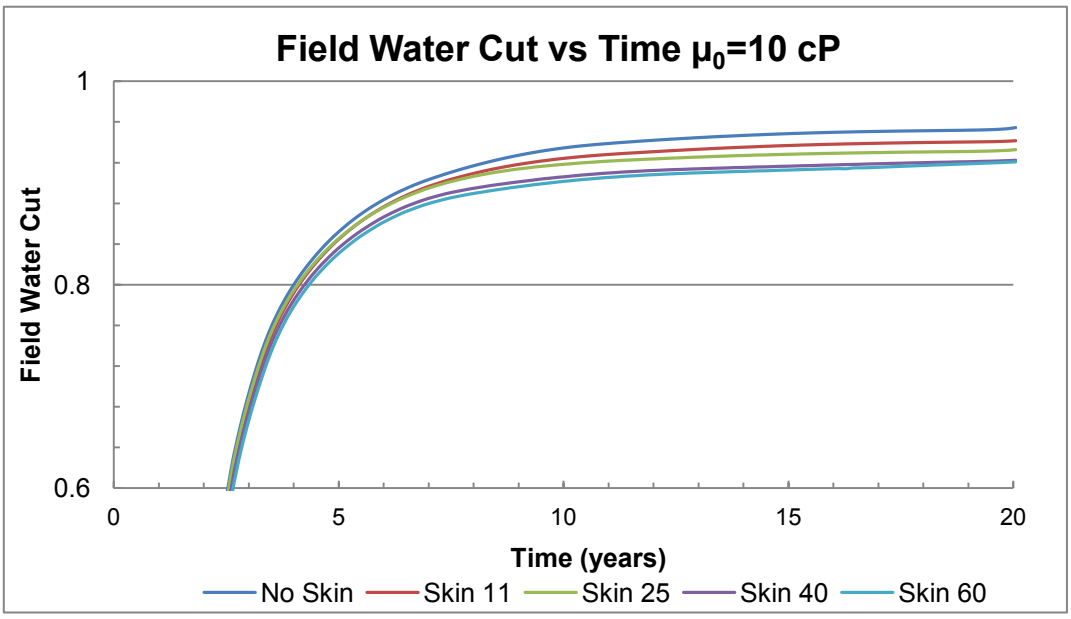

b)

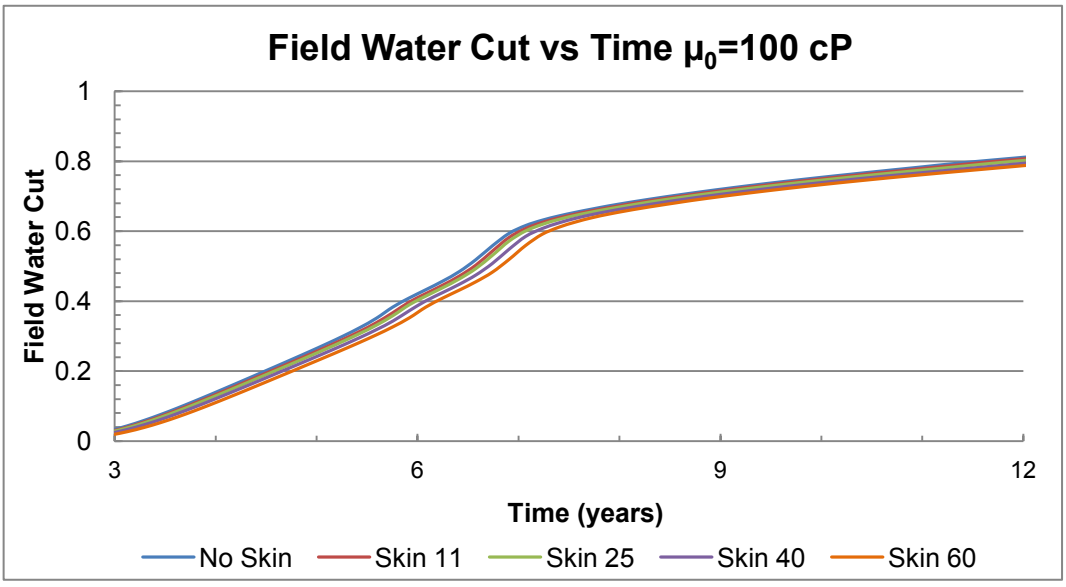

c)

FIGURE 14: WATER CUT, DURING INJECTION OF "RAW" AND OF "CLEAN" WATER, VS REAL TIME IN TWO-ZONE RESERVOIR

a) 1 cP; b) 10 cP; c) 100 cP

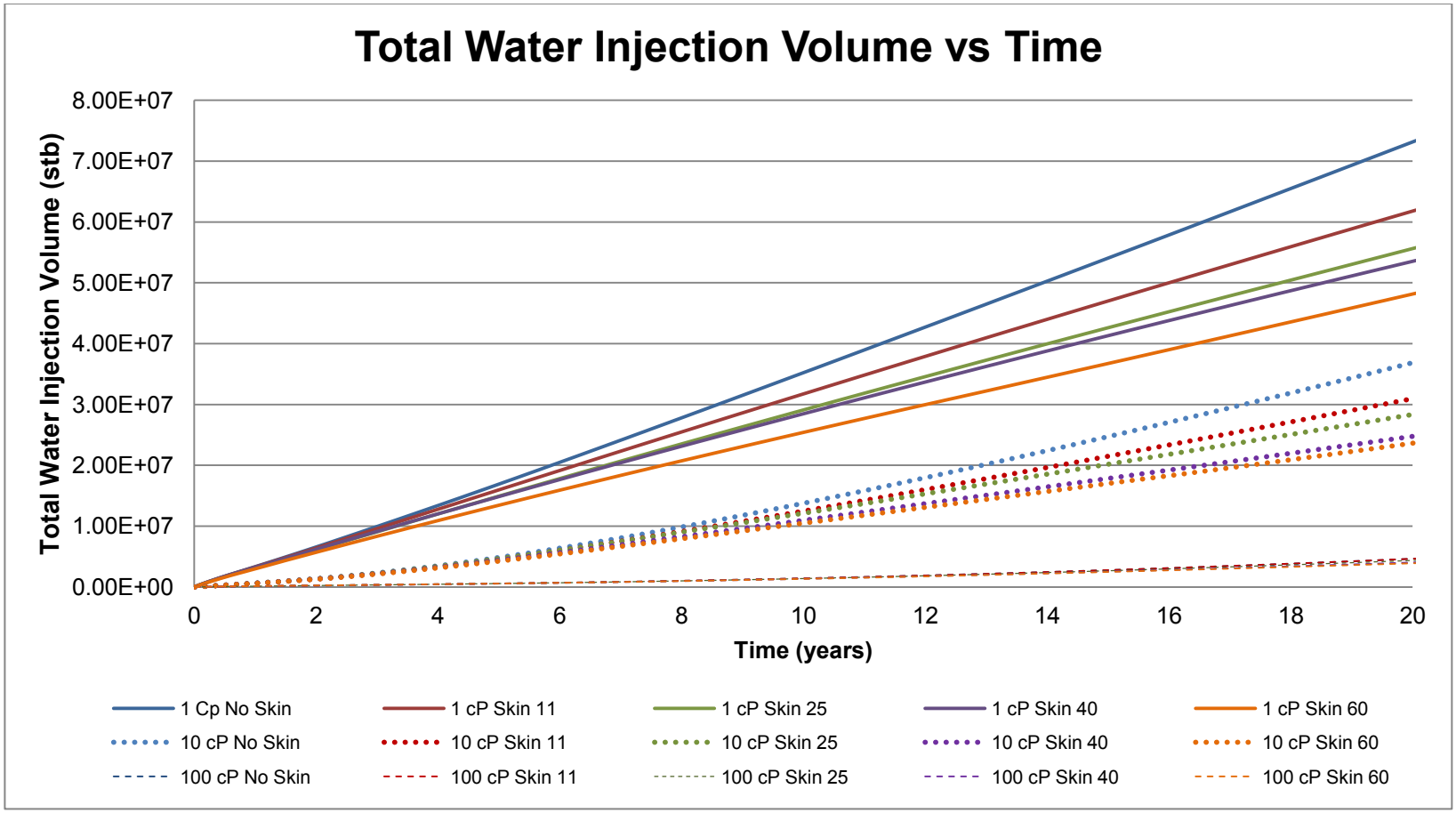

FIGURE 15: VOLUME OF INJECTED WATER VS REAL TIME FOR INJECTION OF "RAW" AND OF "CLEAN" WATER IN TWO-ZONE RESERVOIR

Curves 1, 2, 3, 4 and 5 correspond to injection of clean water and of suspensions resulting in skin factors 11, 25, 40 and 60 after 1 PVI, respectively. Solid, dotted and dashed curves correspond to oil viscosities 1 cP, 10 cP and 100 cP, respectively.

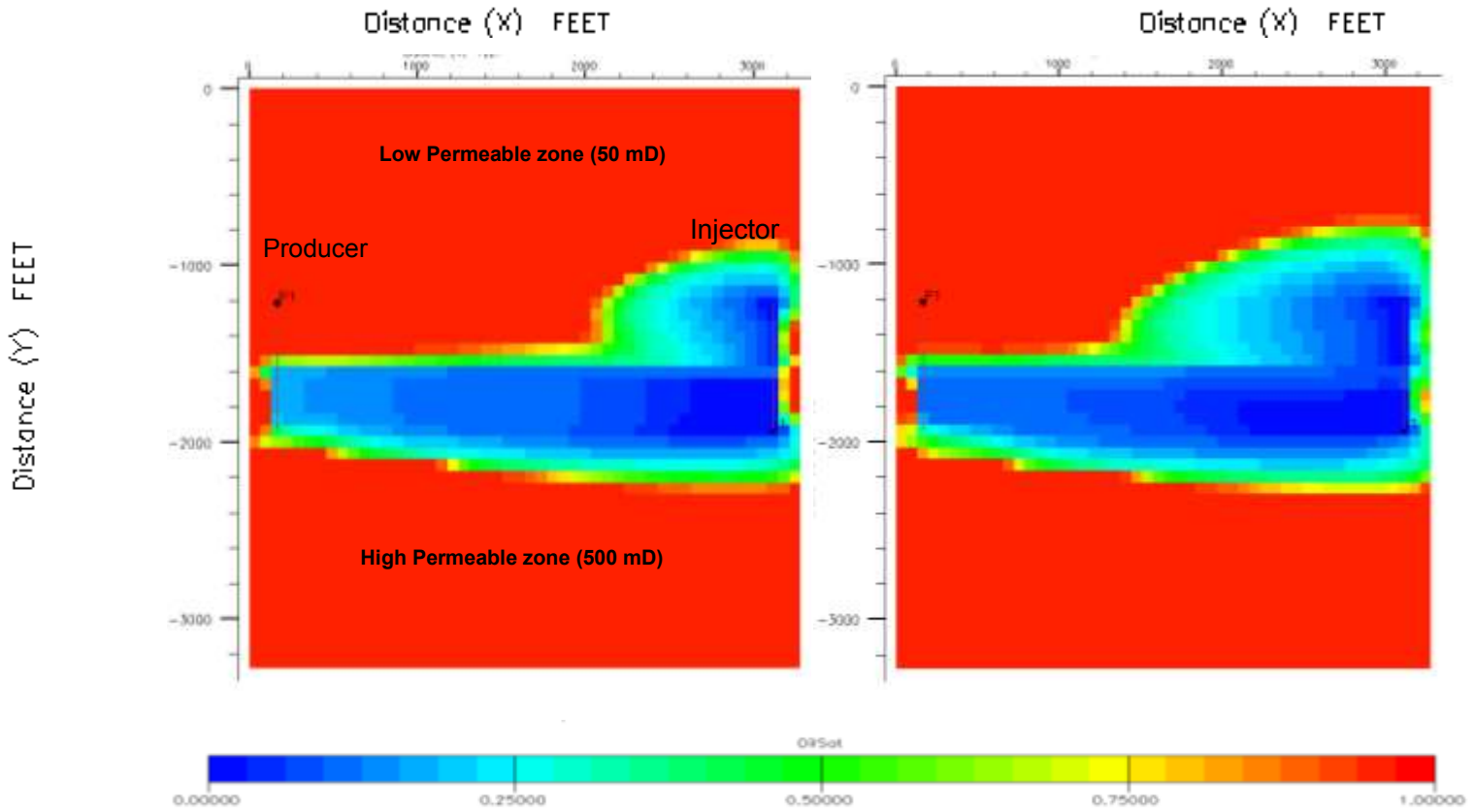

a) b)

FIGURE 16: IMPROVED SWEEP EFFICIENCY WITH INJECTIVITY DAMAGE AFTER 1 PVI IN TWO-ZONE RESERVOIR

a) Sweep efficiency with no damage after 1 PVI for 1 cP ; b) Sweep efficiency with damage (skin= 60) after 1 PVI for 1 cP

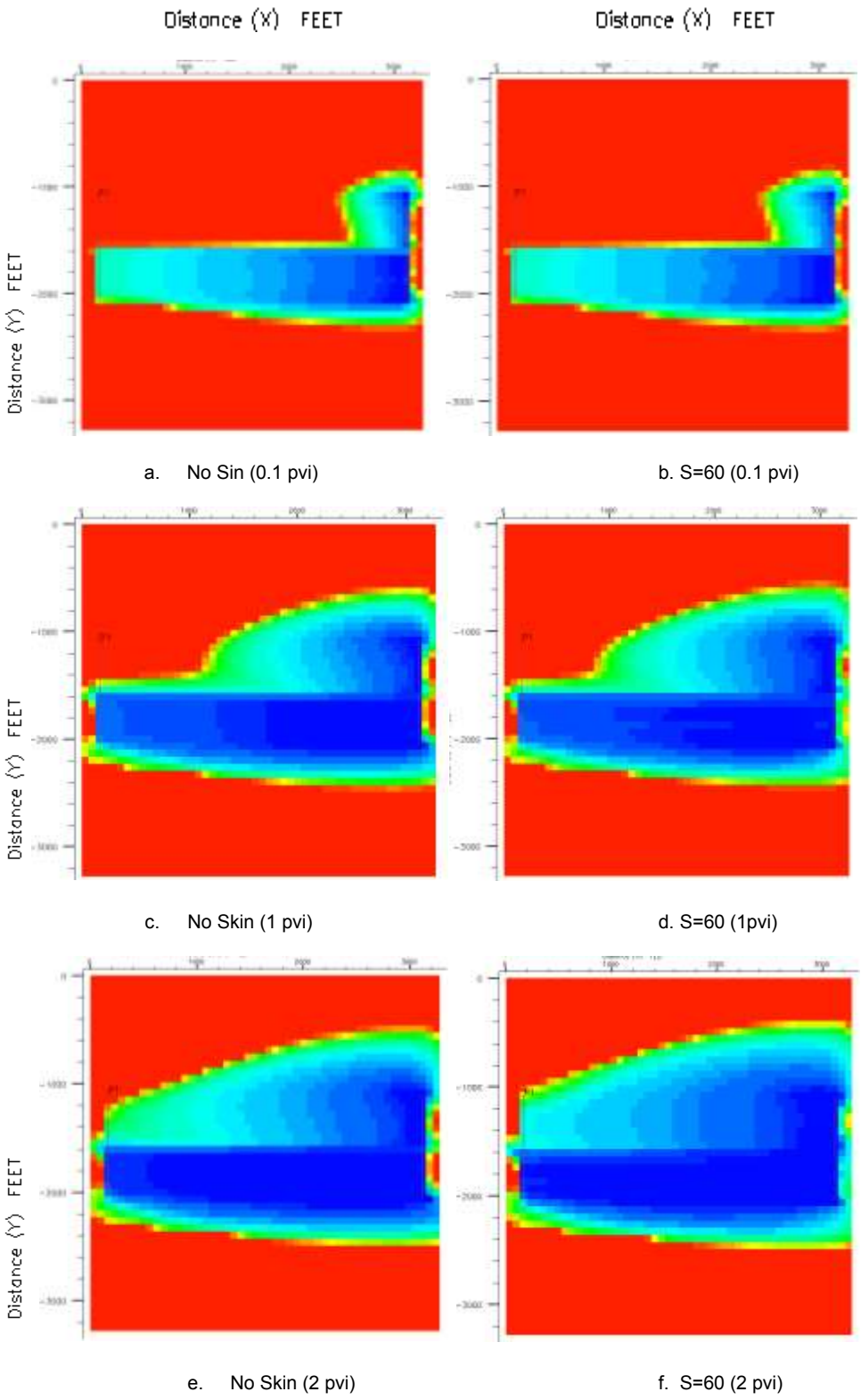

a. No Sin (0.1 pvi) b. S=60 (0.1 pvi)

c. No Skin (1 pvi) d. S=60 (1pvi)

e. No Skin (2 pvi) f. S=60 (2 pvi)

FIGURE 17: SWEEP EFFCICIENCY INCREASE DUE TO SKIN FACTOR DISTRIBUTED ALONG THE HORIZONTAL INJECTOR; THE CASE OF "LONG" HW

2.4.2 HOMOGENOUS RESERVOIR WITH OVERLAPPING WELLS:

2.4.2.1 Horizontal injector perpendicular to the horizontal producer:

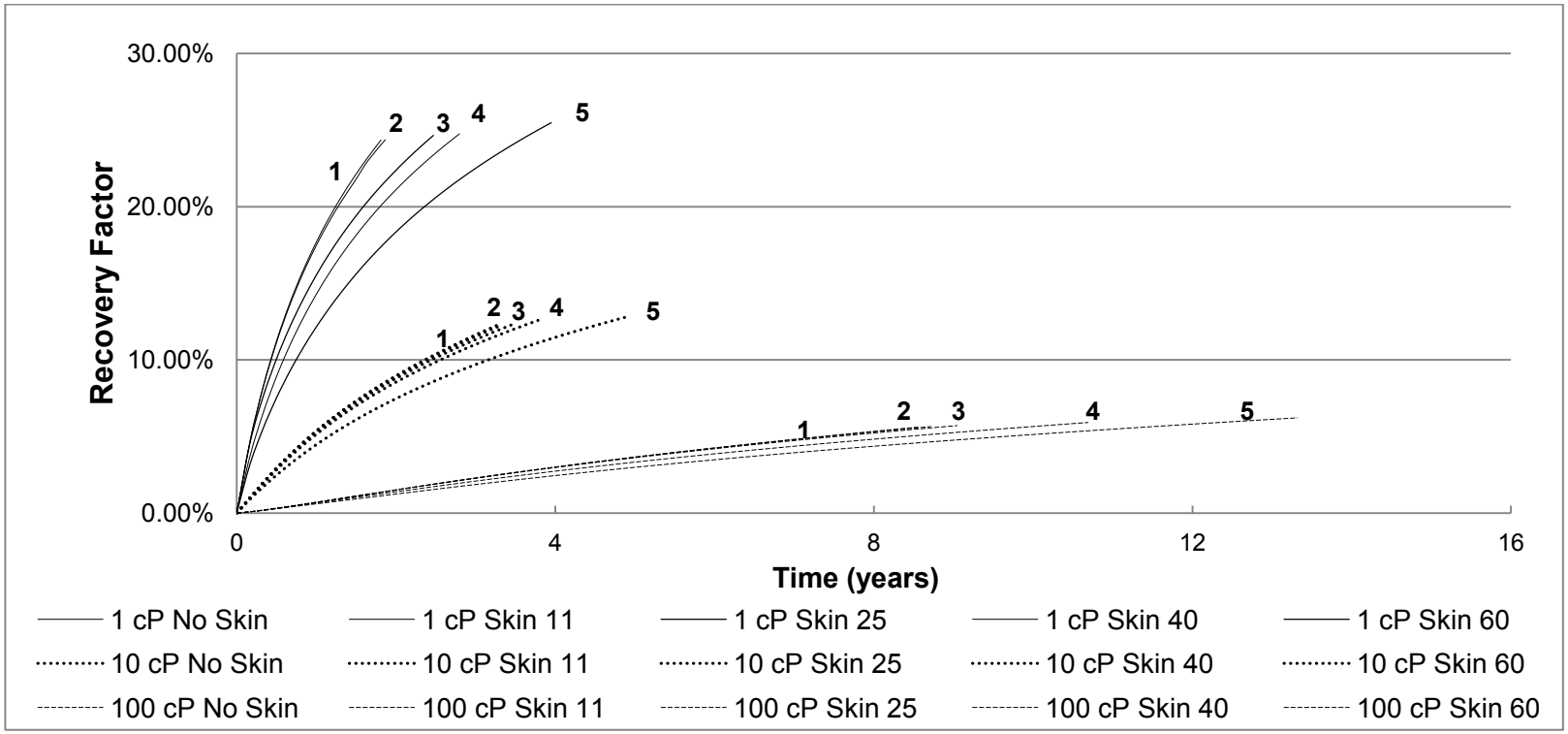

FIGURE 18: RECOVERY FACTOR (OF "RAW" AND OF "CLEAN" WATER INJECTION) VS REAL TIME (YRS) FOR PERPENDICULAR OVERLAPPING WELLS IN HOMOGENEOUS RESERVOIR

Curves 1, 2, 3, 4 and 5 correspond to injection of clean water and of suspensions resulting in skin factors 11, 25, 40 and 60 after 1 PVI, respectively. Solid, dotted and dashed curves correspond to oil viscosities 1 cP, 10 cP and 100 cP, respectively.

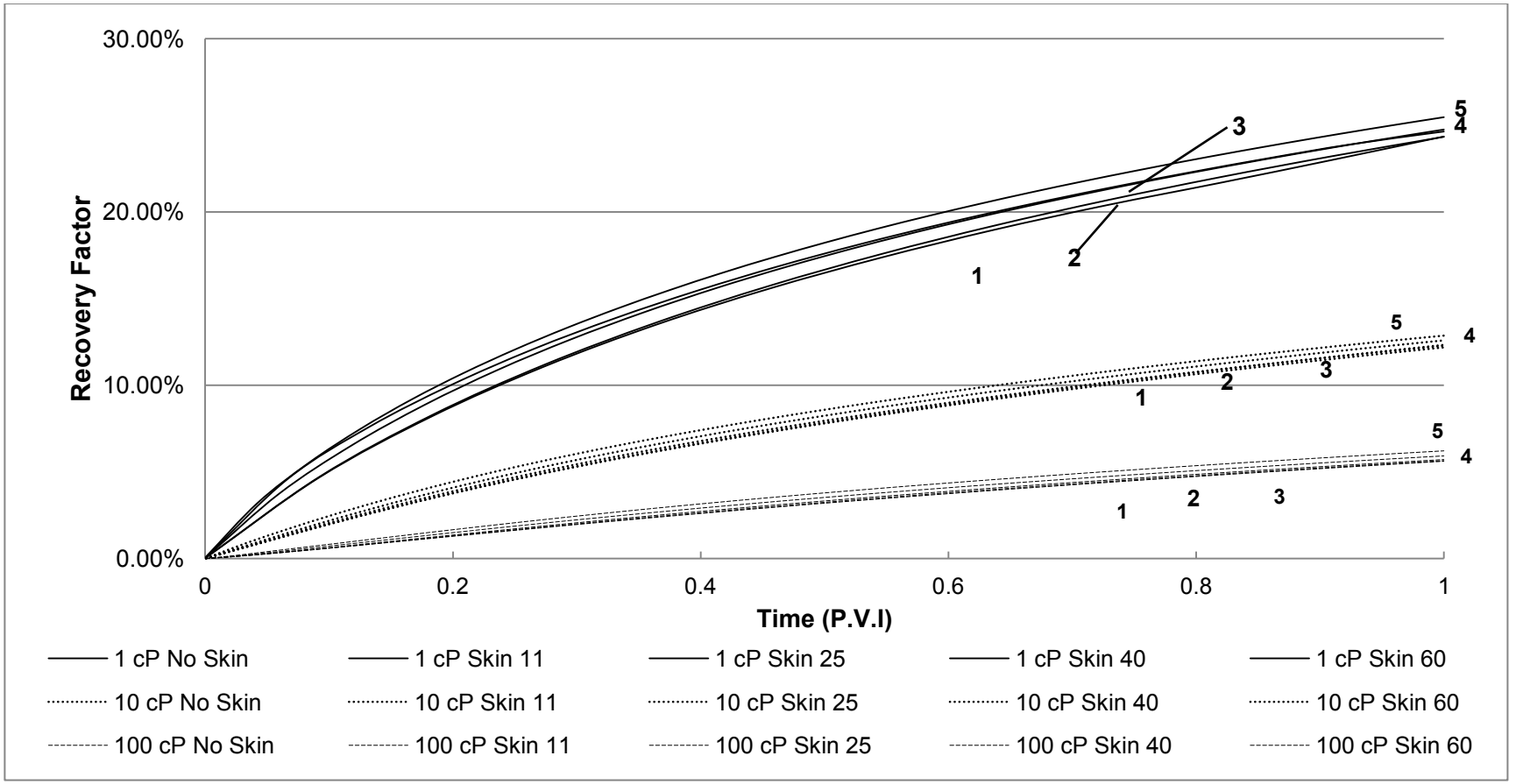

FIGURE 19: RECOVERY FACTOR (OF "RAW" AND OF "CLEAN" WATER INJECTION) VS TIME (PVI) FOR PERPENDICULAR OVERLAPPING WELLS IN HOMOGENEOUS RESERVOIR

Curves 1, 2, 3, 4 and 5 correspond to injection of clean water and of suspensions resulting in skin factors 11, 25, 40 and 60 after 1 PVI, respectively. Solid, dotted and dashed curves correspond to oil viscosities 1 cp, 10 cp and 100 cp, respectively

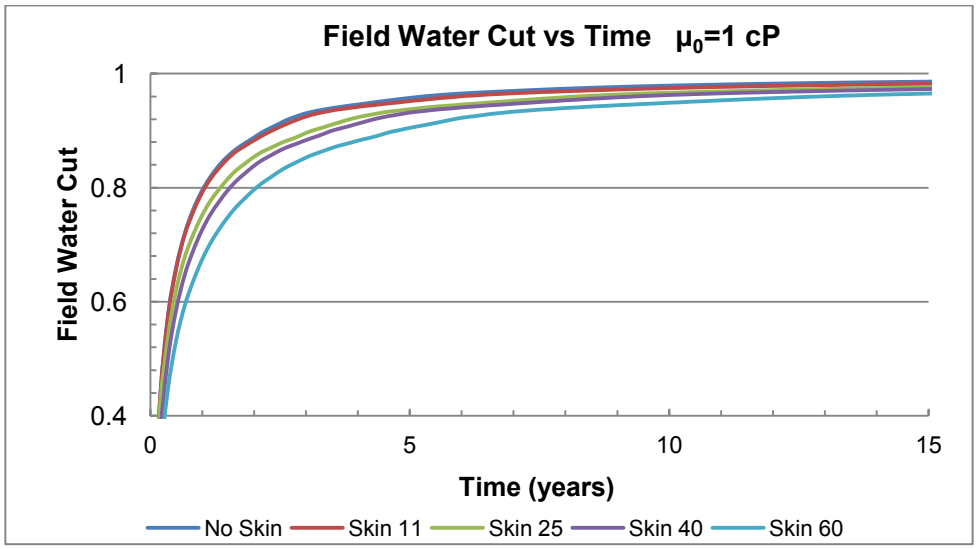

a)

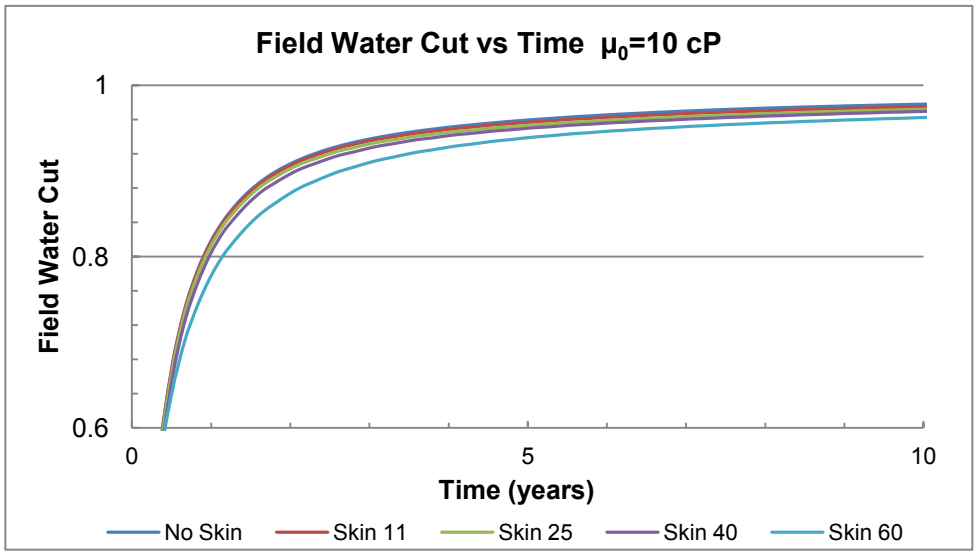

b)

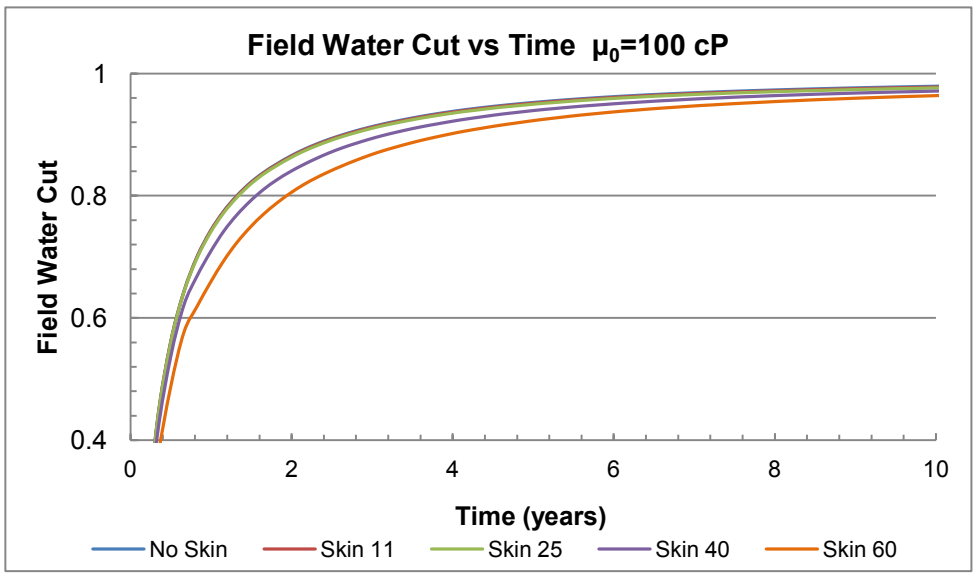

c)

FIGURE 20: WATER CUT, DURING "RAW" AND "CLEAN" WATER INJECTION, VS REAL TIME FOR PERPENDICULAR OVERLAPPING WELLS IN HOMOGENEOUS RESERVOIR.

a) oil viscosity is 1 cp, b) oil viscosity is 10 cp, c) oil viscosity is 100 cp

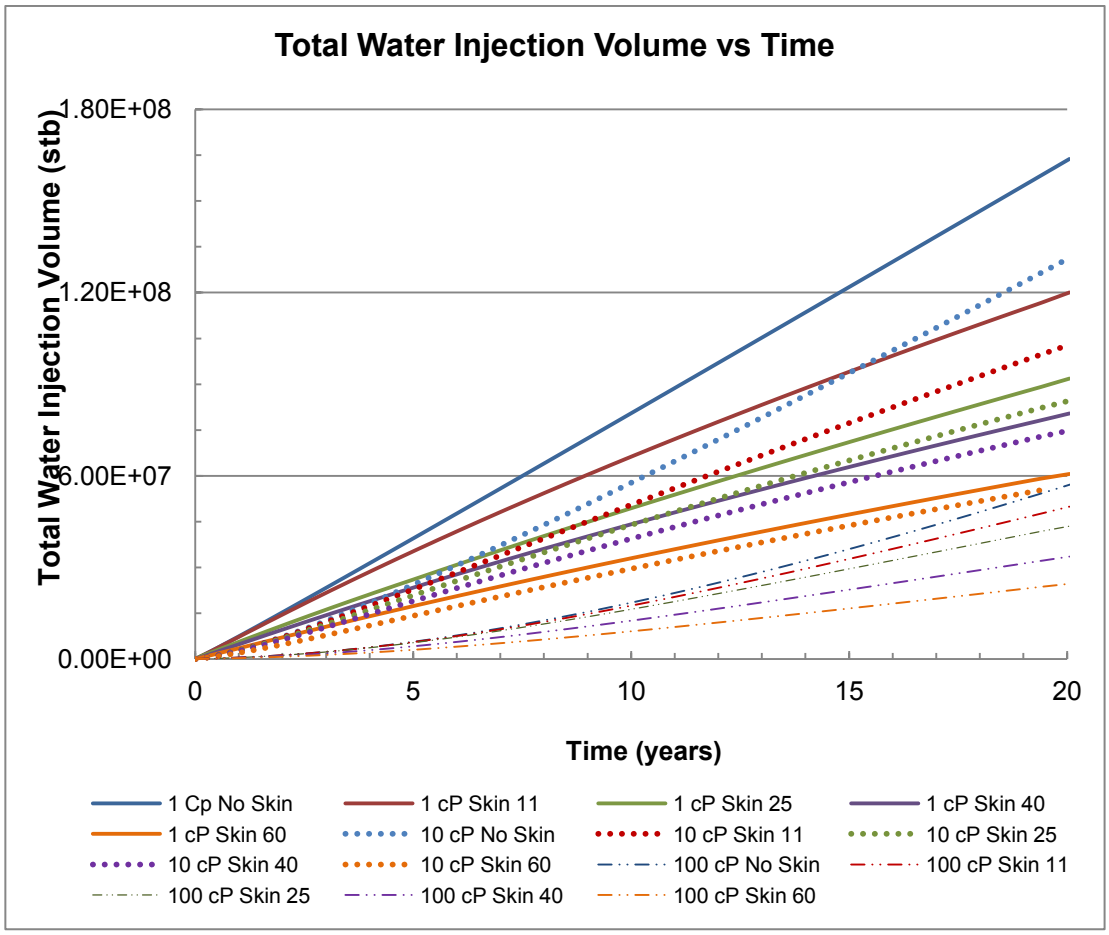

FIGURE 21: WATER INJECTED VOLUME VS REAL TIME FOR PERPENDICULAR OVERLAPPING WELLS IN HOMOGENEOUS RESERVOIR

Solid, dotted and dashed curves correspond to oil viscosities 1 cp, 10 cp and 100 cp, respectively

2.5 Discussion

2.5.1 Parallel Horizontal Injector and Producer in Thin Horizontal Reservoir with High and Low Permeability Zones

Figure 16 a) and b) present saturation fields after 1 PVI for the cases with and without skin, respectively. Fast breakthrough and low sweep took place for the case with no skin. It is seen that the sweep is higher in the high permeability zone. The bulk of water enters the high permeability zone; therefore resulting in the higher induced skin around the part of well in this zone as skin is a monotonically increasing function of the volume of injected water. The increased skin along the sections of the horizontal well located in highly permeable zone yields the reduction of invaded water in this zone. Automatically, the difference of fluxes is redirected into the low permeable zone, resulting in its better sweep. Figure 16b shows increased water saturation in the low permeability zone if compared with Figure 16a.

The homogenization of the injectivity profile by induced skin also results in better sweep behind the injector. Figure 16 shows some oil trapped near to the zone boundary. Two water fluxes in different permeability zones reach the boundary behind the injector at different times and start moving in opposite directions, resulting in trapped oil behind the injector. Induced skin leads to a decrease of time difference of front arrival to the impermeable boundary, which results in some decrease of trapped oil.

TABLE 5: INCREMENTAL RECOVERY FACTOR BY "RAW" WATER INJECTION COMPARED TO "CLEAN" WATER INJECTION IN VOLATILE OIL 1CP TWO-ZONE RESERVOIR.

Cases	Recovery Factor (RF) at 1 p.v.i.	Recovery Increase compared to "No Skin" case
No Skin	27.54%	-
Skin = 11	27.96%	0.42%
Skin = 25	28.53%	0.99%
Skin = 40	29.06%	1.52%
Skin = 60	29.42%	1.88%

The effect of the induced injectivity skin, non-uniformly distributed along horizontal well, on the recovery factor *vs* injected volume of water is presented in

Figure 12 for three cases of volatile, conventional and heavy oils. The damage-free injection of clean water is considered along with injection of four poor quality waters resulting in different injectivity impairment. The injectivity damage parameters for four cases are presented in Table 2. For all oil viscosities, the higher is the skin the higher is the incremental recovery factor after 1 pvi. If compared with clean water flooding, injection of particulate suspension into volatile oil reservoir yielding S=60 after 1 pvi causes 1.8% of incremental recovery. The effect is less pronounced for higher viscosity oils – incremental recovery of 0.8% for 100 cp oil after 1 PVI (Figure 13). The incremental recovery by raw water injection in volatile oil (1 cP) is summarized in Table 5.

Despite the decreasing of incremental recovery with increasing oil viscosity, the relative effect of non-uniform distribution of the induced injectivity skin along horizontal well does not decrease since the recovery is lower for heavy oils. For the case of high skin S=60 presented in Figure 13, the incremental recovery factors for oil viscosities 1, 10 and 100 cp are 1.88%, 1.43% and 0.9%, respectively, while the absolute recovery factors are 29.09%, 16.63% and 8.98%. So, the ratios of the incremental recovery and the recovery factor (relative incremental recoveries) are 0.065, 0.086 and 0.1, respectively. Thus, the relative incremental recovery is the highest for heavy oils.

Along with the positive effect of sweep efficiency increase due to injectivity profile homogenization, the induced skin yields the negative effect of flux and total rate reduction (the total rate is the sum of those for produced oil and water). Figure 11 exhibits recovery factor versus real time for three different viscosity oils during injection of clean water along with injection of four different quality waters. The higher is the skin the lower is the recovery factor. Yet, the difference between the recovery curves is negligible. For volatile oil reservoir, the recovery factor for clean waterflooding after 10 years is 35.37% while for S=60 it is lower at 34.25%. Finally, the negative effect of rate decrease is compensated by the positive effect of sweep increase.

As it follows from Figure 11, the amount of produced oil versus real time is almost independent of the induced skin. Therefore, the comparison between the

recovery efficiency indicators at the same production time means “at the same amount of produced oil”.

Figure 14 shows how the water cut curve depends on the value of the induced skin. Figure 14a, b and c show the water cut curves for volatile, conventional and heavy oils, respectively. The higher is the induced skin the lower is the water cut. For waterflooding in the volatile oil field, water cut reduction increases from 4% after 2 years of injection up to 7% after 8 years of injection. The reduction of water cut by induced skin yields the reduction of the amount of injected water for the same volume of produced oil (Figure 15). The effect of induced skin is more pronounced for the case of a volatile oil – the amount of injected clean water after 10 years of injection is 1.5 times higher than that for poor quality water causing S=60. The effect is weaker for the case of conventional oil: the amount of injected clean water is 1.3 times higher than for the poor quality water. The effect almost disappeared for heavy oils – dashed curves 1, 2, 3, 4 and 5 in Figure 15 almost coincide.

Finally, the main advantage of the induced homogenization of the injectivity profile is the reduction of the volume of injected water for the same amount of produced oil. Since the balance of injected and produced fluids is maintained during the waterflood cases under consideration, the absolute reduction in injected water is equal to that in produced water under the same amount of produced oil. Like in the polymer flooding, the physics effect of improved recovery during injection of water with particles is the decreasing of water flux in swept zones. So, the IOR effects are also similar: the decreased amount of injected and produced water and some recovery increase after a long injection period (Lake 1989).

Figure 17a, c and e show areal saturation distribution during injection of suspension, while Figure 17b, 19d and 19f illustrate water injection without skin. Figure 17a and b present saturation distributions in the reservoir after 0.1 pvi; Figure 17c and d show saturation distribution after 1 pvi while Figure 17e and f show saturation field after 2 pvi. The main effect is the partial redirection of injected water into the low permeable zone due to high induced skin at the horizontal well section in the high permeability zone. A minor effect of sweep

increase due to induced skin at the beginning of water injection (0.1 pvi) was observed. One can see the higher sweep in low permeability zone and the water saturation decrease in highly permeable area if compared with that of clean water flood at 1 pvi. The significant increase of sweep in low permeability zone after 2 pvi is apparent. In terms of the overall recovery, the incremental recovery factor increases up to 5% at 1 pvi and up to 9% after 2 pvi.

The dynamics of displacement presented in Figure 17 allows comparing the effect of induced injectivity damage on incremental recovery for vertical and horizontal wells. For the case of vertical injector in thin two-layer-cake reservoir, the injected water bypasses the damaged zone near to the vertical injector by moving vertically along a short distance from low permeability to high permeability layer and enters the high velocity path. Almost all incremental flux in low permeability layer, induced by high skin in the high permeability layer, enters the high permeability layer. Distribution of fluxes along the layers remains the same downstream of the damaged area. It diminishes the effect of inhomogeneous skin profile on the waterflood sweep efficiency. Figure 17 exhibits the case where the distance between wells has the same order of magnitude to the inter-zone distance. As in the thin two-layer-cake reservoir, the induced skin creates an additional resistance to flow in the high permeability zone and leads to an additional water flux entering the low permeability zone. Since the inter-zone distance is significantly higher than the distance between the high permeability and low permeability layers, the pressure gradient across the boundary is significantly lower in 2-zone reservoir. It allows for incremental flux in low permeable zone, caused by the injection rate redistribution due to the induced skin, to not fully move into highly permeable zone but displace more oil from the low permeability zone.

2.5.2 HOMOGENOUS RESERVOIR WITH OVERLAPPING WELLS

2.5.2.1 Perpendicular overlapping wells in homogeneous reservoir

The effect of injectivity profile homogenization by the skin, induced by utilizing poor quality water, for bottom-up injection in the system of horizontal injector and producer is investigated. The homogeneous rectangular reservoir was waterflooded by a horizontal injector below the horizontal producer (Figure 9). The geometrical placement of wells in the reservoir is symmetrical with respect to planes x= 500 m and y= 500 m. The corresponding reservoir and formation damage properties are given in Table 3 and Table 4. The constant pressures along both wells are assumed, i.e. the pressure losses due to fluid flows in well columns are neglected.

The speed along the shortest stream line AB in Figure 9 highly exceeds those along the stream lines between the well heels and toes (curves CD and FE, respectively) that pass the remote areas near to the rectangular vortexes. This explains the poor sweep in periphery areas (Bedrikovetsky 1993). The plugging by poor quality water occurs preferentially along the streamlines with higher speed, where the larger volumes of injected particles yield the higher particle retention concentrations. This occurrence constitutes to a natural conformance control by diverting the fluid from the zones, swept by high speed streamlines, to low speed zones which results in more uniform displacement of oil (enhanced sweep). In the case of two-zone reservoir, the effect of different speed along the streamlines was due to the heterogeneity of the reservoir, while in the bottom-up injection case it is due to the more complex geometry of stream lines.

The competitive factors of the improved sweep due to the redirection of water flux into the peripheral areas and of the reduced flux due to induced skin are the same as that in the two-permeability-zone reservoir. Yet, the gravity brings the additional complexity to the displacement process. The higher is the flow velocity in the gravity stable displacement the lower is the recovery (Lake 1989; Bedrikovetsky 1993). Plugging the high speed stream lines causes the recovery increase while the flow acceleration in low speed streamlines yields the decrease

of the recovery factor. The complex interaction of the above gravity effects with the skin induced factors can be revealed by 3d numerical simulation.

The recovery factor versus time in pvi is presented in Figure 19 for the injection of clean water and four cases of suspension injection. For the case of high skin S=60, the incremental recovery factors for volatile, conventional and heavy oils after 1 PVI are 1.13%, 0.58% and 0.51%, respectively. Since the absolute recovery factors after 1 pvi are 24.34%, 12.29% and 5.62%, the ratios between the incremental recovery factors and the absolute recovery factors are 0.046, 0.047 and 0.090. Despite the incremental recovery factor decreases with increase of oil viscosity, the relative incremental recovery increases.

TABLE 6: INCREMENTAL RECOVERY FACTOR BY "RAW" WATER INJECTION COMPARED TO "CLEAN" WATER INJECTION IN VOLATILE OIL 1CP IN HOMOGENEOUS RESERVOIR.

Cases	Recovery Factor (RF) at 1 p.v.i.	Recovery Increase compared to "No Skin" case
No Skin	24.34%	-
Skin = 11	24.36%	0.02%
Skin = 25	24.65%	0.31%
Skin = 40	24.75%	0.41%
Skin = 60	25.75%	1.41%

Figure 18 presents the recovery factor *vs* real time for three cases of different viscosity oils and four skin values along with clean water flooding. The lower is the skin factor the higher is the recovery. The induction of skin due to poor quality water flooding (S=60) results in decreasing of the recovery factor after 2 years of injection by 7.16% for volatile oil, by 1.49% for conventional oil and by 0.27% for heavy oil. Yet, the induced skin, that homogenizes the injectivity profile, causes the water cut to decrease (Figure 20). The water cut decrease, if compared between the clean water injection and injection of poor quality water resulting in skin S=60, for volatile oil is 13% for 5 months injection and 7.5% for 3-year injection. The water cut reduction decreases for more viscous oils. For the case of heavy oil, the water cut decrease is 8% for 5 months injection and 4.4% for 3 years of injection.

The effect of water cut reduction yields the significant reduction of injected and produced water volumes (Figure 21). The injected water volume after 10-year injection is decreased by injection of poor quality water by 2.5 times for volatile oil, 2 times for conventional oils and 2.13 times for heavy oils.

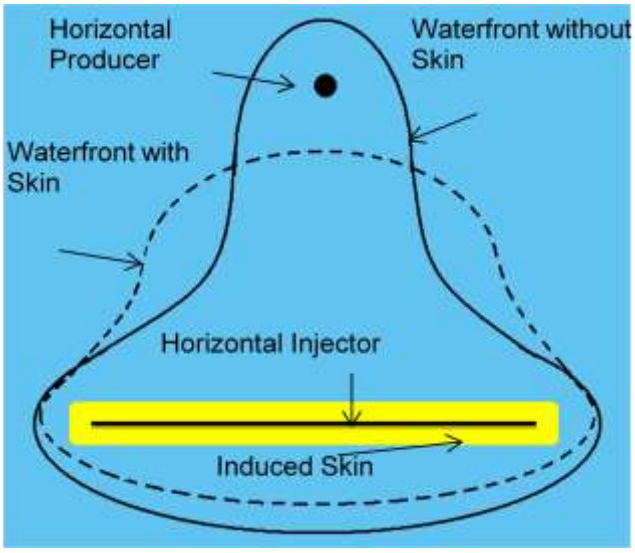

FIGURE 22: SHOWING EFFECT OF SKIN IN HOMOGENEOUS RESERVOIR WITH OVERLAPPING WELLS

2.6 SUMMARY

The skin factor in injection wells due to the injection of particulated water monotonically increases with time. The analytical model provides explicit formulae for skin factor versus injected water volume. The option of water injection with a constant skin factor is already available in most black-oil simulators. Periodical recalculation of accumulated skin after injection of equal volumes using the analytical model allows for implementation of the injectivity decline model into a reservoir simulator for waterflooding. The ECLIPSE 100 black-oil reservoir simulator with implemented option of injectivity decline was applied for study of the effect of poorly treated water injection on sweep efficiency during waterflooding.

The injection of raw water causes formation injectivity damage due to the capture of particles by rock and the external filter cake formation. The damage results in a more uniform injectivity profile along the horizontal well. This continuous homogenization of the injectivity profile during waterflooding yields the redirection of some injected water from the more permeable (higher swept) zones into the low permeable (lower swept) zones. The induced injection skin with waterflooding yields a reduced water-cut if compared with “clean” water injection – the water cut reduction occurs soon after the water breakthrough and remains up to 7-13% during a significant part of the production period. So, the water cut is lower for the case of raw water injection. It also results in some sweep increase. Yet, the induced skin results in some delay in reaching the given recovery factor if compared with the injection of „clean‟ water due to production and injection rates reduction.

The above effects are more pronounced for volatile oils and can be relatively small for heavy oils.

The effects of water cut reduction and delayed IOR for raw water injection are similar to those of polymer flooding, since both technologies result in decrease of the injected water mobility.

The main positive effect of waterflooding with raw water, causing a decrease of injectivity index, is the economic benefit due to savings on injected water treatment. The latter is applied for poorly treated seawater injection as well as for the re-injection of produced water. The advantage of savings on water treatment is especially important for off-shore waterfloods, where the limited and expensive space in platforms yields a high cost of water treatment. Another important advantage is savings due to reduction of injected and produced waters. The disadvantage is the total production rate reduction due to the induced skin factor, which may cause some reduction in oil production rate. This disadvantage is negligible for waterflooding in two-permeability-zone reservoir, where the effect of decreased water cut compensates the effect of the total rate decrease. Yet, some reduction in oil production was observed for bottom-up waterflooding. The final decision on utilizing this method must be made after performing the quantitative economic analysis, which is outside the scope of this work.

The above conclusions are valid for the idealized reservoir model adopted in this work: the reservoir pressure does not rise to the level of the fracturing pressure, deformation and geo-mechanics effects are negligible, simple two-zone heterogeneity was considered. The application of the poor quality water injection in concrete oilfields requires more complex reservoir model and economic analysis.

It is expected that the application of poor quality aqueous suspension may also result in a reduction of water cut and an increase of sweep efficiency for extended fractured injectors and for different configurations of horizontal and slanted wells (Bachman et al. 2003).

2.7 CONCLUSIONS:

The analytical model for injectivity impairment due to poor quality injected water can be implemented in black oil reservoir simulator. Simulation of lateral waterflooding in two-permeability-zone reservoir and of bottom-up flood in homogeneous reservoir with horizontal injector and producer allows the following conclusions to be drawn:

- Injection of poor quality water results in in-homogeneously distributed skin factor as the skin varies along the well according to the injection rate variation;
- The induced skin yields a partial homogenization of the injectivity profile;
- Poor quality water injection results in significant reduction of injected and produced water if compared with the clean water flooding and in some increase of sweep efficiency while causing the total production rate reduction;
- The negative effect of the total rate reduction is compensated by the positive effect of water cut reduction for lateral flood of a two-permeability-zone reservoir where the induced skin does not affect the oil production history;
- The induced skin causes some reduction in oil production rate for bottom-up flooding;
- The incremental recovery factor is higher for lower viscosity oils. Yet, the ratio between the incremental recovery factor and the recovery factor after 1 PVI increases with increasing oil viscosity;
- The feasibility of poor quality water flooding is a subject to detailed economic analysis.

CHAPTER 3: SWEEP INCREASE DUE TO INDUCED FINES MIGRATION AND FORMATION DAMAGE:

3.1 LITERATURE REVIEW:

3.1.1 FINES MIGRATION THEORY:

Formation damage can also be observed from the mobilization of formation fines during low salinity water injection. It has been recognized that the mobilization of small solid particles, present in the pore spaces of all sandstone reservoirs and not held in place by the natural cementations during deposition, can contribute to severe formation damage (Muecke 1979). Various researches have focused on investigating the effectiveness of low salinity waterflooding, which is presently considered as a very prospective EOR method. These investigations studied on the effects of water salinity on wettability, relative permeability, capillary pressure and residual oil saturation (Tang & Morrow 1999; Jerauld et al. 2008; Rivet et al. 2010; Takahashi & Kovscek 2010). These effects appear to be separate phenomena from the movement of fines but may occur simultaneously with fines migration. Some low salinity core flood studies have reported the release of significant amounts of fines (Bernard 1967; Tang & Morrow 1999; Pu et al. 2010), while others have reported no evidence of fines migration (Yildiz & Morrow 1996; Jerauld et al. 2008; Lager et al. 2008; Rivet et al. 2010) but with additional oil recovery. This work only considers the effects of fines migration to provide mobility control and does not consider changes to the residual oil saturation or relative permeability curves as a result of injecting low salinity water.

Classical filtration theory describes particle detachment with consequent migration and pore plugging for single phase flow. The kinetic relationships for particle detachment have been proposed by Shapiro & Stenby (2000 & 2002); Tufenkj (2007); Yuan & Shapiro (2010). Particle retention, represented by the filtration coefficient, is described by a rigorous theory that considers interactions between particle-to-grain and particle-to-particle within the formation rock (Nabzar et al. 1996; Tufenkji & Elimelech 2004; Chauveteau et al. 1998; Bedrikovetsky et al. 2010). The empirical detachment coefficient can be determined from extensive experimental data (Ju et al. 2007; Tufenkji 2007). Another limitation of this model is that the retention concentration and

permeability would eventually reach the asymptotical stabilization when time tends to infinity (Bedrikovetsky et al. 2010). It exhibits a delayed response to an abrupt change in fluid velocity or composition, which does not agree with the near instantaneous response seen in laboratory experiments (Miranda & Underdown 1993; Ochi & Vernoux 1998; Khilar & Fogler 1998). The mechanical equilibrium of a particle was not taken into account in the classical filtration model (Li et al. 2006; Yuan & Shapiro 2010).

The modified particle detachment model uses the maximum (critical) retention function instead of a kinetics expression to describe the rate of particle detachment. In this model, particle capture continues according to classical deep bed filtration theory until the concentration of retained particles reaches a maximum determined by the static equilibrium of forces acting on a particle. Changes to fluid velocity or composition may abruptly reduce the maximum retained concentration below the current retained concentration causing the instantaneous release of particles. To simplify the model, all particles are assumed to be spheres of equal radii and the same material. (Bedrikovetsky et al. 2010)

The main forces considered to act on a particle on the surface of a pore or internal particle cake are drag, lift, gravity and a total electrostatic force Figure 23.

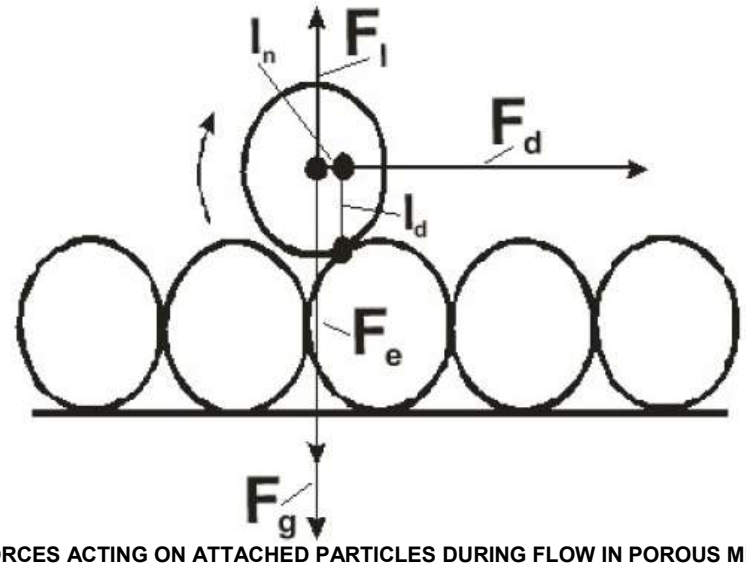

FIGURE 23: FORCES ACTING ON ATTACHED PARTICLES DURING FLOW IN POROUS MEDIA (TORQUE BALANCE ON A SINGLE PARTICLE) (BEDRIKOVETSKY ET AL. 2010)

Drag and lift are caused by the flow of fluid over a particle and act to detach the particle from the pore wall. Both forces increase with increasing flow velocity, particle radius and the fluid viscosity. The gravity force is the buoyant weight of the particle. For small particles of low to moderate density the gravity force is insignificant compared to the magnitude of the other forces, hence it can often be ignored. The total electrostatic force describes the interaction of a particle and pore wall at very small separations and is independent of fluid velocity. For the purposes of this model, the total electrostatic force is taken as the maximum value of the sum of the van der Waals, electrical double layer and Born forces as described by Derjaguin, Landau, Verwey and Overbeek (DLVO) theory (Bedrikovetsky et al. 2010). The Van Der Waals force depends primarily on the Hamaker constant and is largely independent of changes to water composition. However, the electrical double layer force does depend on water composition, specifically ionic strength and pH (Hunter 2001). Hence it is via the electrical double layer force that changes to salinity and pH affect the force balance and maximum retention concentration. Typically for clastic reservoir rocks, the total attractive electrostatic force decreases as the water salinity decreases. The dependency on pH is usually more complicated. A limitation of this modeling approach is that, to be accurate, it must consider all significant forces acting on a particle. The above forces are considered to be the most significant though others exist, for example, adhesion forces for full two phase flow and non-DLVO surface forces (Khilar & Fogler 1998; Takahashi & Kovscek 2010).

The static equilibrium of a particle is determined by the balance of torques from the main forces (Rahman et al. 1994; Civan 2007; Freitas & Sharma 2001). The dimensionless erosion number is introduced as the ratio between the detaching and attaching torques:

$$\varepsilon = \frac{F_d l_d + F_f l_n}{(F_e + F_s) l_n} \tag{15}$$

Where: F_d, F_l, F_e and F_s are drag, lifting, electrostatic and gravity forces, respectively; l_d and l_n are the corresponding levers for the drag and normal forces.

A particle is released if the erosion number exceeds unity. This may occur due to an increase in the drag and lift forces, because of an increase in flow velocity, or a decrease in the electrostatic force, because of a decrease in the water salinity or other change in water composition. The maximum concentration of retained particles is a function of the erosion number for any porous media (Bedrikovetsky et al. 2010).

$$\sigma = \sigma_{cr(\varepsilon)} \tag{16}$$

Where: σ: concentration of retained particles; σ_{cr}: maximum concentration of retained particles.

The derivation of equation for an average cylindrical capillary of the porous medium is presented in Appendix F.

Following Pang & Sharma (1994), Bachman et al. (2003) and Mojarad & Settari (2007), it is assumed that the inverse to normalized permeability $k_{(\sigma)}/k_0$ is a linear function of the retained particle concentration:

$$\frac{k_0}{k(\sigma)} = 1 + \beta\sigma = R_a$$

$$Where: \quad k_0 : reservoir\ initial\ permeability; \tag{17}$$

$$k_{(\sigma)} : reservoir\ permeability\ with\ (\sigma)\ retained\ particle\ concentration.$$

The formation damage coefficient for straining is assumed to be much greater than that for attachment, i.e. the detachment of fines causes a negligibly small permeability increase while the plugging of pore throat results in a significant decrease of permeability due to straining of detached particles (Figure 24).

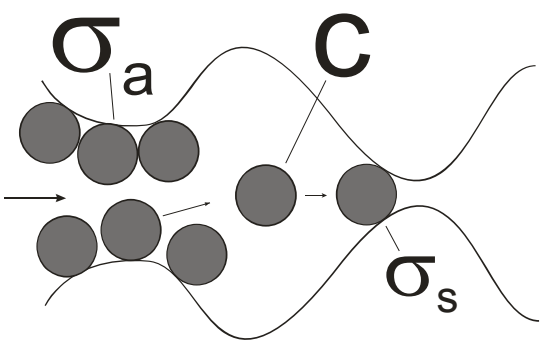

FIGURE 24: STRAINING OF DETACHED PARTICLES IN A SINGLE PORE (BEDRIKOVETSKY ET AL. 2010).

The ratio of ($k_{(\sigma)}/k_0$) also represents how much the reservoir permeability has been declining due to fines migration during low salinity injection. "σ" constant in equation (16) corresponds to the concentration of strained particles.

The model for fines release and permeability decline was compared to experimental coreflood data from the literature (Lever & Dawe 1984). In their work, coreflood experiment with a natural sandstone core sample was water flooded with decreasing salinity and its effect on the core"s permeability was recorded.

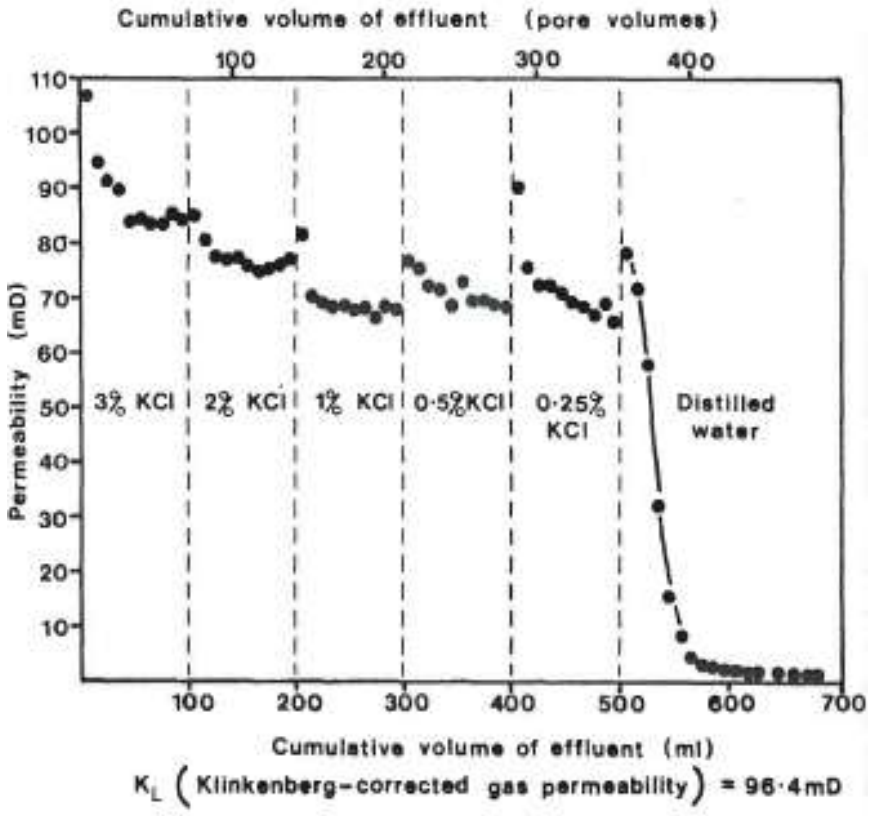

FIGURE 25: PERMEABILITY OF THE HOPEMAN SANDSTONE TO KCL BRINES (LEVER & DAWE, 1984).

It was observed that the core"s permeability decreases with declining water salinity. However when distilled water was flushed through the core, the permeability dropped drastically compared to the original permeability (Lever & Dawe 1984). As the concentration of strained particles is equal to the concentration of detached particles minus the concentration of particles produced at the core effluent, the curve of stabilized permeability versus salinity curve from Figure 25 could be recalculated into the maximum retention function by using equation (16) (shown in Figure 26).

NOTE:
This figure is included on page 54 of the print copy of the thesis held in the University of Adelaide Library.

FIGURE 26: DEPENDENCY OF RETAINED PARTICLE CONCENTRATION EROSION NUMBER (ZEINI ET AL. 2011)

The maximum retention function $\sigma_{cr}(\varepsilon)$ shows that the salinity required to release all mobile particles is greater than zero. This has significant practical implications as it demonstrates that only low, not zero, salinity may be required to release all attached particles. (Zeini et al. 2011)

3.1.2 *MECHANISM FOR IMPROVED SWEEP EFFICIENCY DUE TO FINES MIGRATION*

The above observations, that fines migration can cause permeability decline because of changes in water composition, are sufficient to warrant the consideration of the effects of induced fines migration on waterflooding performance. During waterflood, the rapid water breakthrough can be a significant problem, leading to high water cut at producing wells and lower volumetric sweep efficiency for a given volume of injected water. The problem is particularly pronounced for a mobility ratio significantly greater than unity or where the variation of permeability across the reservoir is significant.

Mobility control techniques, such as polymer flooding, may be employed to reduce a high mobility ratio by increasing the viscosity of the injected water or decreasing the effective permeability to water of the reservoir in the water

swept zone behind the flood front (Lake 1989). Such techniques decrease the fractional flow of water in the reservoir and hence decrease the water cut at the producing wells. The volumetric sweep efficiency for a given volume of injected water is also increased. Fines release, due to the alteration of the chemistry of the injected water, and the consequent decrease in permeability, may be able to provide mobility control and hence the ability to improve waterflood performance. Since the mobilization of fines by changing the chemistry of the injected water can only take place in the water-swept zone, only the effective permeability to water of the reservoir is reduced, reducing the mobility ratio. However, the main disadvantage of mobility control is that, for a given injection rate, the induced formation damage results in an increased injection pressure.

For a layered-cake reservoir in either a gravity-dominated situation or where reservoir permeability increases with depth, water propagates preferentially in the highly permeable zones, with slow displacement of the oil in low permeability zones. A further slowing of the displacement front in the low permeability zone occurs after water breakthrough in highly permeable zones and the creation of an injector/producer channel filled by high mobility water. Formation damage induced by mobilized fines in the swept zone tends to make the permeability distribution across the reservoir more uniform. Hence, the induced formation damage causes the breakthrough period increase and improved sweep efficiency for a given volume of injected water. (Zeini et al. 2011)

3.1.3 BASIC EQUATIONS FOR FINES MIGRATION UNDER 2-PHASE FLOW

The system of two-phase flow in porous media with varying water salinity that lifts the fine particles will be discussed in this study. For simplicity, we assume that volumetric concentrations of attached and retained particles are negligibly small if compared with porous space, i.e. the fine particles retention does not affect porosity. We also assume no diffusion and capillary pressure.

Finally, the system of governing equations for two-phase oil-water flow with fines mobilization due to decrease of water salinity and consequent reduction of relative permeability for water consists of equations for total incompressible flux of carrier water and oil, for volumetric balance of incompressible water, for

mass balance of suspended, attached and strained particles, for either attachment retention rate or the maximum attachment function, for size exclusion retention rate, for advective-diffusive mass transfer of salt in porous space with retained fines and for modified Darcy"s law accounting for permeability reduction due to fines straining:

$$\nabla\left(U\right)=0$$

$$\phi\frac{\partial s}{\partial t}+U\nabla f\left(s,\sigma_s\right)=0,\ f\left(s,\sigma_s\right)=\left[1+\frac{k_{ro}\left(s\right)\mu_w\left(1+\beta\sigma_s\right)}{k_{rw}\left(s\right)\mu_o}\right]^{-1}$$

$$\frac{\partial}{\partial t}\left[\phi sc+\sigma_a+\sigma_s\right]+U\nabla\left(cf\right)=0$$

$$\sigma_a=\sigma_a\left(\varepsilon,s\right),\ \varepsilon=\varepsilon\left(\gamma,U\middle/\phi-\sigma_a-\sigma_s\right)$$

$$\frac{\partial\sigma_s}{\partial t}=\lambda_s cU\frac{f}{\phi s},$$

$$\frac{\partial}{\partial t}\left[\phi\gamma\right]+\nabla\left(\gamma U\right)=0$$

$$U=-k\left[\frac{k_{rw}\left(s\right)}{\mu_w\left(1+\beta\sigma_s\right)}+\frac{k_{ro}\left(s\right)}{\mu_o}\right]\nabla p$$

Where: c: concentration of suspended particles (ppm); s: water saturation
γ: brine ionic strength (mol/L); f: fractional flow of water (18)

The important difference between particle release under one phase and two-phase flows is saturation dependency of the maximum retention function. It reflects the fine particles release from the rock surface wetted by water only.

Introduce dimensionless co-ordinates, time and concentrations

$$x_D=\frac{x}{L},t_D=\frac{1}{\left(\phi-\sigma_{a0}\right)}\int_0^t q\left(t\right)dt,S=\frac{\sigma}{\left(\phi-\sigma_{a0}\right)c^0},C=\frac{c}{c^0},U=\frac{q}{L^2},\varepsilon_D=\frac{\alpha_L}{L}=\frac{D}{LU},$$

$$P=\frac{kp}{U_0\mu L}=\frac{kpL}{q_0\mu},u=\frac{U}{U_0}$$

(19)

Where: x_D: dimensionless coordinate; S: dimensionless concentration of deposited particles
ε_D: inverse of Peclet number $(\text{dimensionless diffusion})$; P: dimensionless pressure
u: dimensionlessvelocity

Here the case of fully saturated attached fines system is considered. It occurs during injection of low salinity water into oilfield, where the attached fines with

maximum concentration are in contact with water with continuously decreasing salinity.

In dimensionless co-ordinates, the system becomes:

$$\nabla(u) = 0$$

$$\frac{\partial s}{\partial t_D} + u\nabla f(s, S_s) = 0,\ f(s, S_s) = \left[1 + \frac{k_{ro}(s)\,\mu_w\left(1 + \beta\phi c^0 S_s\right)}{k_{rw}(s)\,\mu_o}\right]^{-1}$$

$$\frac{\partial}{\partial t_D}\left[sC + S_a + S_s\right] + u\nabla(Cf) = 0$$

$$S_a = S_a(\varepsilon, s),\ \varepsilon = \varepsilon\left(\gamma, U/\phi\right)$$

$$\frac{\partial S_s}{\partial t_D} = (\lambda_s L) C |u| \frac{f}{s},$$

$$\frac{\partial(\gamma s)}{\partial t_D} + u\nabla(\gamma f) = 0$$

$$U = -k\left[\frac{k_{rw}(s)}{\mu_w\left(1 + \beta\phi c^0 S_s\right)} + \frac{k_{ro}(s)}{\mu_o}\right]\nabla p$$

Where: S_a : dimensionlessconcentration of attached particles (20)

S_s : dimensionless concentrationof strained particles

(Zeini et al. 2011)

3.1.4 LARGE SCALE APPROXIMATION

Consider the large scale case, where the free run of fine particle before being captured is significantly smaller than the reservoir size, i.e. the dimensionless filtration coefficient for straining

$$\lambda_s L >> 1 \tag{21}$$

Tending $\lambda_s L$ to infinity in left hand side of the third eq. (6) under limited retention rate and flow velocity results in dimensionless suspended concentration tending to zero, C<<1. Ignoring C in third eq (6) leads to

$$S_s = S_{a0} - S_a(\varepsilon, s) \tag{22}$$

Eq. (8) means that in large scale approximation, the lifted fines are immediately captured by size exclusion in porous media.

System (6) becomes

$$\begin{aligned}
&\nabla(u) = 0, \qquad S_s = S_{a0} - S_a(\varepsilon, s), \\
&\frac{\partial s}{\partial t_D} + u\nabla f\left(s, S_{a0} - S_a(\varepsilon, s)\right) = 0,\ f\left(s, S_{a0} - S_a(\varepsilon, s)\right) = \left[1 + \frac{k_{ro}(s)\,\mu_w\left(1 + \beta\phi c^0\left(S_{a0} - S_a(\varepsilon, s)\right)\right)}{k_{rw}(s)\,\mu_o}\right]^{-1} \\
&S_a = S_a(\varepsilon, s),\ \varepsilon = \varepsilon\left(\gamma, U/\phi\right) \\
&\frac{\partial(\gamma s)}{\partial t_D} + u\nabla(\gamma f) = 0 \\
&U = -k\left[\frac{k_{rw}(s)}{\mu_w\left(1 + \beta\phi c^0\left(S_{a0} - S_a(\varepsilon, s)\right)\right)} + \frac{k_{ro}(s)}{\mu_o}\right]\nabla p
\end{aligned} \tag{23}$$

System (9) describes low salinity waterflooding with fines lifting, migration, capture and subsequent permeability damage. (Zeini et al. 2011)

3.1.5 OVERVIEW OF POLYMER FLOODING AND ITS MODELING IN ECLIPSE SIMULATOR:

Polymer flooding has been widely used as a mobility control enhanced oil recovery method, in which the flowing rates of both the injected (displacing) and displaced fluids through the reservoir are altered. The main aim of mobility control method is to improve the sweep efficiency during the displacement of oil by water. (Green & Willhite 1998)

The mobility of each fluid phase is determined using the following equation:

$$\lambda_i = \frac{k_i}{\mu_i}$$

$$Where: \ \lambda \ is \ the \ fluid \ mobility; \ i \ is \ the \ fluid \ phase \ (water, \ oil, \ etc.) \qquad (24)$$
$$\mu \ is \ the \ fluid \ viscosity$$

During the displacement process, the mobility ratio between the displacing and displaced fluids is:

$$M = \frac{\lambda_{Displacing}}{\lambda_{Displaced}} = \frac{\lambda_{Water}}{\lambda_{Oil}} \qquad (25)$$

$$Where: \ \text{M is the mobility ratio}$$

The mobility ratio is critical as it represents the areal and vertical sweep of the displacement process. It is preferable when the mobility ratio is less than 1 as it shows that the mobility of displacing fluid is less than that of the displaced fluid (Green & Willhite 1998). For instance during the displacement of oil by injected water, less mobile water means more gradual displacement front (piston-like displacement). More mobile oil means that the oil always travels in front of the less mobile water; thus, prevent the early water breakthrough and improve the sweep efficiency.

During polymer flooding, a certain concentration of high molecular weight polymer is mixed with injected water to increase the water viscosity significantly (Green & Willhite 1998). Based on the mobility equation (25), the higher is the fluid viscosity the lower is the fluid mobility. This helps to slow down the water movement through the reservoir and improve the sweep efficiency.

When the polymer solution is injected into the reservoir, some of the polymer is absorbed into the rock surface, which contributes to the loss of polymer during the injection process. The relative permeability of the polymer solution is further declined due to the polymer adsorption. In Eclipse simulator, it has been assumed that the permeability decline is proportional to the amount of adsorbed polymer. (Schlumberger 2007)

In order to determine the rock permeability decline, Eclipse requires specifications of the residual resistance factor for a particular rock type. The water permeability damage in Eclipse modeling is determined as:

$$\frac{k_0}{k} = R_k = 1 + (RRF - 1)\frac{C_a}{C_{a,\max}} \tag{26}$$

Where: k_0: water initial permeability; k: polymer solution permeability; RRF: residual resistance factor of the formation rock; C_a: adsorbed polymer concentration; $C_{a,max}$: maximum adsorbed polymer concentration.

(Schlumberger 2007)

As the polymer adsorbed concentration reaches the maximum concentration, the rock permeability decline will be equal to the residual resistance factor:

$$\begin{aligned} &\frac{C_a}{C_{a-\max}} = 1 \quad \rightarrow R_k = 1 + RRF - 1 \\ &\rightarrow R_k = RRF \end{aligned} \tag{27}$$

3.2 COUPLED SIMULATION OF INDUCED DAMAGE FROM FINES MIGRATION AND RESERVOIR MODELS:

Alteration of water salinity affects the attached concentration stronger than the velocity alteration. Therefore, we neglect the velocity dependency of the maximum concentration of attached fines. It is also assumed that the maximum retention concentration is independent of water saturation.

Introduce small adsorption $c_a(\gamma)$ into equation (28):

$$\nabla(u)=0, \qquad S_s = S_{a0} - S_a(\gamma),$$

$$\frac{\partial s}{\partial t_D} + u\nabla f\left(s, S_{a0} - S_a(\gamma)\right) = 0,\ f\left(s, S_{a0} - S_a(\gamma)\right) = \left[1 + \frac{k_{ro}(s)\mu_w\left(1+\beta\phi c^0\left(S_{a0} - S_a(\gamma)\right)\right)}{k_{rw}(s)\mu_o}\right]^{-1}$$

$$S_a = S_a(\gamma)$$

$$\frac{\partial\left(\gamma s + \delta c_a(\gamma)\right)}{\partial t_D} + u\nabla(\gamma f) = 0, c_a(\gamma) = S_{a0} - S_a(\gamma) \tag{28}$$

$$U = -k\left[\frac{k_{rw}(s)}{\mu_w\left(1+(RRF-1)\dfrac{S_{a0}-S_a(\gamma)}{S_{a0}}\right)} + \frac{k_{ro}(s)}{\mu_o}\right]\nabla p$$

Here δ is small parameter. The resistance factor is presented as

$$1+(RRF-1)\frac{S_{a0}-S_a(\gamma)}{S_{a0}} \tag{29}$$

leading to the following expression for the maximum resistance factor RRF:

$$RRF = 1+\beta S_{ao} \tag{30}$$

Finally, the system of equations for 2-phase flow with varying water salinity and fines mobilisation can be “translated” into the polymer flooding model with the formulae (29) and (30).

3.3 SIMULATION MODELS AND RESERVOIR DESCRIPTIONS:

The options of waterflood with normal, low salinity waterflooding and polymer flooding are simulated to compare their effect on the recovery factor. In order to test the robustness of low salinity water injection in against different heterogeneity degree, two simulation models of a simple 5-layered-cake reservoir (Figure 27) and of a highly heterogeneous reservoir SPE9 (Figure 28) are investigated. The permeability profile for 5-layer-cake reservoir is chosen in the way that the recovery factor with normal waterflooding is almost the same as that for reservoir model SPE9.

The inverted 5-spot well pattern is utilized in both cases, in which there are four producers at the corners and one injector at the center of the reservoir. The reservoir design parameters are summarized in Table 7.

TABLE 7: PARAMETERS USED FOR 5-LAYERED-CAKE RESERVOIR

Parameters of the geological model	Value used Two Zone Study
Node numbers	10 x 10 x 5
The length of the reservoir (m)	350
The width of the reservoir (m)	350
The thickness of the reservoir (m)	90
The length of wells (m)	86
Initial Reservoir Pressure (Psi)	3000
Viscosity of Water (cP)	1
Viscosity of Oil (cP)	9
Initial Oil Saturation	0.75
Initial Porosity	0.12
Initial Horizontal Permeability (mD)	5, 10, 20, 30 & 150
Initial Vertical Permeability (mD)	2

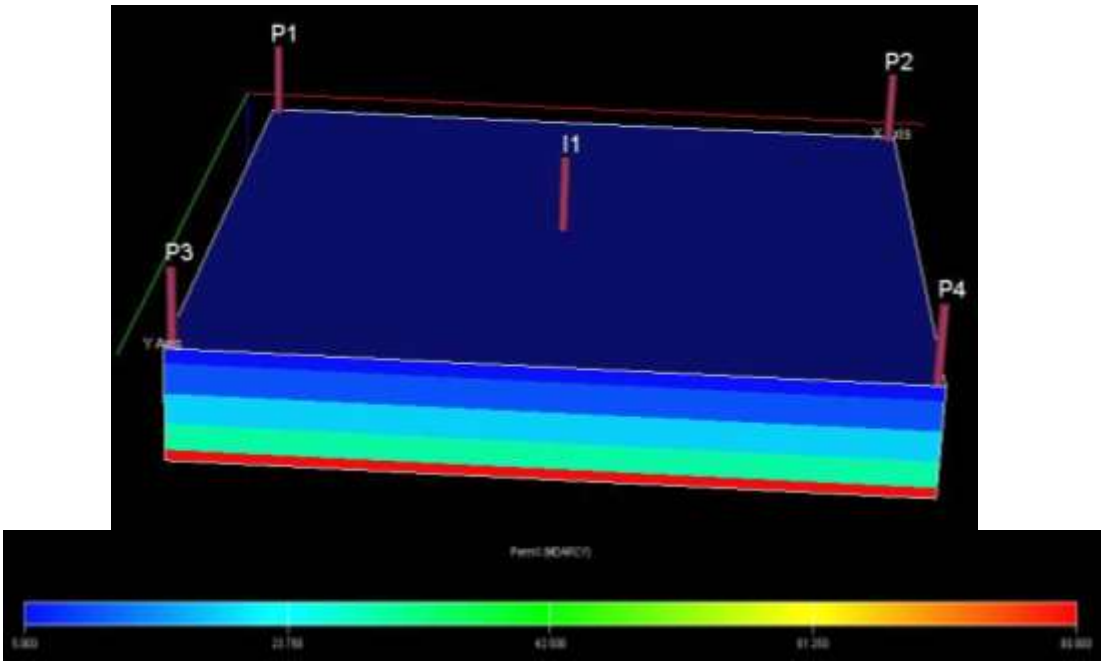

FIGURE 27: PERMEABILITY PROFILE FOR 5-LAYER-CAKE RESERVOIR

The SPE9 reservoir was created in the ninth SPE comparative solution project (Killough, 1995) with the heterogeneity degree provided by a geostatistically-based permeability field, which makes it more realistic to demonstrate a real-field application. However due to the large dimensions of the original reservoir, a crop out section of SPE9 is used with all the original heterogeneity and properties intact. The dimensions of the reservoir are the same to that of the 5-layered-cake reservoir.

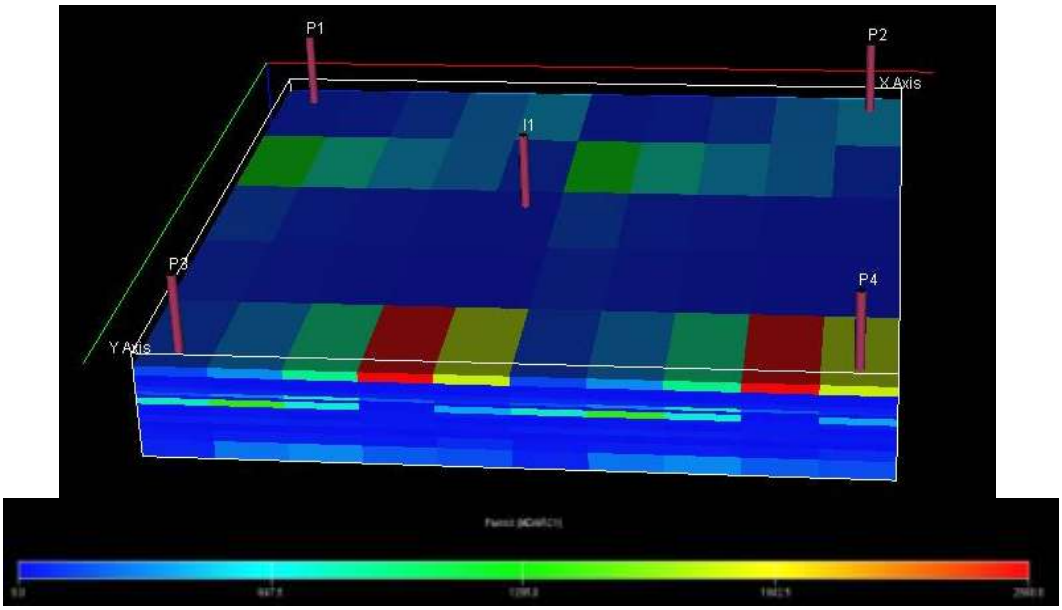

FIGURE 28: PERMEABILITY PROFILE FOR HIGHLY HETEROGENEOUS SPE9 RESERVOIR

3.4 WATERFLOODING AND POLYMER INJECTION SCHEME:

The polymer injection scheme is designed based on the injection scheme implemented in Daqing oilfield in China (Wang et al. 2008). The polymer-solution oil viscosity is a critical parameter in polymer injection as the more viscous the injected solution, the more effective the polymer flooding. The polymer used in this case was partically hydrolyzed polyacrylamide polymer (HPAM) with the viscosity properties as follow.

NOTE:
This figure is included on page 64 of the print copy of the thesis held in the University of Adelaide Library.

FIGURE 29: VISCOSITY VS POLYMER CONCENTRATION (GAO & SU, 2004)

The injection schedule implemented is:

- Stage 1: Initial Polymer Solution (concentration of 1000 mg/L) is injected for a limited period.
- Stage 2: Reducing the polymer concentration to 700 ppm and then 400 ppm.
- Stage 3: After sufficient polymer has been injected, the polymer slug is displaced through the reservoir by injecting water (chase water).

The injection is controlled on injection rate so that comparisons can be made of the displacement efficiency of each enhanced recovery method on the same volume of injected water. However since the addition of polymer increases the injected solution"s viscosity by 20-40 times, this will hence require a higher injection pressure to achieve the same rate as that of waterflooding. Thus, the injection rate during polymer flooding is designed so that the injector"s bottom-hole pressure does not exceed the fracturing pressure of the reservoir.

The “normal” and “low salinity” waterflooding will then be designed at the same injection rate.

3.5 RESULTS

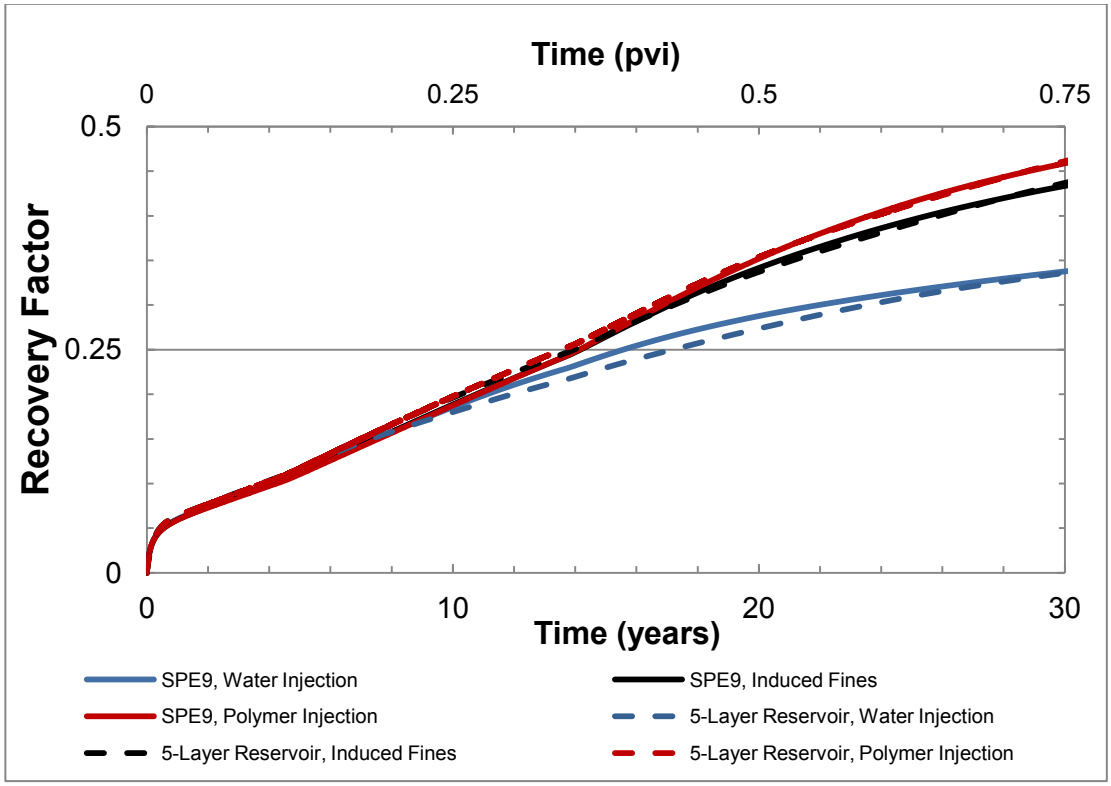

FIGURE 30: RECOVERY FACTOR (OF "CLEAN" WATER INJECTION, POLYMER AND LOW SALINITY WATER INJECTION) VS REAL TIME (YRS) OF "NORMAL" AND OF "LOW SALINITY" WATER

Solid and dashed curves correspond to SPE9 and 5-layer-cake reservoir, respectively.

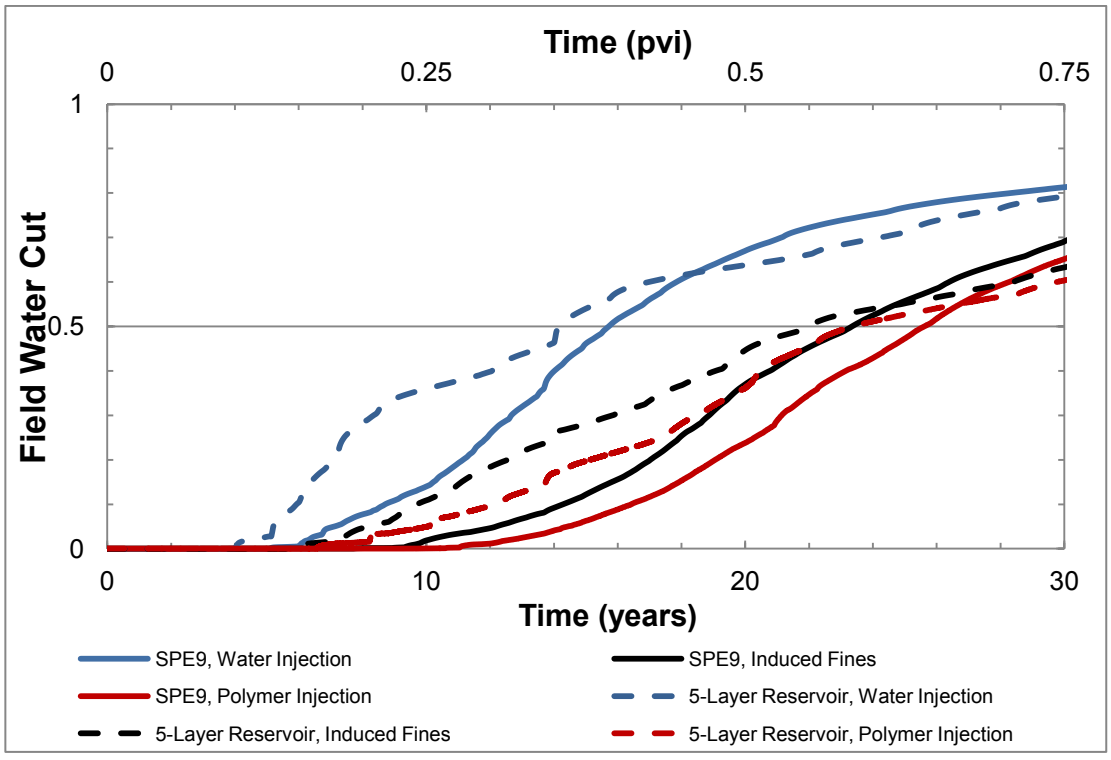

FIGURE 31: WATER CUT (OF "CLEAN" WATER INJECTION, POLYMER AND LOW SALINITY WATER INJECTION) VS REAL TIME

Solid and dashed curves correspond to SPE9 and 5-layer-cake reservoir, respectively.

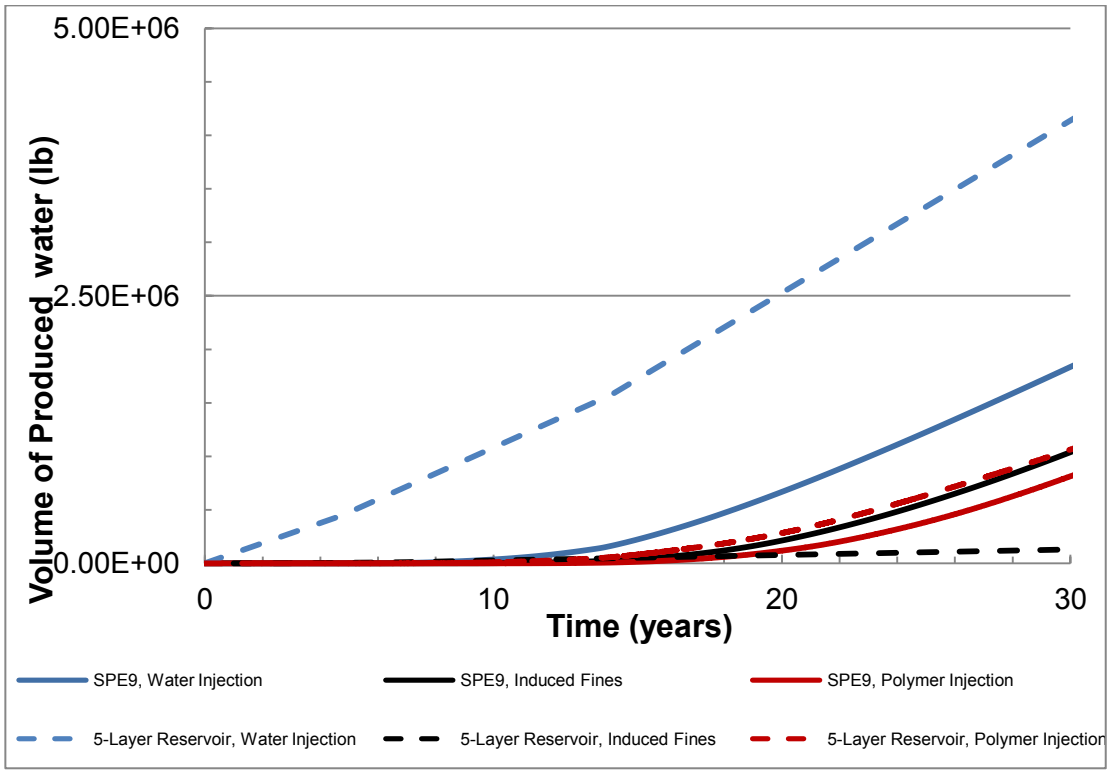

FIGURE 32: WATER PRODUCED VOLUME (OF "CLEAN" WATER INJECTION, POLYMER AND LOW SALINITY WATER INJECTION) VS REAL TIME

Solid and dashed curves correspond to SPE9 and 5-layer-cake reservoir, respectively.

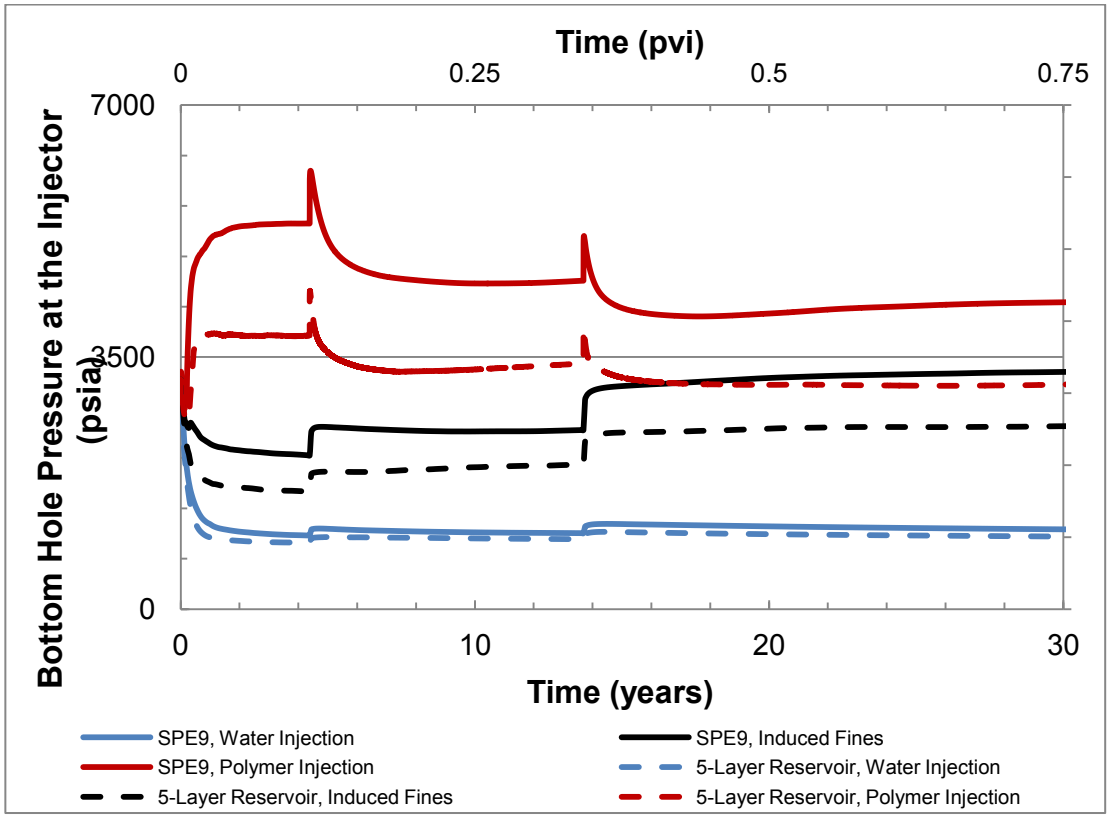

FIGURE 33: INJECTION PRESSURE (OF "CLEAN" WATER INJECTION, POLYMER AND LOW SALINITY WATER INJECTION) VS REAL TIME

Solid and dashed curves correspond to SPE9 and 5-layer-cake reservoir, respectively.

3.6 DISCUSSION

Implementing low salinity waterflooding with fines mobilization into reservoir simulator shows that the main effects of induced fines migration on waterflooding with monitored injection rate between the injectors and producers are:

- Significant increase in recovery factor compared to normal waterflooding
- Significant reduction in watercut compared to normal waterflooding

Three options of waterflood with low salinity, normal water and polymer flooding have been simulated for a 5-layer-cake reservoir and a heterogeneous reservoir model SPE9. Figure 27 and Figure 28 present 3D image of the 5-spot pattern for 5-layer-cake and SPE9 reservoirs studied in this work. The permeability profile for 5-layer-cake reservoir is selected in a way that the recovery with normal waterflooding is almost the same as that for reservoir model SPE9 to aid in the investigation of the effect of heterogeneity profile on the performance of low salinity waterflooding. The polymer resistance factor is chosen to have almost the same permeability damage as that for fines migration and straining.

The recovery factors for three flooding options are obtained for both reservoirs, which are plotted in Figure 30 and the results are as following:

TABLE 8: RECOVERY FACTORS VS REAL TIME FOR NORMAL WATERFLOOD, LOW SALINITY WATERFLOOD AND POLYMER FLOOD AFTER 30 YEARS

Cases	Recovery Factor (RF) after 30 years	Incremental Recovery Factor
SPE9		
- Normal Waterflood	33.77%	-
- Low Salinity Waterflood	43.53%	9.76%
- Polymer Flooding	45.87%	12.1%
5-Layer Cake Reservoir		
- Normal Waterflood	33.59%	-
- Low Salinity Waterflood	43.94%	10.35%
- Polymer Flooding	46.13%	12.54%

In both reservoirs, low salinity water injection and polymer flooding deliver significantly higher increase in recovery factor compared to that of the normal

waterflooding case (Table 8). Even though polymer flooding has the highest incremental recovery increase, it requires much higher injection pressure due to the highly viscous injected solution compared to the required injection pressure in normal waterflood and low salinity waterflood (as illustrated in Figure 33). For low salinity waterflooding, the injection pressure, at any stages during the injection, is around 2.25 times less than that required for polymer flooding while still delivering a significant incremental recovery increase. Polymer flooding is also a more expensive option compared to low salinity waterflooding due to the polymer acquiring cost and operational costs.

As shown in Figure 31, the water breakthrough time is delayed by 3 years and by 5 years for low salinity waterflood and polymer flooding respectively compared to that of the normal waterflood. In polymer flooding, the high viscosity of the polymer solution would reduce the water phase"s mobility considerable, ensuring that the water travels slower than the displaced oil to prevent the formation of water fingering. Whilst, in low salinity waterflooding, the induced formation leads to the reduction in water"s effective permeability in the water-swept zone and helps to slow down the advancing water finger. For SPE9 reservoir, the water breakthrough for normal waterflood occurs after 6 years comparing to that after 9 and 11 years for low salinity waterflooding and polymer flooding, respectively. This is a good indication that the injected water front travels at a slower velocity than the displaced oil and thus, allows it to sweep more oil from the reservoir. Consequently, the volumes of produced water in low salinity waterflood and polymer flood are also considerably less than that in normal waterflood as illustrated in Figure 32 as they remain longer in the reservoir to sweep a more extensive area. The polymer desorption effect is neglected in this case to obtain the optimum performance of polymer flooding to compare to the effects of low salinity water injection.

The results of this investigation show that the induced fines migration from low salinity waterflooding can accelerate the production of oil. However, the total volume of technically recoverable oil remains unchanged because the model did not consider other effects resulting from the injection of low salinity water, including the alteration of relative permeability, wettability and capillary pressure. For example, the injection of low salinity water can decrease the residual oil

saturation, resulting in a higher total oil recovery than for a normal waterflood (Bernard 1967; Tang & Morrow 1999; Rivet et al. 2010; Takahashi & Kovscek 2010), presently considered the main benefit of low salinity waterflooding. Hence the results of this analysis, obtained under the assumption of constant residual oil saturation, may underestimate the total benefit of low salinity waterflooding. To get a more complete understanding, the combined effects would have to be captured by the same model.

Finally, for a same amount of injected water, the main advantage of low salinity waterflooding is the significant increase in incremental recovery factor and significant decrease of produced water volume over time compared to the normal water flooding. In comparison to polymer flooding, even though the performance of low salinity waterflood is slightly less effective, low salinity waterflood is cheaper as it requires lower injection pressure and less acquiring cost it as it is more abundant. A detailed and comprehensive economic analysis would be necessary to verify this point but it is out of the scope of this study.

3.7 CONCLUSION:

- Since permeability decline with decreasing the salinity of the injected water is explained by simultaneous particle detachment and size exclusion, the mathematical model for fines migration contains equation for kinetics of particle straining and also the maximum retention function describing fine particles mobilization.
- Mathematical model for waterflooding using low salinity water to induce fines migration with subsequent permeability damage in large scale approximation is equivalent to that of polymer flooding without adsorption
- Introduction of vanishing adsorption allows using the polymer flood black oil simulator to model waterflood with induced fines migration.
- If compared with normal waterflooding, low salinity waterflooding with release and straining of fines results in improved sweep efficiency and reduction in produced and injected water. Yet, it also results in some decreasing of oil production rates.
- The higher is the layer-cake reservoir heterogeneity, the higher is the incremental oil recovery with induced fines migration.
- Injection of low salinity slug with saline water drive can be implemented as an improvement of the continuous fresh water injection. In this case, the unwept zone will remain almost undamaged, while delaying the water fingering and improve the sweep efficiency.
- The effect of induced fines is an increase of sweep efficiency. Therefore, the method is mostly effective in reservoirs with large scale heterogeneity. In particular, sweep increase in layer-cake reservoir exceeds that in the reservoir with SPE-9-type heterogeneity.

CHAPTER 4: SWEEP INCREASE DUE TO WATER ISOLATION DURING PRESSURE DEPLETION:

4.1 SIMULATION MODELS AND RESERVOIR DESCRIPTIONS

Permeability decline during low salinity water flooding (LSW) is a well known phenomenon, explained by fines mobilization, capture and consequent pore plugging. One of the main reasons for low gas recovery in gas fields with strong water support is the early water invasion, leading to the abandonment of production wells with high water cut.

So in a gas fields with strong aquifer support, it is proposed to take advantage of the induced formation damage from LSW in order to increase gas recovery by implementing short time injection fresh water into a watered-up abandoned gas well. This would result in a permeability decline around this well, i.e. exactly in the area, where the water finger propagates, leading to a delayed water breakthrough into gas producers and consequently, a lower water cut. Figure 34 illustrates the water invasion profile for normal depletion case and for the case with a limited low salinity water injection. The water finger profile us the same for both cases til time "t_1". However with the introduction of fresh water (low salinity water), at time "t_2", the water encroachment is delayed compared to the "normal depletion case. The invaded water would then be redirected around the low permeable block to displace more gas and prolong the effective life of the field considerably.

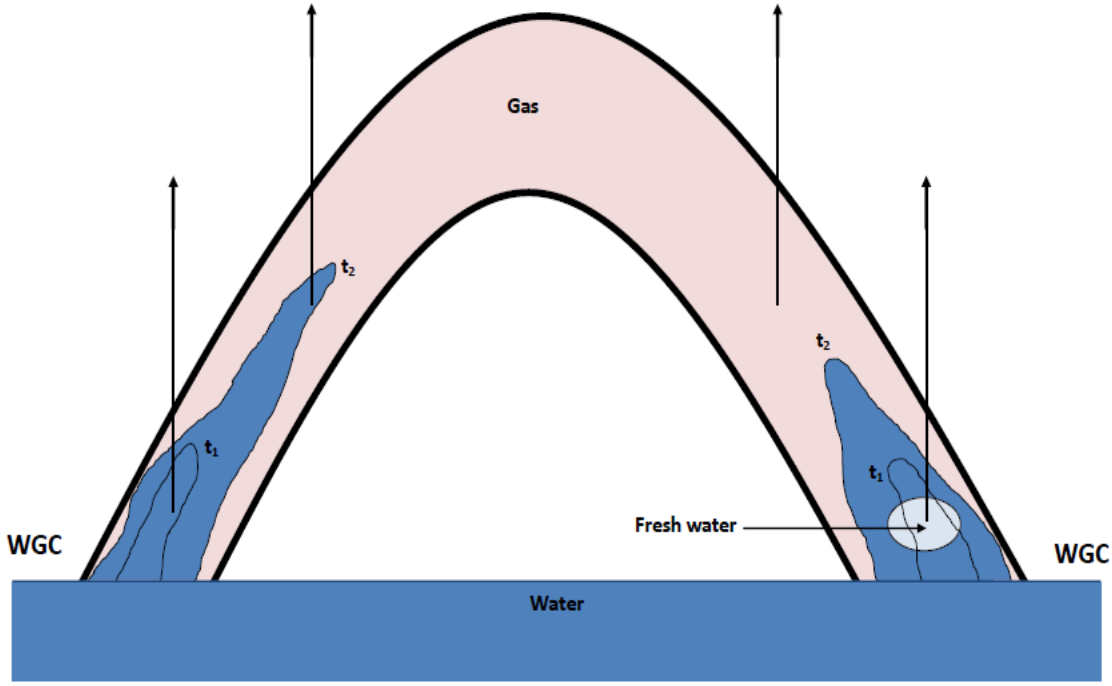

FIGURE 34: WATER INVASION PROFILE DURING NORMAL DEPLETION AND DURING LOW SALINITY WATERFLOODING

The reservoir heterogeneity is represented by a layered reservoir with permeability ranging from 50 mD to 1500 mD (shown in Figure 35). The design parameters for the reservoir models are included in Table 9.

TABLE 9: PARAMETERS USED FOR GAS RESERVOIR WITH A STRONG UNDERLYING AQUIFER

Parameters of the geological model	Value
Node numbers	50 x 50 x 20
RESERVOIR PROPERTIES	
– **The length of the reservoir (m)**	675
– **The width of the reservoir (m)**	500
– **The thickness of the reservoir (m)**	30.5
– **The length of wells (m)**	23
– **Initial Reservoir Pressure (Psi)**	4500
– **Viscosity of Water (cP)**	1
– **Initial Oil Saturation**	0.78
– **Initial Porosity**	0.2
– **Initial Horizontal Permeability (mD)**	50, 500, 1000 and 1500
– **Initial Vertical Permeability (mD)**	10
– **Injection Pressure (psi)**	5500
– **Distance between well (m)**	300
AQUIFER PROPERTIES	
– **The length of the aquifer(m)**	1270
– **The width of the aquifer (m)**	500
– **The thickness of the aquifer (m)**	30.5
– **Initial Aquifer Pressure (Psi)**	4500
– **Initial Permeability (mD)**	300

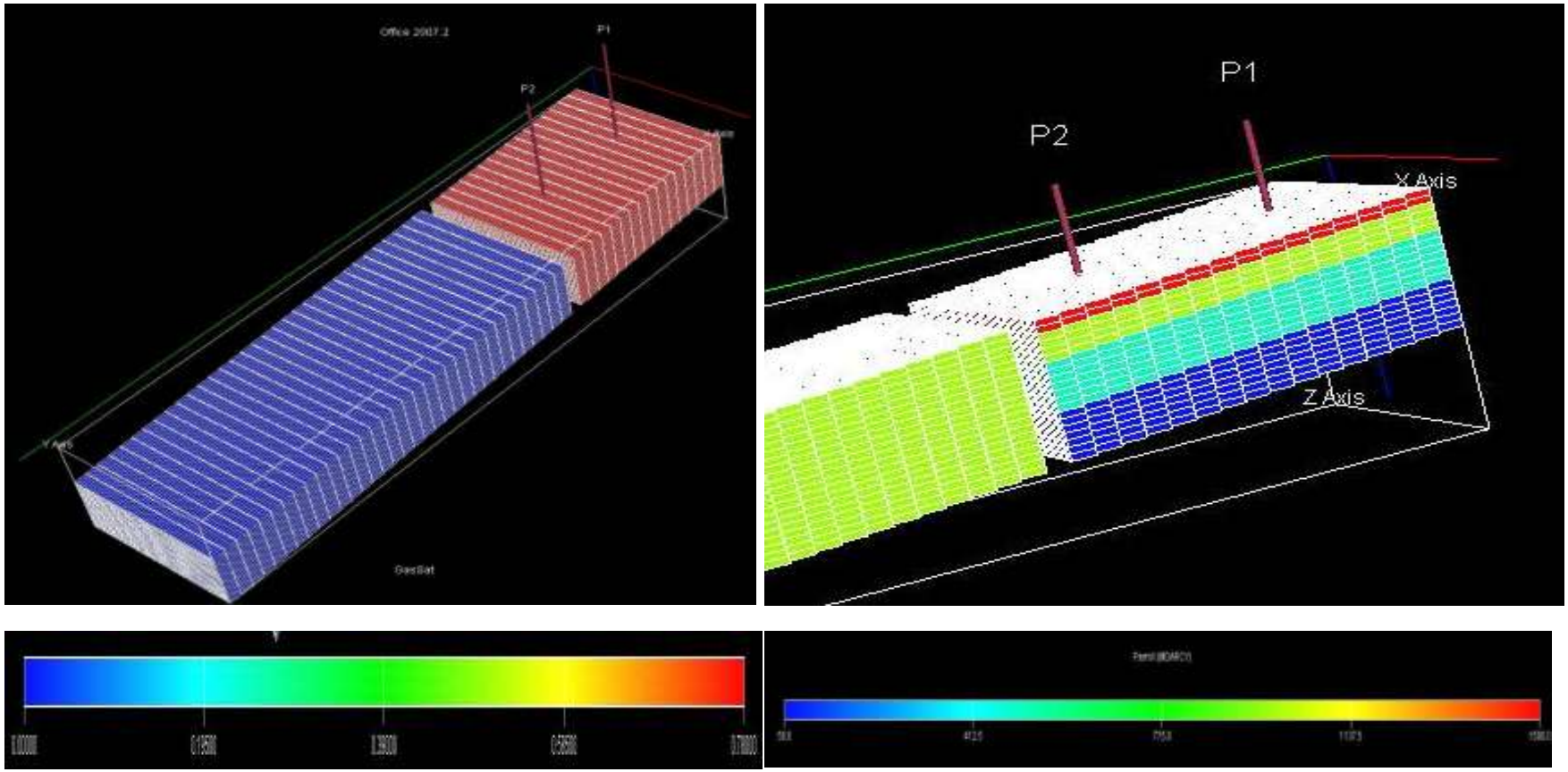

a) Gas Saturation b) Reservoir Permeability

FIGURE 35: 3D VISUALIZATION OF GAS RESERVOIR WITH UNDERLYING AQUIFER

As pressure drawdown occurs during the production, a low pressure area is formed around the producers, leading to the formation of water finger propagating to the producers. Consequently, this causes a low recovery factor by the time the well reaches its economical water cut limit (at 0.3). Hence, it is proposed that as the down-dip „P2" producer is watered out as seen in Figure 36, it would then be converted into an injector to inject low salinity water for a short period of time, which will mobilize formation fines and cause fines migration. Eventually, the formation fines would be captured causing permeability decline around the well. This creates an additional resistance to delay the aquifer encroachment towards the up-dip „P1" producer, allowing for additional gas production from the reservoir before reaching the watercut limit itself.

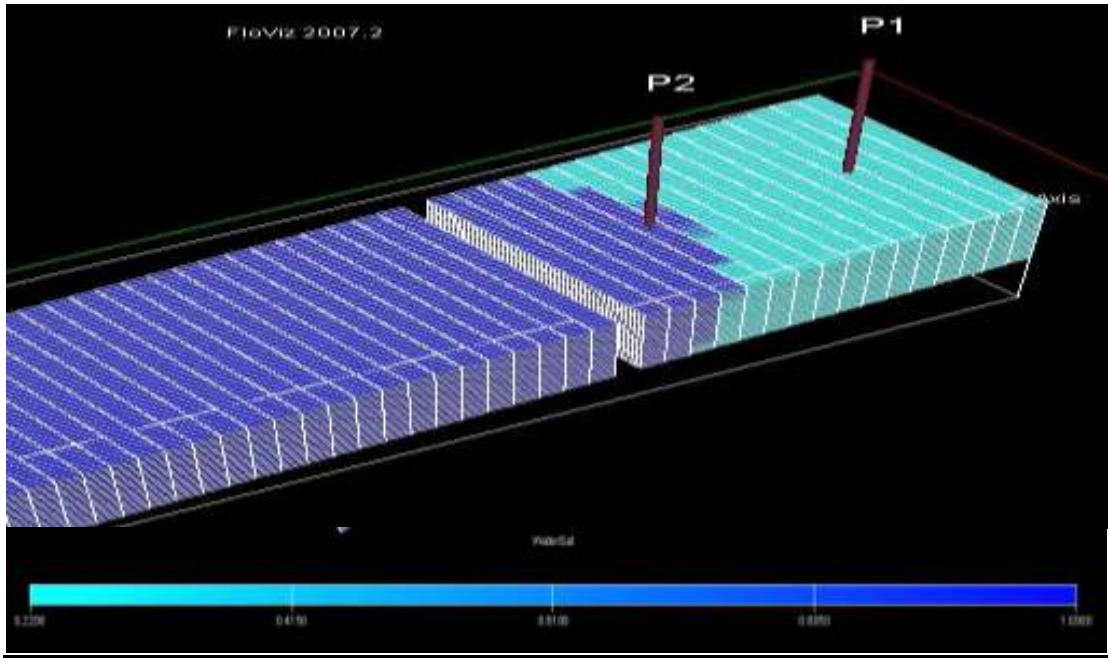

FIGURE 36: AQUIFER ENCROACHMENT TOWARDS THE PRODUCERS IN A DIPPING GAS RESERVOIR

In Australia, there are numbers of oil reservoirs being supported by strong aquifers, which poses a challenge on controlling the water encroachment in order to improve the sweep efficiency of the reservoir. Hence, a case study is also done on an oil reservoir with similar characteristics to test the robustness of this method in delaying water encroachment and hence improve the recovery factor of the reservoir. The economic water cut limit for oil reservoir is controlled to be at 0.9.

Sensitivity analysis investigates the impact of the injection period and the oil viscosity towards the overall incremental recovery with the injection period ranging from 2 days to 2 years and the oil viscosity from 1 cP to 100 cP.

4.2 RESULTS

4.2.1 GAS RESERVOIR

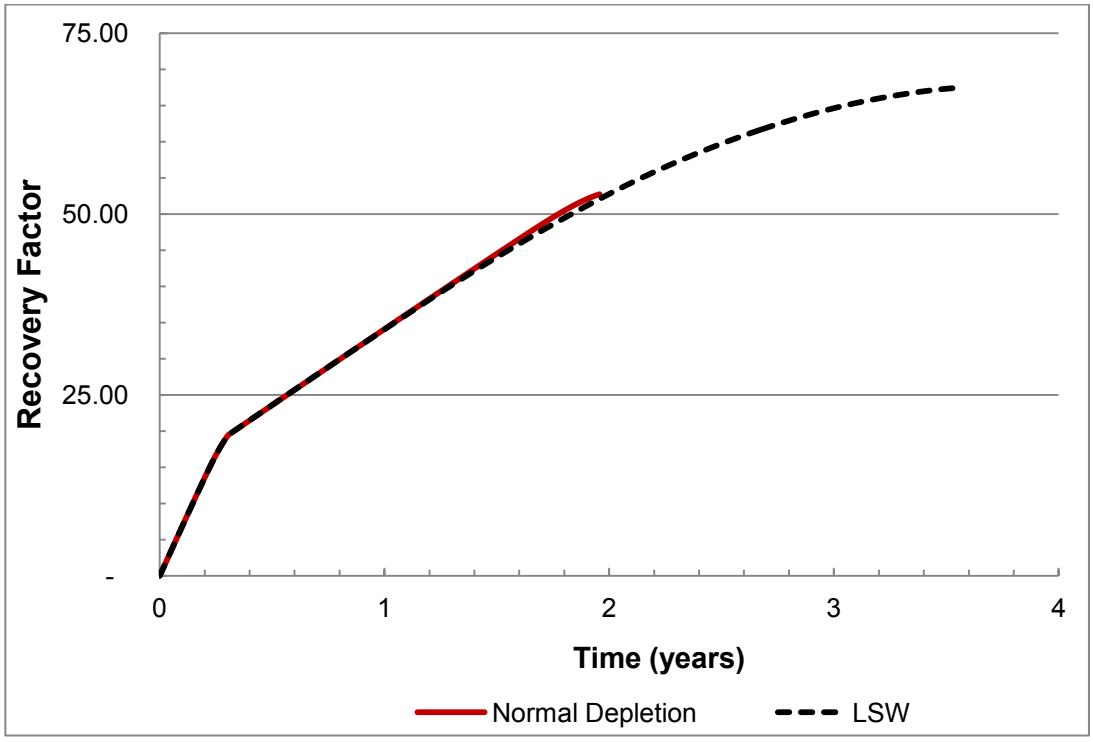

FIGURE 37: RECOVERY FACTOR, WITH NORMAL DEPLETION AND WITH INDUCED FINES MIGRATION, VS REAL TIME

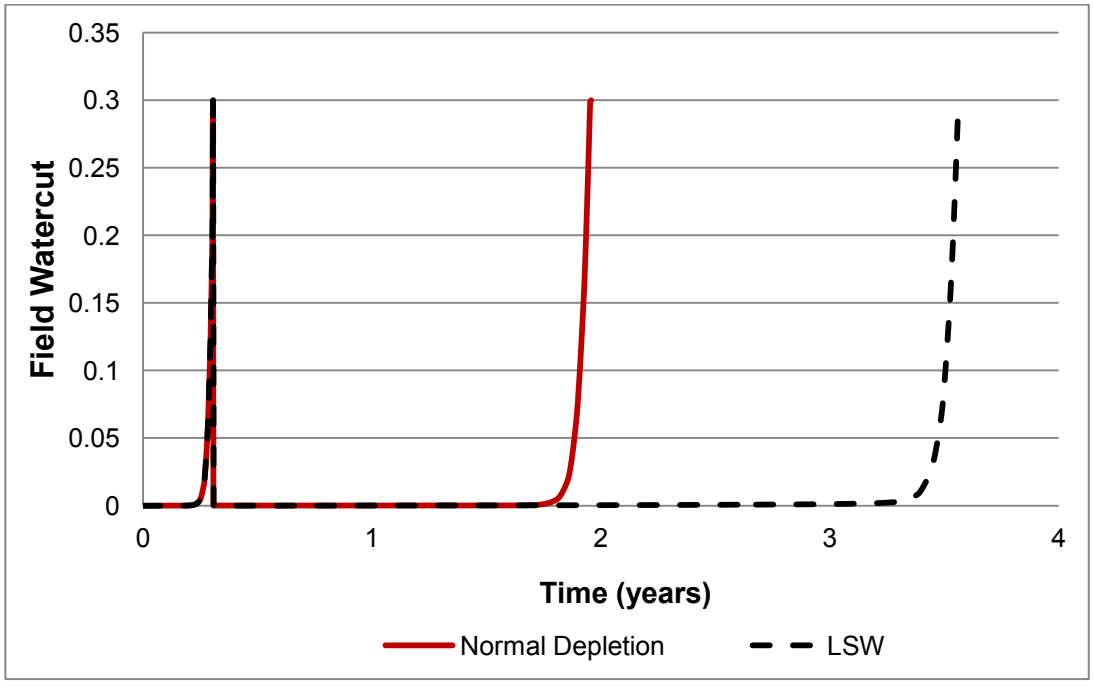

FIGURE 38: FIELD WATER CUT, WITH NORMAL DEPLETION AND WITH INDUCED FINES MIGRATION, VS TIME

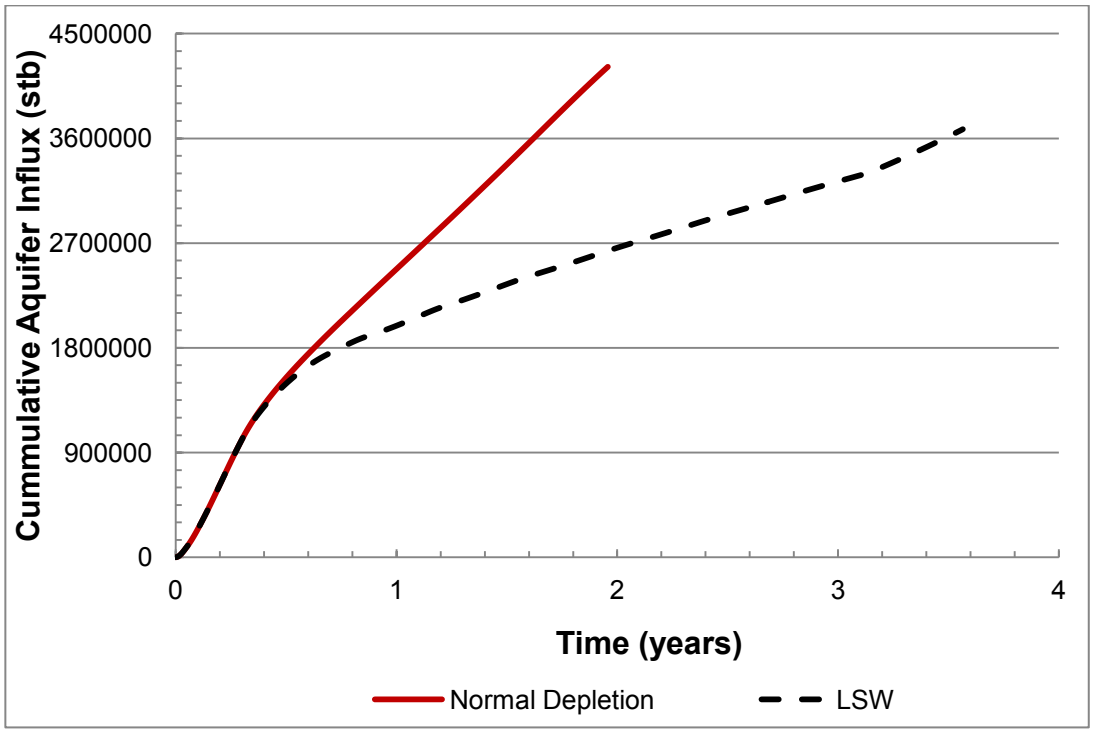

FIGURE 39: CUMMULATIVE AQUIFER INFLUX, WITH NORMAL DEPLETION AND WITH INDUCED FINES MIGRATION, VS TIME

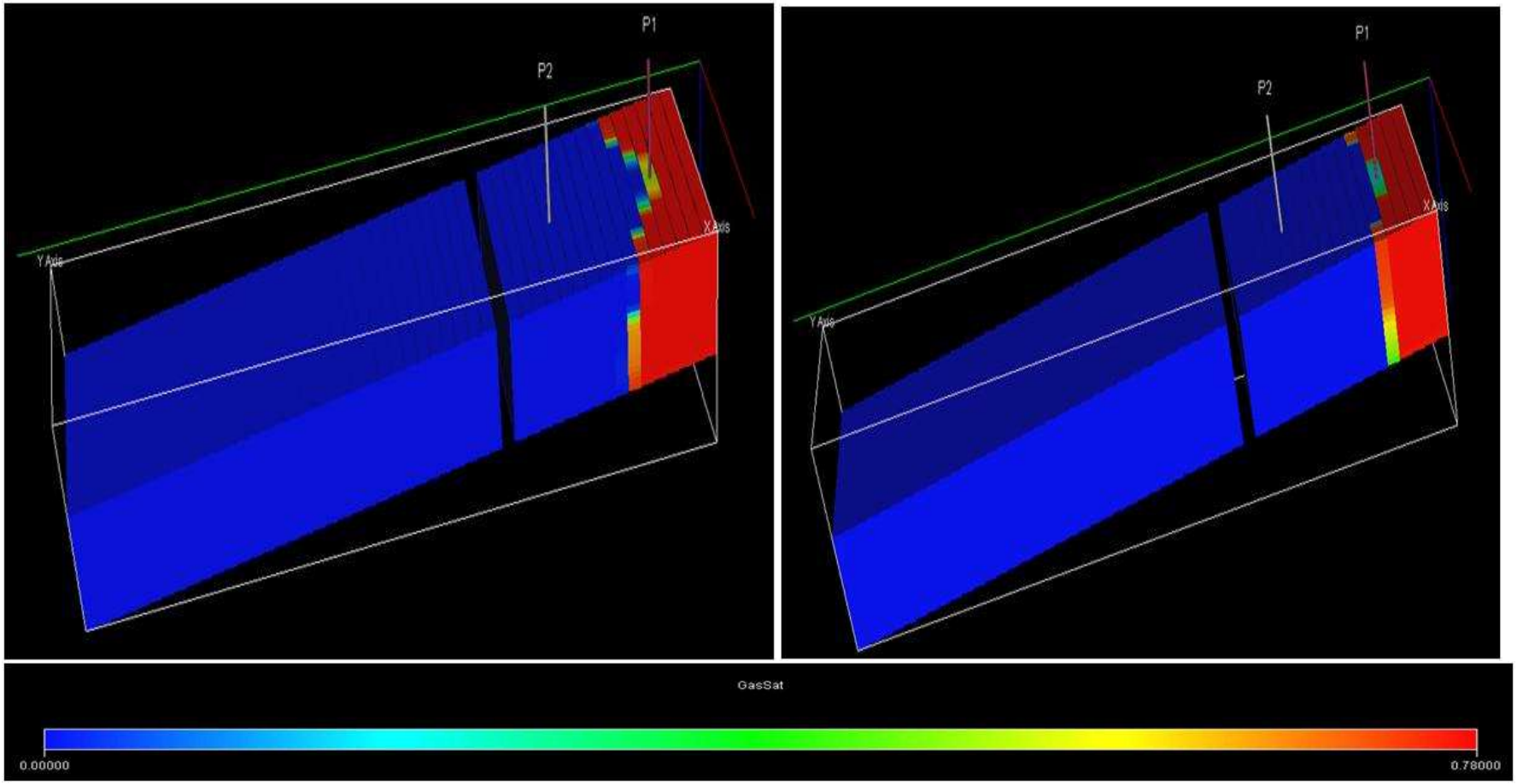

a) Normal Production b) With limited low salinity injection

FIGURE 40: RESIDUAL GAS AT ABANDONMENT FOR NORMAL DEPLETION AND WITH LIMITED LOW SALINITY INJECTION

4.2.2 OIL RESERVOIR

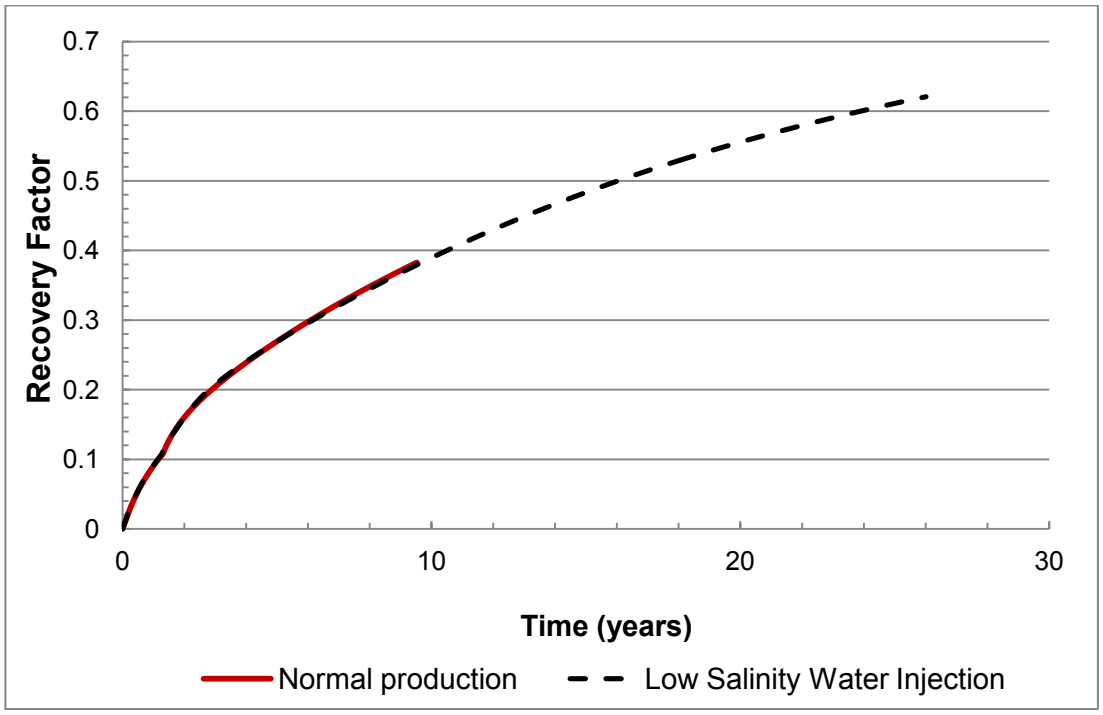

FIGURE 41: RECOVERY FACTOR, WITH NORMAL PRODUCTION AND WITH INDUCED FINES MIGRATION, VS REAL TIME

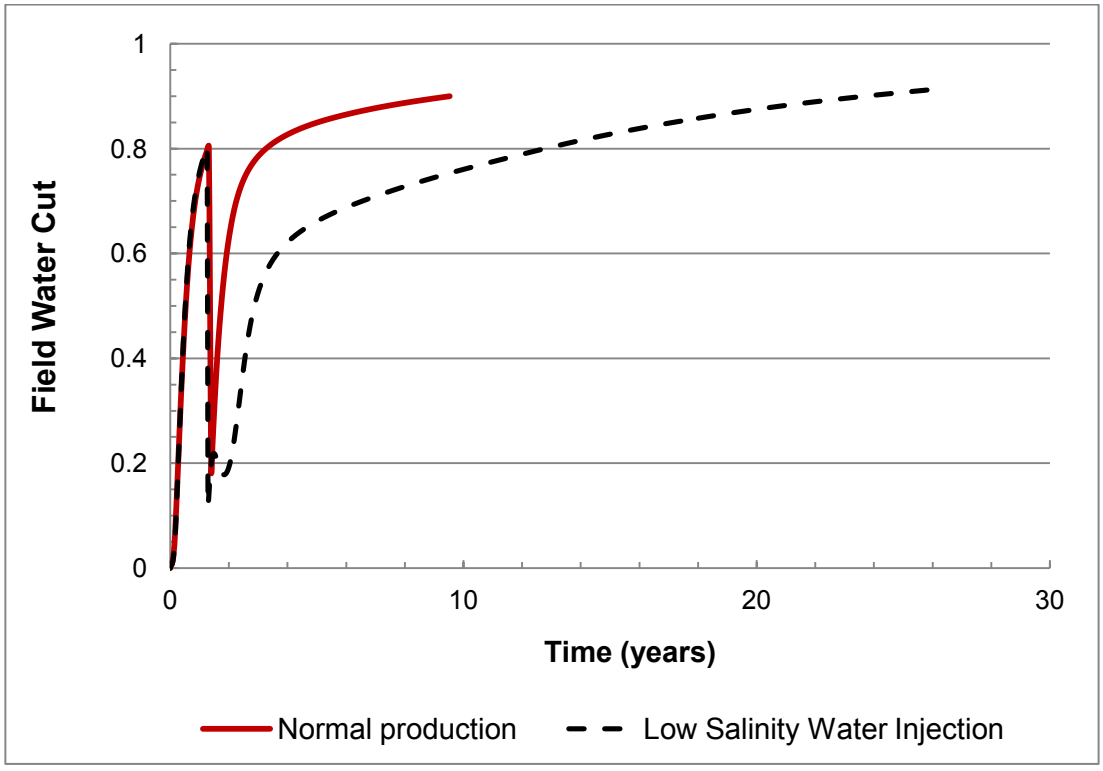

FIGURE 42: FIELD WATER CUT, WITH NORMAL DEPLETION AND WITH INDUCED FINES MIGRATION, VS REAL TIME

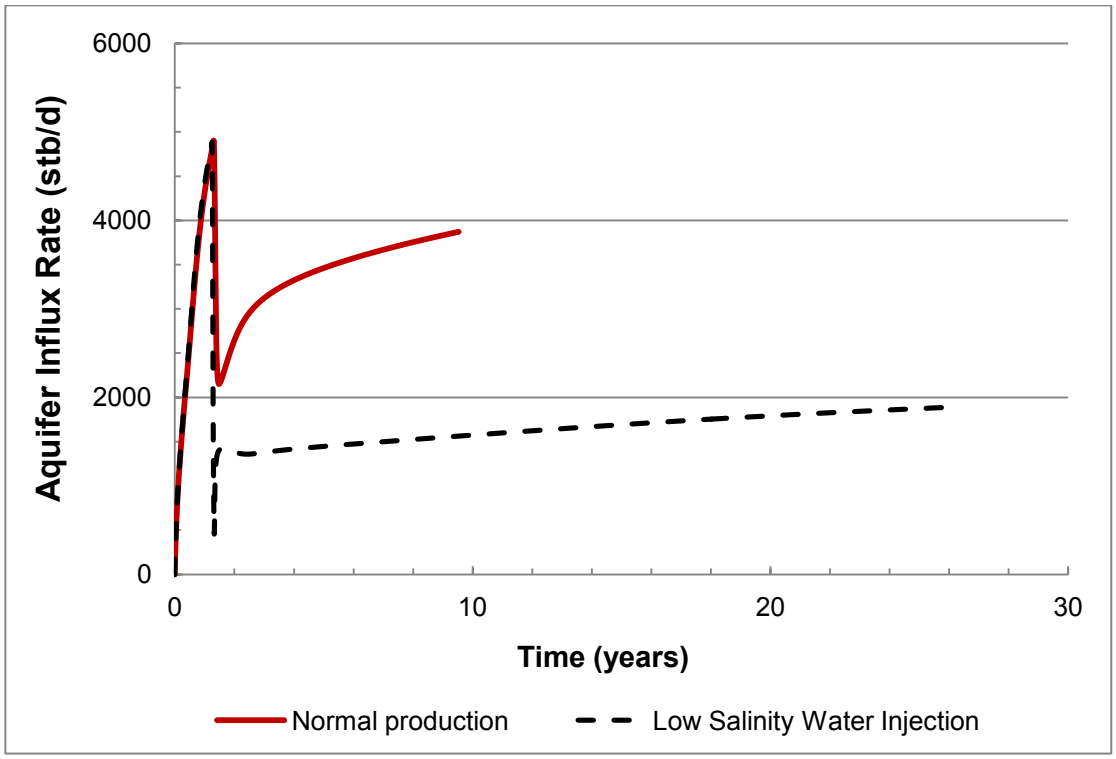

FIGURE 43: AQUIFER INFLUX RATE, WITH NORMAL DEPLETION AND WITH INDUCED FINES MIGRATION, VS REAL TIME

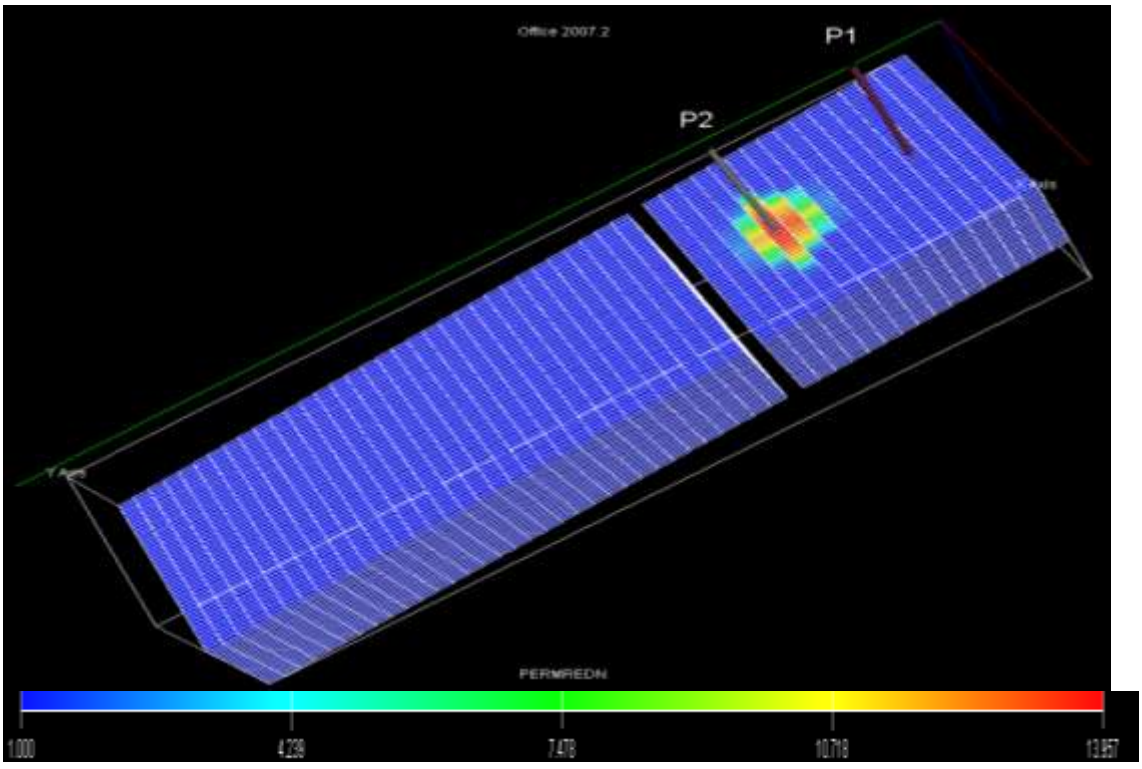

FIGURE 44: LOW PERMEABILE ZONE, RESULTED FROM FINES MIGRATION, DURING LOW SALINITY WATER INJECTION

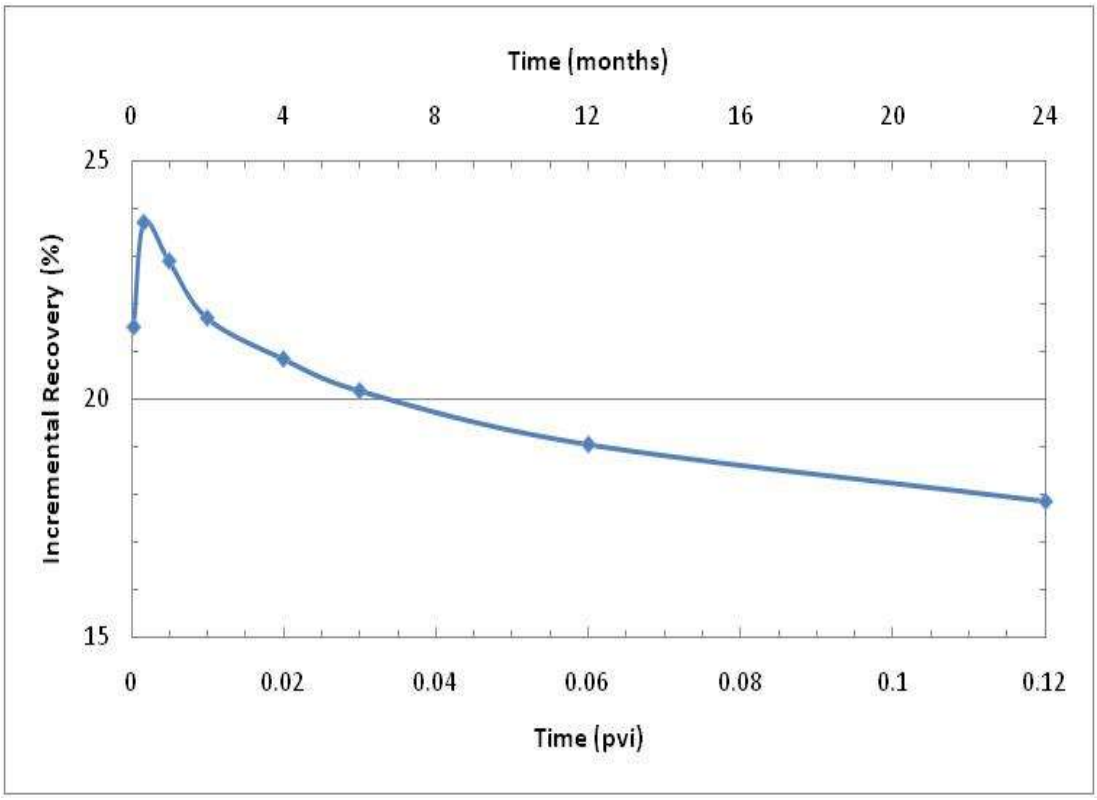

FIGURE 45: SENSITIVITY ANALYSIS FOR VARIOUS PORE VOLUME INJECTED ON LOW SALINITY WATER INJECTION PERFORMANCE

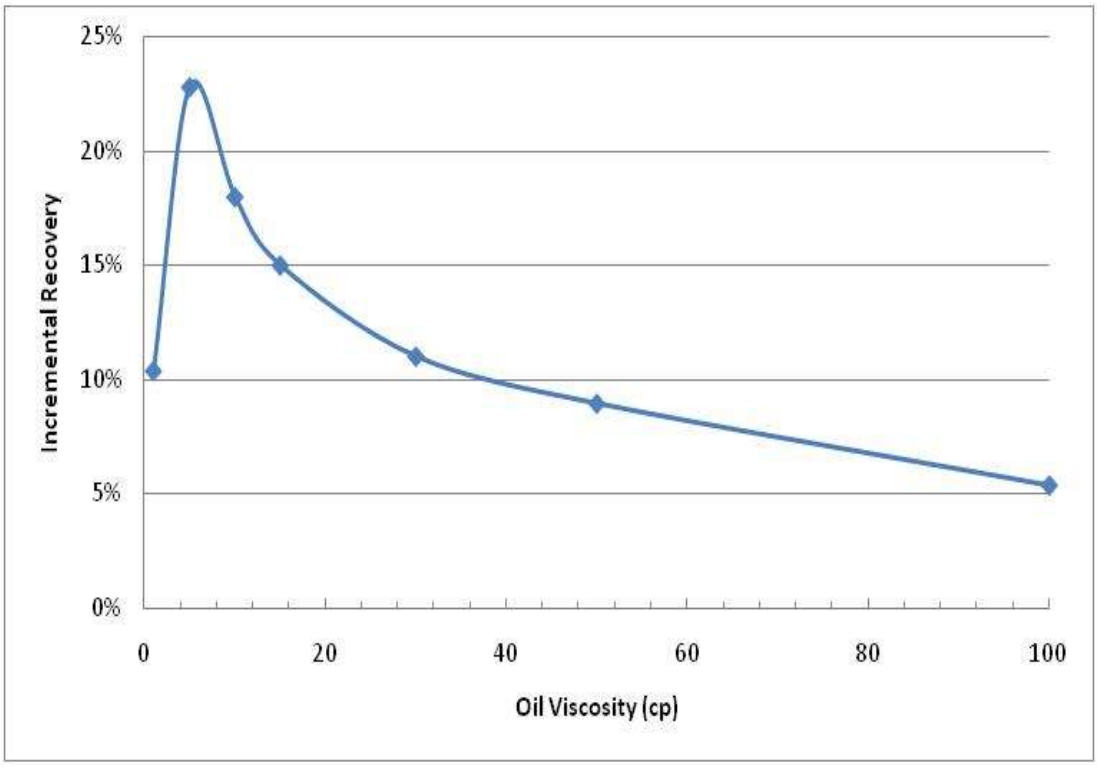

FIGURE 46: SENSITIVITY ANALYSIS FOR OIL VISCOSITY ON LOW SALINITY WATER INJECTION PERFORMANCE

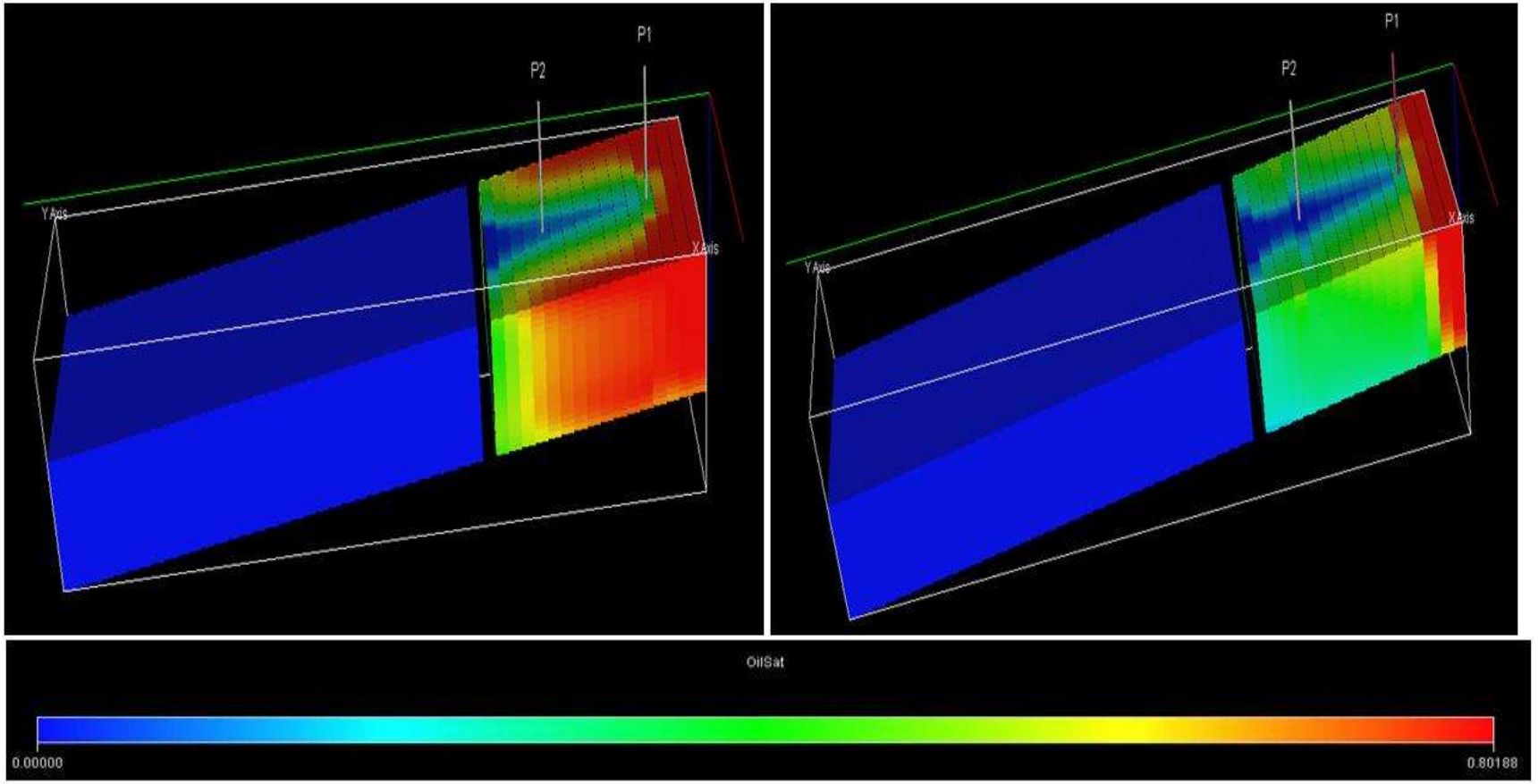

a) Normal Depletion b) With limited low salinity injection

FIGURE 47: RESIDUAL OIL AT ABANDONMENT WITH NORMAL DEPLETION AND WITH INDUCED FINES MIGRATION

4.3 DISCUSSION

As shown in Figure 36, during gas field depletion with strong aquifer support, with the lowest pressure region near to the production wells P2 and P1 being the wellbore pressure (P_w), the center of the invaded water finger would move pass well P2 and watered-out the well (at watercut of 0.3 for gas wells), making it uneconomical to continue the production. During normal depletion, the water finger then continues to propagate towards the up-dip well P1 and water-out the well, leaving a significant amount of residual gas behind. However, injecting a small amount of low salinity water into the abandoned well P2 mobilizes the formation fines and subsequently causing the induced formation damage on the neighboring region around the wellbore. The low permeable block created adds resistance to the water finger propagation towards P1, leading to the prolonged production life of the field.

Figure 37 shows the recovery factor of the cases of normal depletion at 53% (continuous line) compared to 65% of the case with limited low salinity water injection (dashed line). It can be seen that the recovery factor for “normal depletion” case is slightly higher than that with low salinity water injection from 1.5 year to 2 year due to the induced formation damage caused by fines migration. However, the formation of low permeable block would obscure the advancing water tongue and redirect the water flow to sweep the peripheral area. Thus, the production life of the field is prolonged by another 2 years with low salinity waterflooding, resulting in the 12% incremental recovery. It can also be confirmed from the field watercut vs real time curve (Figure 38) that the induced formation damage slows down the water finger propagation by 2 years. Production of gas and water via well P2 is the same for both cases while the injection of small portion of fresh water prolongs the production via well P1. Along with the positive effect of increase of recovery factor, the cumulative aquifer influx for the case with induced damage is significantly less than that of the normal depletion case.

After 2 years of production, the cumulative aquifer influx for normal depletion is 4,150,000 stb compared to 2,700,000 stb for the case with induced damage (Figure 39). This also translates to a significant reduction in the volume of produced water at well P1 with limited low salinity water injection compared to

that of the normal depletion case. The ability to prolong a production life of a gas field is important as gas market depends on the local‟s demand and it requires a constant and steady supply throughout the contract life. Thus by implementing a limited low salinity water injection, it would allow for more cost effective operation as less production wells required to produce the additional gas from the reservoir and lower water handling costs.

The investigation is then extended to an oil reservoir with similar configuration and the results for both cases of “normal depletion” and “limited low salinity water injection” are as following:

TABLE 10: RECOVERY FACTOR AND FIELD LIFE FOR "NORMAL DEPLETION" CASE AND "WITH LIMITED LOW SALINITY WATER INJECTION" CASE

Case	Recovery Factor (%)	Field Life (years)
Normal Depletion	38%	9
With limited low salinity WF	61%	31

Similar to gas reservoir, in oil reservoirs, the lowest pressure near to the producer is the bottom-hole pressure (P_w). Thus, the water finger invades and follows the lowest pressure streamline, which passes through the producer‟s borehole. In order to delay the water encroachment, a small amount of low salinity water is injected into P2, after the well has been watered-out and abandoned, to mobilize formation fines and create a low permeable zone which will act as a resistance barrier to the water finger‟s propagation to the up-dip well P1 (as shown in Figure 44). As a result, instead of following the lowest pressure streamline, the water finger would be diverted to sweep the neighboring area, leading to the improved sweep efficiency and higher recovery factor.

Figure 41 shows that the oil field‟s life is considerably prolonged from 10 years with „normal depletion‟ to 26 years with „limited low salinity water injection‟, resulting in the increase of 23% in oil recovery factor. A significant delay in the propagation of the water finger towards the up-dip well P1 is depicted in Figure 42. At 10 years after production commenced, while well P1 during “normal depletion” case is already watered out (at water cut of 0.9), the water cut at well P1 in a case with “low salinity water injection” is only at 0.75. Additionally, the

aquifer influx rates for both cases in Figure 43 shows that there is less water invaded into the reservoir, thus, less water would be produced at the producers. Hence, the application of low salinity water injection has many advantages in improving the sweep efficiency, increasing the oil recovery factor and delaying the water invasion into the producers.

Sensitivity analysis was conducted on the impacts of oil viscosity and amount of low salinity water injected on the effectiveness of this method (results as shown in Figure 45 and Figure 46). According to Figure 45, the highest production occurs with 10-day fresh water injection or at 0.0017 pvi. Longer injection time (greater amount of low salinity water injected) would cause an early breakthrough of the fresh water via the high permeability layer at the up-dip well P1. Thus, it is important to determine the optimal volume of injected water for the best results.

Then, based on Figure 46, the application of low salinity water injection remains effective for light oil, volatile oil and heavy oil reservoirs with oil viscosity ranging from 1 cP to 100 cP. However, it is found that for layered cake reservoirs, volatile oil reservoir would be the best candidate for this method as it resulted in 23% in recovery increase compared to the “normal depletion” scenario. Figure 47 shows the 3D illustrations of the final sweep for “normal depletion” and “with low salinity water injection”, in which the remaining oil saturation in “normal depletion” is significantly higher than that of the case with “low salinity water injection”.

4.4 CONCLUSION:

- Injection of fresh water slug into an abandoned well results in a significant recovery factor increase due to the longer production period for both oil and gas reservoirs.

- Depending on the reservoir geometry, size, distance from the WOC and transport properties, the time of fresh water injection varies between weeks and months. The typical size of the injected bank is selected from the conditions of partial filling of the reservoir cross-section.

- The typical incremental recovery factor for oil is 10-20% for gas is 5-12%.

- Typical values for prolonged period of production wells life is 2 years for gas reservoirs and 15 years for oil reservoirs.

CHAPTER 5: FINAL CONCLUSIONS AND RECOMMENDATIONS:

5.1 CONCLUSIONS:

Based on the results of this research, the main conclusions can be drawn:

- The technology of raw water injection was developed using Eclipse waterflood BlackOil simulator with modelling of injectivity decline along the well due to plugging of porous media by injected particles. The induced skin growth yields a partial homogenization of the injectivity profile and improved sweep efficiency.

- The technology of low salinity water injection have been developed using Eclipse reservoir modelling with polymer injection option, which can describe mobilization of fines particles, their migration, capture and subsequent permeability decline. In comparison to normal waterflood, low salinity waterflooding results in improved sweep efficiency and reduction in produced and injected water volume.

- The main physics mechanism of incremental oil recovery found is the diversion of the injected water into unswept zones due to plugging the swept zone by capture particles.

- The proposal of a new technology of small bank of fresh water injection into watered-up and abandoned production wells result in lifting of reservoir fines, their migration and plugging the path for invaded aquifer water. It results in a decrease of water production and prolongation of oil or gas production from wells.

5.2 RECOMMENDATIONS:

- Further researches are to be conducted to improve Eclipse accommodate skin calculations. This would help to eliminate the errors that occur from transitioning between Excel and Eclipse.

- It is recommended that if further investigations are carried out a higher injection rate is used as this will assist to generate results in a more realistic time scale. This can be achieved by setting a high bottom-hole pressure at the injector.

- Further researches on incorporating the effects of fines migration on relative permeability, wettability and capillary pressure to obtain more accurate results.

- Detailed economic analyses are necessary to verify the applicability and advantages of raw waterflooding and fresh waterflooding over normal waterflood method.

NOMENCLATURE

SYMBOLS:

A	area, L^2, m^2
c	concentration, ppm
C	normalized concentration
c_a	polymer adsorption isotherm
c^o	initial concentration of suspended particles
D	diffusion coefficient, L^2/T. m^2/s
E_r	erosional factor
f	fractional flow of water
F_d	drag force, MLT^{-2}, N
F_e	electrostatic force, MLT^{-2}, N
F_g	gravitational force, MLT^{-2}, N
F_l	lifting force, MLT^{-2}, N
h	thickness, L, m.
II	injectivity index
J	impedance
k	absolute permeability, L^2 , mD
k_o	initial absolute permeability, L^2 , mD
k_{ro}	oil relative permeability
k_{rw}	water relative permeability
k_{rwor}	relative permeability in presence of residual oil, L^2, m^2
L	reservoir size, L, m
l_d	lever for drag force, L, m
l_n	lever for normal force, L, m
m, m_c	slope
P	dimensionless pressure
p	pressure, $ML^{-1}T^2$, Pa
Q	volumetric flow rate, L^3T^{-1}, m^3/s
q	Q/h, L^2/T, m^2/s
S	dimensionless concentration of deposited particles
s	water saturation
S_a	dimensionless concentration of attached particles
S_{ao}	initial dimensionless concentration of attached particles
S_s	dimensionless concentration of strained particles
t	time, T, s
t_D	dimensionless time, PVI
U	physical (interstitial) flow velocity, LT^{-1}, m/s
u	dimensionless physical (interstitial) flow velocity
U_o	initial physical (interstitial) flow velocity, LT^{-1}, m/s
x	position of oil-water interface, L, m
x_D	dimensionless coordinate
M	mobility ratio

R_k *permeability decline ratio*

GREEK SYMBOLS

α_L *dispersivity coefficient, L, m*
α *critical porosity fraction*
γ *brine ionic strength, molL^{-3}, mol/lit*
ϕ *porosity*
μ_o *oil dynamic viscosity, ML^{-1}T^{-1}, cP*
μ_w *water dynamic viscosity, ML^{-1}T^{-1}, cP*
β *formation damage coefficient*
ε *torque ratio*
ε_D *inverse to Peclet number (dimensionless diffusion)*
λ *dimensionless filtration coefficient*
λ' *filtration coefficient, L^{-1}, 1/m*
λ_s *filtration coefficient for straining, L^{-1}, 1/m*
ρ *dimensionless radius*
σ *volumetric concentration of captured particles, L^{-3}, 1/m^3*
σ_a *volumetric concentration of attached particles, L^{-3}, 1/m3*
σ_{ao} *initial volumetric concentration of attached particles, L^{-3}, 1/m3*
σ_s *volumetric concentration of strained particles, L^{-3}, 1/m3*

SUBSCRIPTS

0 *initial*
c *contour*
cf *cross-flow*
p *permeate*
t *at time (t)*
tr *transition*
i *fluid phase*

ABBREVIATIONS

RRF *maximum resistance factor*

REFERENCES

Altmann, J & Ripperger, S 1996, „Particle deposition and layer formation at the crossflow microfiltration", *Journal of Membrane Science*, vol. 124, no. 1, pp 119-128.

Bachman, R, Harding, T, Settari, A & Walters, D 2003, „Coupled simulation of reservoir flow, geomechanics, and formation plugging with application to high-rate produced water reinjection". *SPE 79695 presented at the SPE Reservoir Simulation Symposium*, Houston, Texas, USA, 3-5 February.

Bedikovetsky, P, Marchesin, D, Hime, G, Alvarez, A & Marchsin, AO 2002, „Porous media deposition damage from injection of water with particles", *paper presented at the 8th European Conference on the Mathematics of Oil Recovery*, 3-6 September 2002, Germany.

Bedrikovetsky, P 1993, *Mathematical theory of oil and gas recovery-with applications to ex-USSR oil and gas fields*, Vol. 4, ed G. Rowan, Kluwer Academic Publishers, The Netherlands.

Bedrikovetsky, P 2009, „Formation damage note", Australian School of Petroleum, University of Adelaide.

Bedrikovetsky, P, da Silva, MJ, Fonseca, DR, de Souza, AG & Furtado, C 2005, „Well-history-based prediction of injectivity decline during seawater flooding", *paper presented at the SPE 6th European Formation Damage Conference*, 25-27 May 2005, The Netherlands.

Bedrikovetsky, P, Mackay, E, Monteiro, RP, Patricio, F & Rosario, FF 2006, „Injectivity impairment due to sulphate scaling during PWRI: analytical model", *SPE paper 100512 presented at the SPE Int. Oilfield Scale Symposium*, Aberdeen, Scotland, UK, 30 May-1 June.

Bedrikovetsky, P, Siqueira, FD, Furtado, C and de Souza, ALS 2010, „Modified particle detachment model for colloidal transport in porous media", *Transport in Porous Media,* vol. 86, no. 2, pp. 353-383.

Bernard, GG 1967, „Effect of floodwater salinity on recovery of oil from cores containing clays", *paper SPE 1725 presentaed at the SPE California Regional Meeting*, Los Angeles, California, USA, 26-27 October.

Bernard, GG 1967, „Effect of floodwater salinity on recovery of oil from cores containing clays", *Paper SPE 1725 presented at the SPE California Regional Meeting*, Los Angeles, California, USA, 26-27 October.

Chauveteau, G, Nabzar, L & Coste, J 1998, „Physics and modelling of permeability damage induced by particle deposition", *Paper SPE 39463 presented at the SPE Formation Damage Control Conference*, Lafayette, Louisiana, USA, 18-19 February.

Civan, F 2000, *Reservoir formation damage*, Gulf Publising Company, Texas, USA.

Civan, F 2007, *Reservoir formation damage: fundamentals, modelling, assessment, and mitigation,* 2nd Ed., Gulf Professional Publishing, USA.

Civan, F 2010, „Non-isothermal permeability impairment by fines migration and deposition in porous media including dispersive transport", *Transport in Porous Media*, vol. 85, no. 1, pp. 233-258.

Dake, LP 2004, *The practice of reservoir engineering, developments of petroleum science*, Elsevier.
Ding, DY 2010, „Coupled simulation of near-wellbore and reservoir models", *Journal of Petroleum Science and Engineering*, vol. 76, pp. 21-36, Elsevier.

Farshbaf Zinati, F, Farajzadeh, R, Currie, PK & Zitha, PLJ 2007, „Modeling of external filter-cake buildup in radial geometry", *paper prepared for presentation at the European Formation Damage Conference*, 30 May-1 June 2007, Scheveningen, The Netherlands.

Freitas, A & Sharma, M 2001, „Detachment of particles from surfaces: an Afm study", *Journal of Colloid and Interface Science*, vol. 233, no. 1, pp. 73-82.

Gao, S &Su, Y 2004, „The development project design on polymer flooding for the Central of Xing4-5 in Daqing", Yearly Report, issue 12, no. 16-17, Chinese Government.

Green, DW & Willhite, GP 1998, *Enhanced Oil Recovery*, Society of Petroleum Engineering, Texas, USA.

Hadia, N, Chauhari, L, Mitra, SK, Vinjamur, M & Singh, R 2006, „Experimental investigation of use of horizontal wells in waterflooding", *Journal of Petroleum Science and Engineering*, vol. 56, pp. 303-310.

Hunter, RJ 2001, *Foundations of Colloid Science*. 2nd ed., New York: Oxford University Press, USA.

Jerauld, G, Webb, K, Lin, C & Seccombe, J 2008, „Modelling low-salinity waterflooding", SPEREE vol. 11, no. 6, pp. 1000-1012. SPE-102239-PA.

Joshi, SD 1991, *Horizontal Well Technology*, Penn Well Publishing Company, Tulsa, OK, p. 12.

Joshi, SD, Ding, W & Hall, K 1993, „A simulation study of waterflooding using combinations of horizontals and vertical wells", *SVIP 005 presented at Tenth Petroleum Engineering Conference of the SPE of Venezuela*, Puerto La Cruz, Venezuela, October 20-25.

Ju, B, Fan, T, Wang, X & Qiu, X 2007, „A New simulation framework for predicting the onset and effects of fines mobilization". *Transport in Porous Media*, vol. 68, no. 2, pp. 265-283.

Khambharatana, F, Thomas, S & Farouq Ali, SM 2000, *Numerical simulation and experimental verification of oil recovery by macroemulsion floods*, Society of Petroleum Engineer, Brazil.

Khilar, K and Fogler, H 1998, *Migrations of Fines in Porous Media,* Kluwer Academic Publishers, Dordrecht/London/Boston.

Lake, LW 1989, *Enhanced Oil Recovery*, Prentice-Hall, New Jersey.

Lever, A & Dawe, R 1984, „Water-sensitivity and migration of fines in the Hopeman sandstone", *Journal of Petroleum Geology*, vol. 7, no. 1, pp. 97-107.

Li, X, Lin, CL, Miller, JD & Johnson, WP 2006, „Role of grain-to-grain contacts on profiles of retained colloids in porous media in the presence of an energy barrier to deposition", *Environmental science & technology*, vol. 40, no. 12, pp. 3769-3774.

Minssieux, L, Nabzar, L, Chaveteau, G & Longeron, D 1998, „Permeability damage due to asphaltene deposition: experimental and modeling aspects", *Institut Francais du Petrole*, vol. 53, no. 3.

Miranda, RM & Underdown, DR 1993, „Laboratory measurement of critical rate: a novel approach for quantifying fines migration problems", *paper SPE 25432 presented at the SPE Production Operations Symposium*, Oklahoma City, Oklahoma, USA.

Mojarad, R & Settari, A 2007, „Coupled numerical modelling of reservoir flow with formation plugging", *Journal of Canadian Petroleum Technology*, vol. 46, no. 3, pp. 54-59.

Muecke, TW 1979, „Formation fines and factors controlling their movement in porous media", *Journal of Petroleum Technology*, vol. 31, pp. 144–150

Muhammad, A 2008, „Taking advantage of Injectivity Damage to improve Reservoir Sweep in Horizontal Wells", Honours Thesis, Australian School of Petroleum (ASP), Australia.

Mungan, N 1965, „Permeability reduction through changes in ph and salinity", Journal of Petroleum Technology (JPT), vol. 17, no. 12, pp. 1449-1453, SPE-1283-PA.

Nabzar, L, Chauveteau, G & Roque, C 1996, „A New model for formation damage by particle retention", *paper SPE 31119 presented at the SPE Formation Damage Control Symposium*, Lafayette, Louisiana, USA, 14-15 February.

Nguyen, TKP, Hage, A 2009, „Improved oil recovery by raw water injection", Honours Thesis, Australian School of Petroleum, Australia.

Nunes, M, Bedrikovetsky, P, Newbery, B, Paiva, R, Furtado, C & de Souza, AL 2005, „Theoretical definition of formation damage zone with applications to well stimulation", *Journal of Energy Resources Technology*, vol. 132, no. 3.

Ochi, J & Vernoux, JF 1998, „Permeability decrease in sandstone reservoirs by fluid injection - hydrodynamic and chemical effects", *Journal of Hydrology*, vol. 208, no. 3, pp. 237-248.

Pang, S & Sharma, MM 1997, „A model for predicting injectivity decline in water-injection wells", *SPE Formation Evaluation*, vol. 12, no. 3, pp. 194-201. SPE- 28489-PA.

Pu, H, Xie, X, Yin, P & Morrow, N 2010, „Low-salinity waterflooding and mineral dissolution", *paper SPE 134042 presented at the SPE Annual Technical Conference and Exhibition*, Florence, Italy, 19-22 September.

Rahman, S, Arshad, A & Chen, H 1994, „Prediction of critical condition for fines migration in petroleum reservoirs", *paper SPE 28760 presented at the SPE Asia Pacific Oil and Gas* Conference, Melbourne, Australia, 7-10 November.

Rivet, S, Lake, L & Pope, G 2010, „A coreflood investigation of low-salinity enhanced oil recovery", *paper SPE 134297 presented at the SPE Annual Technical Conference and Exhibition*, Florence, Italy, 19-22 September.

Schlumberger 2007, *Eclipse Technical Description*. Schlumberger, Australia.
Shapiro, A & Stenby, E 2000, „Factorization of transport coefficients in macroporous media", *Transport in Porous Media,* vol. 41, no. 3, pp. 305-323.

Shapiro, A & Stenby, E 2002, *Multicomponent Adsorption: Principles and Models. In Adsorption: theory, modelling, and analysis*, Marcel Dekker, New York, USA, chap 6, p. 375.

Sharma, M, Pang, S & Wennbarg, KE 1997, „Injectivity decline in water injection wells: an offshore Gulf of Mexico case study", *Society of Petroleum Engineers*, The Netherlands.

Sharma, MM, Pang, S, Wennberg, KE & Morgenthaler, LN 1997, „Injectivity decline in water-injection wells: an offshore Gulf of Mexico case study", *SPE 38180 presented at the SPE European Formation Damage Conference held in The Hague*, 2–3 June.

Soo, H & Radke, CJ 1986a, „A filtration model for the flow of dilute stable emulsions in porous media: I. theory", *Chemical Engineering Science,* vol. 41, pp. 263–272.

Soo, H and Radke, CJ 1986b, „A filtration model for the flow of dilute stable emulsions in porous media: I. Parameter evaluation and estimation", *Chemical Engineering Science,* vol. 41, pp. 273–281

Takahashi, S & Kovscek, AR 2010, „Wettability estimation of low-permeability, siliceous shale using surface forces", *Journal of Petroleum Science and Engineering*, vol. 75, no. 1-2, pp. 33-43.

Tang, G & Morrow, N 1999. „Influence of brine composition and fines migration on crude oil/brine/rock interactions and oil recovery", *Journal of Petroleum Science and Engineering*, vol. 24, no. 2, pp. 99-111.

Tufenkji, N & Elimelech, M 2004, „Correlation equation for predicting single-collector efficiency in physicochemical filtration in saturated porous media", *Environmental Science Technology*, vol. 38, no. 2, pp. 529-536.

Tufenkji, N 2007, *Colloid and Microbe Migration in Granular Environments: A Discussion of Modelling Methods. In Colloidal Transport in Porous Media*, ed Frimmel, FH, von der Kammer, F, Flemming, FC, Springer-Verlag, Berlin, Germany.

Valdya, R & Fogler, H 1992, „*Fines migration and formation damage: influence of pH and ion exchange'*, SPE Petroleum Engineering, vol. 7, no. 4, pp. 325-330. SPE-19413-PA.

Wang, D, Shao, Z & Wang, J 2008, „Key aspects of project design for polymer flooding at the daqing oil field", *SPE-109682 paper presented at the 2007 SPE Annual Technical Conference and Exhibition*, Anaheim, California, 11-14 November.

Yuan, H & Shapiro, A 2010, „A mathematical model for non-monotonic deposition profiles in deep bed filtration systems", *Chemical Engineering Journal*, vol. 166, no. 1, pp. 105-115.

Zeini, A, Machado, F, Bedrikovetsky, P 2011, „Modified Mathematical Model for Fines Migration in Oilfields", *submitted to Society of Petroleum Engineering Reservoir Engineering Journal*, Australia.

APPENDICES

APPENDIX A-FURTHER RESULTS

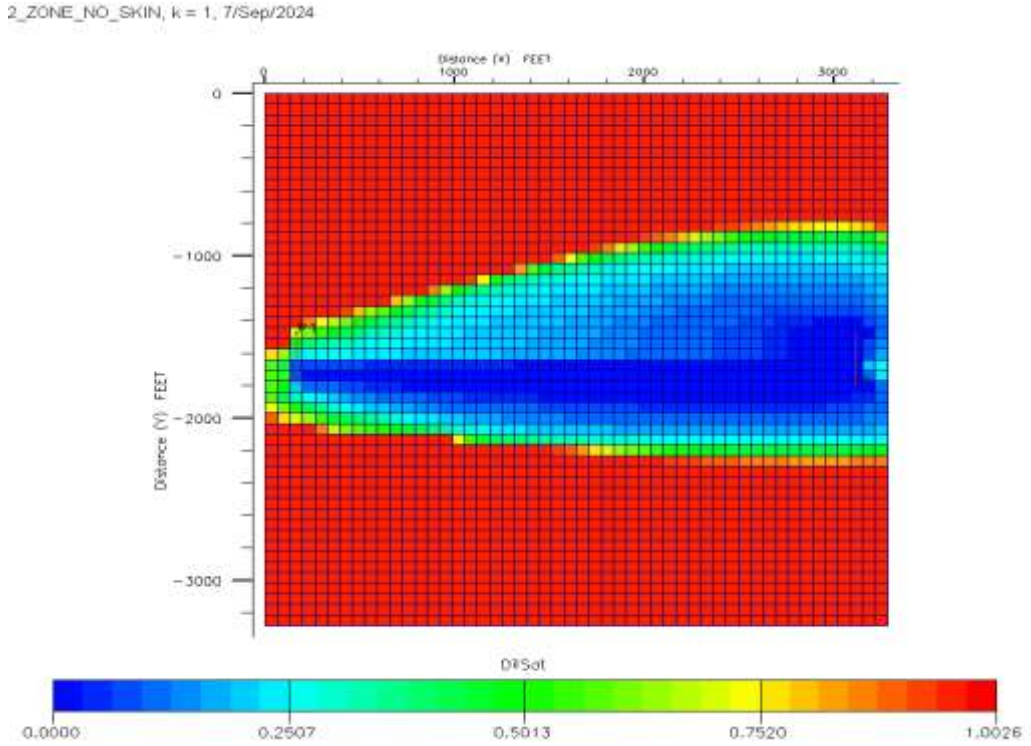

FIGURE 48: VISUALIZATION OF OIL DISPLACEMENT IN TWO ZONE RESERVOIR WITH NO SKIN AFTER 1 P.V.I

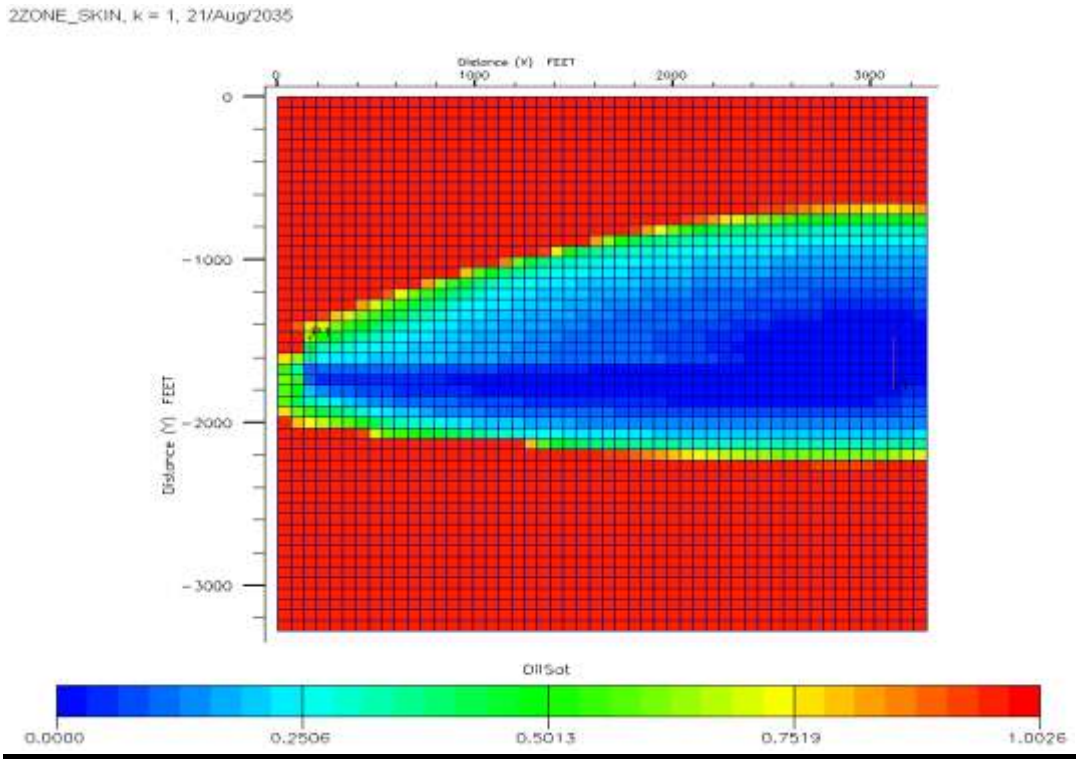

FIGURE 49: VISUALIZATION OF OIL DISPLACEMENT IN TWO ZONE RESERVOIR WITH SKIN AFTER 1 P.V.I

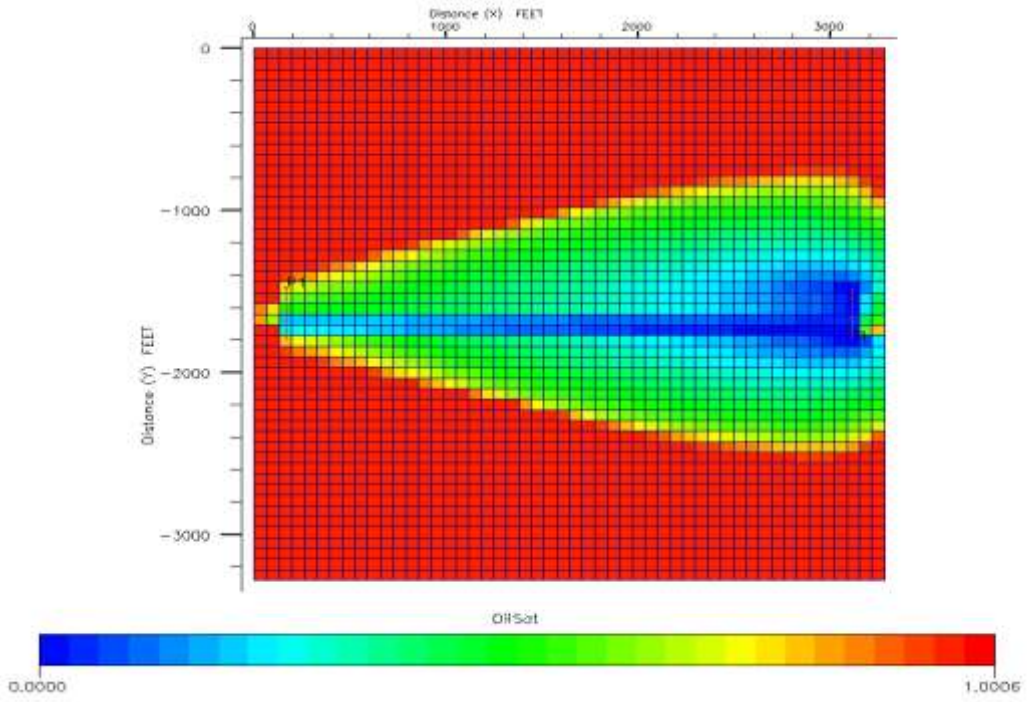

FIGURE 50: VISUALIZATION OF OIL DISPLACEMENT IN HETEROGENEOUS RESERVOIR WITH CHANNEL WITH NO SKIN AFTER 1 P.V.I

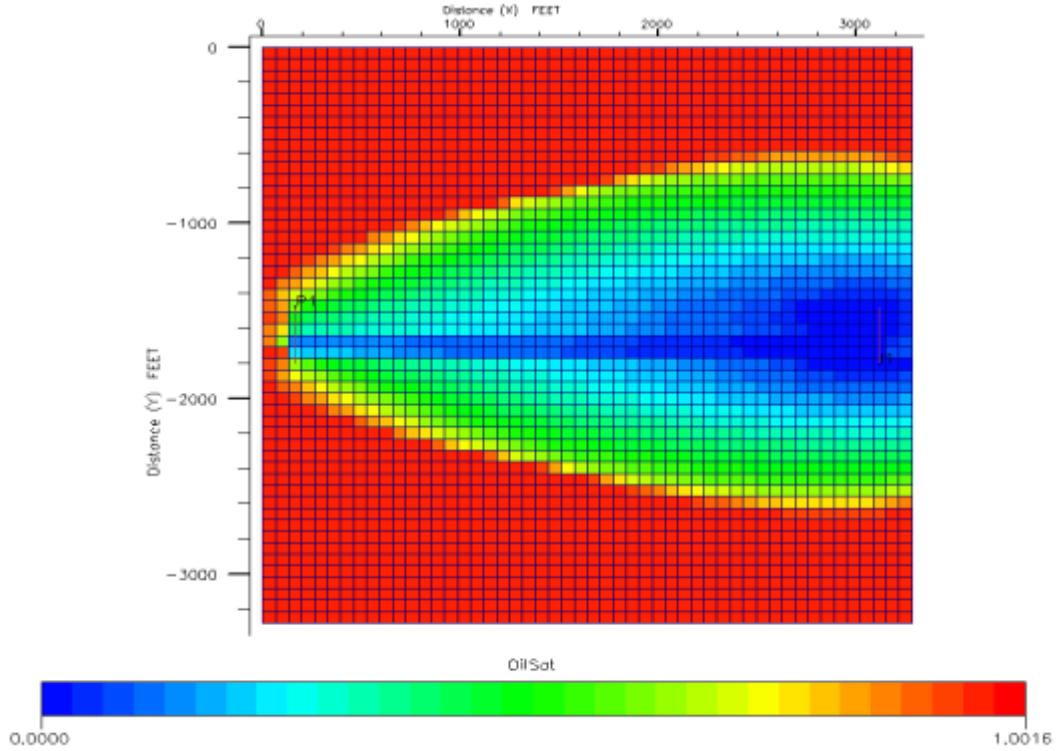

FIGURE 51: VISUALIZATION OF OIL DISPLACEMENT IN HETEROGENEOUS RESERVOIR WITH CHANNEL WITH SKIN AFTER 1 P.V.I

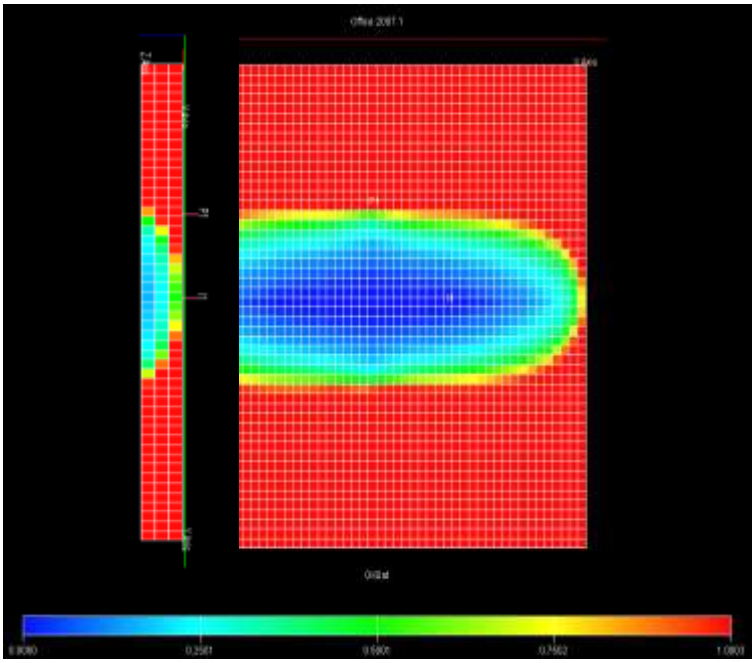

FIGURE 52: VISUALIZATION OF OIL DISPLACEMENT IN HOMOGENEOUS RESERVOIR WITH OVERLAPPING WELLS WITH NO SKIN AFTER 1 P.V.I

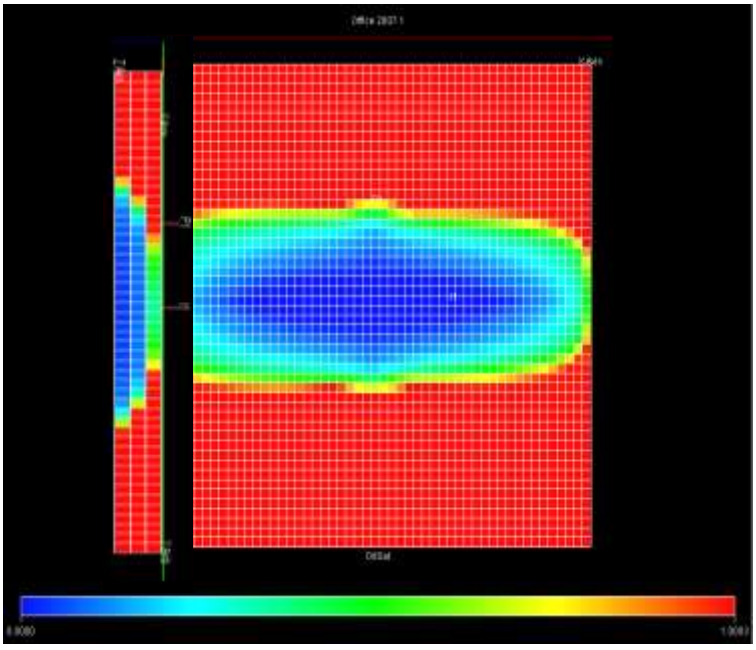

FIGURE 53: VISUALIZATION OF OIL DISPLACEMENT IN HOMOGENEOUS RESERVOIR WITH OVERLAPPING WELLS WITH SKIN AFTER 1 P.V.

APPENDIX B - DEEP BED FILTRATION FORMULATION:

Firstly, the conservation laws for particles are being implemented:

$$c = \frac{N_s}{\phi V};\ \sigma = \frac{N_r}{V};\ V(c\phi + \sigma) = N_r + N_s$$

Where: c: is the concentration (ppm), ø: the porosity

V: is the volume of injected particles (ppm); σ is the retained concentration (ppm)

N_s: is the number of suspended particles; Nr: is the number of retained particles.

Particle number balance in the rock volume V with application of Green‟s formula is:

$$\frac{d}{dt}\int_V (c\phi + \sigma)dx^3 = -\oint_{\partial V}(cU)d\sigma_n = -\int_V div(cU)dx^3$$

Collecting all terms in left hand side and the equation becomes:

$$\int_V \left[\frac{\partial(c\phi + \sigma)}{\partial t} + div(cU)\right]dx^3 = 0$$

So the continuity equation for suspended and retained particles is:

$$\frac{\partial(c\phi + \sigma)}{\partial t} + div(cU) = 0$$

Since water and suspended particles are incompressible:

$$div(U) = 0$$

Thus taking flux term out of the bracket:

$$\frac{\partial(c\phi + \sigma)}{\partial t} + U\nabla c = 0$$

which can be expressed as:

$$\frac{\partial \sigma}{\partial t} = \lambda_{(\sigma)} U c$$

So the retention rate is proportional to the particle flux. Using the definition in which proportionality coefficient (α) is equal to fraction of retained particles per unity length of the particle trajectory, the continuity can be expanded as:

$$\frac{\Delta \sigma}{\Delta t} = \alpha \frac{cUA\Delta t}{Al\Delta t} \qquad with \quad \lambda = \frac{\alpha}{l}$$

Hence, the system of three equations for three unknowns representing the deep bed filtration is derived as:

$$\phi \frac{\partial c}{\partial t} + \frac{q}{2\pi R} \frac{\partial c}{\partial R} = -\frac{\partial \sigma}{\partial t} \qquad (A-1)$$

$$\frac{\partial \sigma}{\partial t} = \lambda' U c \qquad (A-2)$$

$$U = -\frac{k_0 k_{rwor}}{(1+\beta\sigma)\mu} \frac{\partial P}{\partial R} \qquad (A-3)$$

Introducing dimensionless radius, time, concentrations and filtration coefficient:

$$\rho = \frac{r}{R_c} \;\; ; \;\; X = \rho^2 \;\; ; \;\; T = \frac{1}{\phi \pi R_c^2} \int_0^t q_{(\tau)} d\tau \;\; ; \;\; C = \frac{c}{c^0} \;\; ; \;\; S = \frac{\sigma}{\phi c^0} \;\; ; \;\; \lambda = \lambda' R_c$$

Where: S: is the dimensionless concentration, C: is the dimenstionless concentration

T: is the dimenstionless time; ρ: is the dimensionless radius

X: is the dimensionless distance; λ: is the dimensionless filtration coefficient

λ': is the filtration coefficient

B.1 KINETIC EQUATIONS:

Substituting the dimensionless parameters into equation (A-2):

$$\frac{\partial \sigma}{\partial t} = \lambda' Uc$$

Where: U is the velocity (m/s), λ': filtration coefficient (1/m)

Extract porosity out for the left term and divide everything with co. Then substitute the dimensionless deposition (S) and dimensionless concentration (C) and multiply both sides with $\left(\frac{\pi R_c^2}{q}\right)$:

$$\frac{\phi \partial(\phi/\sigma)/c^o}{\partial t} = \frac{\lambda' Uc}{c^o}$$
$$\Leftrightarrow \frac{\phi \partial S}{\partial t} = \lambda' UC$$
$$\Leftrightarrow \frac{\phi \partial S}{\partial t} \cdot \left(\frac{\pi R_c^2}{q}\right) = \lambda' UC \cdot \left(\frac{\pi R_c^2}{q}\right)$$

Where: q is the volumetric flow rate (m^3/s), t is the time (s), R_c is the drainage radius (m),

The derivative of the dimensionless time is:

$$dT = \frac{q}{\phi \pi R_c^2} dt$$

Replace the derivative of dimensionless time and dimensionless filtration coefficient into the above equation,

$$\frac{\partial S}{\partial T} = \lambda' UC \cdot \left(\frac{\pi R_c^2}{q}\right)$$
$$\frac{\partial S}{\partial T} = \frac{\lambda UC \pi R_c}{q}$$

With q is the total flow rate per unit of reservoir thickness:

$$\frac{q}{U} = 2\pi r$$
$$\frac{\partial S}{\partial T} = \frac{\lambda U C \pi R_c}{U 2\pi r}$$
$$\frac{\partial S}{\partial T} = \frac{\lambda C R_c}{2r}$$

Substitute with dimensionless time and the equation becomes:

$$\boxed{\frac{\partial S}{\partial T} = \frac{\lambda C}{2\sqrt{X}}}$$

B.2 CONTINUITY EQUATION:

Similarly, with continuity equation:

$$\phi \frac{\partial c}{\partial t} + \frac{q}{2\pi r}\frac{\partial c}{\partial r} + \frac{\partial \sigma}{\partial t} = 0$$
$$\frac{\partial}{\partial t}(\phi c + \sigma) + \frac{q}{2\pi r}\frac{\partial c}{\partial r} = 0$$

Multiply both sides with $\left(\frac{\pi R_c^2}{q}\right)$:

$$\left[\phi \frac{\partial c}{\partial t} + \frac{q}{2\pi r}\frac{\partial c}{\partial r} + \frac{\partial \sigma}{\partial t} = 0\right] \cdot \left(\frac{\pi R_c^2}{q}\right)$$
$$\left(\frac{\pi R_c^2}{q}\right)\phi \frac{\partial c}{\partial t} + \left(\frac{\pi R_c^2}{q}\right)\frac{q}{2\pi r}\frac{\partial c}{\partial r} + \left(\frac{\pi R_c^2}{q}\right)\frac{\partial \sigma}{\partial t} = 0$$
$$\left(\frac{\pi R_c^2}{q}\right)\phi \frac{\partial c}{\partial t} + \frac{R_c^2}{2r}\frac{\partial c}{\partial r} + \left(\frac{\pi R_c^2}{q}\right)\phi \frac{\partial(\sigma/\phi)}{\partial t} = 0$$

$$dr = \frac{R_c}{2\sqrt{X}}dX$$

so,

$$\left(\frac{\pi R_c^2}{q}\right)\phi \frac{\partial c}{\partial t} + \frac{R_c\sqrt{X}}{r}\frac{\partial c}{\partial X} + \left(\frac{\pi R_c^2}{q}\right)\phi \frac{\partial(\sigma/\phi)}{\partial t} = 0$$
$$\left(\frac{\pi R_c^2}{q}\right)\phi \frac{\partial c}{\partial t} + \frac{\partial c}{\partial X} + \left(\frac{\pi R_c^2}{q}\right)\phi \frac{\partial(\sigma/\phi)}{\partial t} = 0$$

Substitute the dimensionless time into the equation:

$$\frac{\partial c}{\partial T}+\frac{\partial c}{\partial X}+\frac{\partial(\sigma/\phi)}{\partial T}=0$$

Divide all with c^o and substitute the dimensionless concentration and dimensionless deposition particles concentration,

$$\frac{\partial(c/c^o)}{\partial T}+\frac{\partial(c/c^o)}{\partial X}+\frac{\partial(\sigma/\phi c^o)}{\partial T}=0$$
$$\frac{\partial C}{\partial T}+\frac{\partial C}{\partial X}+\frac{\partial S}{\partial T}=0$$

Substitute the dimensionless form of kinetic of deposition equation into the above equation,

$$\frac{\partial C}{\partial T}+\frac{\partial C}{\partial X}+\frac{\lambda C}{2\sqrt{X}}=0$$

$$\boxed{\frac{\partial C}{\partial T}+\frac{\partial C}{\partial X}=-\frac{\lambda C}{2\sqrt{X}}}$$

B.3 DARCY'S LAW

$$U = -\frac{k_0 k_{rwor}}{\mu(1+\beta\sigma)}\frac{\partial p}{\partial r}$$

$$\frac{q}{2\pi r} = -\frac{k_0 k_{rwor}}{\mu(1+\beta\sigma)}\frac{\partial p}{\partial r}$$

Where: P is the pressure (Pa); μ is the viscosity (cP); k is the permeability (mD).

Since $dr = \frac{R_c}{2\sqrt{X}}dX$, we have:

$$\frac{q}{2\pi r} = -\frac{k_0 k_{rwor}}{\mu(1+\beta\sigma)}\frac{2\sqrt{X}\partial p}{R_c \partial X}$$

$$\frac{qR_c}{4\pi r\left(\frac{r}{R_c}\right)} = -\frac{k_0 k_{rwor}}{\mu(1+\beta\sigma)}\frac{\partial p}{\partial X}$$

$$\frac{q}{4\pi X} = -\frac{k_0 k_{rwor}}{\mu(1+\beta\sigma)}\frac{\partial p}{\partial X}$$

Introducing the dimensionless pressure, $P = -\frac{2\pi k_0 k_{rwor} p}{\mu q}$

So,

$$\boxed{\frac{1}{X} = -\frac{2}{(1+\beta\phi c^o S)}\frac{\partial P}{\partial X}}$$

APPENDIX C - IMPEDANCE FORMULATION DURING DEEP BED FILTRATION AND EXTERNAL FILTER CAKE FORMATION:

Expressing the dimensionless pressure gradient from the modified Darcy‟s equation,

$$\frac{1}{X} = -\frac{2}{\left(1+\beta\phi c^{o} S\right)}\frac{\partial P}{\partial X}$$

$$\Delta P = \int_{X_w}^{1} \frac{1+\beta\phi c^{o} S}{2X}\partial X$$

$$\Delta P = \int_{X_w}^{1} \frac{1}{2X}\partial X + \int_{X_w}^{1} \frac{\beta\phi c^{o} S}{2X}\partial X$$

$$\Delta P = \frac{1}{2}\left(\ln 1 - \ln X_w\right) + \frac{\beta\phi c^{o}}{2}\int_{X_w}^{X_w+T} \frac{S(X,T)}{X}\partial X$$

$$\Delta P = -\frac{1}{2}\ln X_w + \frac{\beta\phi c^{o}}{2}\int_{X_w}^{X_w+T} \frac{S(X,T)}{X}\partial X$$

Expand $\frac{S(X,T)}{X}$,

$$\frac{S(X,T)}{X} = \frac{\lambda e^{-\lambda\left(\sqrt{X}-\sqrt{X_w}\right)}}{2X\sqrt{X}}\left(T - X + X_w\right)$$

$$\frac{S(X,T)}{X} = \left\{\frac{\lambda e^{-\lambda\left(\sqrt{X}-\sqrt{X_w}\right)}}{2X\sqrt{X}}T - \frac{\lambda e^{-\lambda\left(\sqrt{X}-\sqrt{X_w}\right)}}{2X\sqrt{X}}\left(X - X_w\right)\right\}$$

Find the integral for the first term from above equation,

$$\frac{\lambda e^{-\lambda\left(\sqrt{X}-\sqrt{X_w}\right)}}{2X\sqrt{X}} = \frac{\lambda}{2}\int \frac{e^{-\lambda\left(\sqrt{X}-\lambda\sqrt{X_w}\right)}}{X\sqrt{X}}\partial X$$

$$= \frac{\lambda}{2}\int \frac{e^{-\lambda\sqrt{X}}e^{\lambda\sqrt{X_w}}}{X\sqrt{X}}\partial X$$

$$= \frac{\lambda e^{\lambda\sqrt{X_w}}}{2}\int \frac{e^{-\lambda\sqrt{X}}}{X\sqrt{X}}\partial X$$

Since $\partial\sqrt{X} = \frac{1}{2\sqrt{X}}\partial X$

$$= \frac{\lambda e^{\lambda\sqrt{X_w}}}{2}\int \frac{e^{-\lambda\sqrt{X}}}{X\sqrt{X}} 2\sqrt{X}\partial\sqrt{X}$$

$$= \lambda e^{\lambda\sqrt{X_w}}\int \frac{e^{-\lambda\sqrt{X}}}{\sqrt{X}^2}\partial\sqrt{X}$$

$$= \lambda e^{\lambda\sqrt{X_w}}\left(-\frac{e^{-\lambda\sqrt{X}}}{\sqrt{X}} - \lambda\int \frac{e^{-\lambda\sqrt{X}}}{\sqrt{X}}\partial\sqrt{X}\right)$$

$$= \lambda e^{\lambda\sqrt{X_w}}\left(-\frac{\lambda e^{-\lambda\sqrt{X}}}{\lambda\sqrt{X}} - \lambda\int \frac{e^{-\lambda\sqrt{X}}}{\lambda\sqrt{X}}\partial\lambda\sqrt{X}\right)$$

$$replace, y = \lambda\sqrt{X}$$

$$= \lambda e^{y_w}\left(-\frac{\lambda e^{-y}}{y} - \lambda\int \frac{e^{-y}}{y}\partial y\right)$$

$$= -\lambda^2 e^{y_w}\left(\frac{e^{-y}}{y} + \int \frac{e^{-y}}{y}\partial y\right)$$

Integral for the second term of the equation above:

$$\frac{\lambda e^{-\lambda\left(\sqrt{X}-\sqrt{X_w}\right)}}{2X\sqrt{X}}\left(X - X_w\right) = \int\left(\frac{\lambda e^{-\lambda\left(\sqrt{X}-\sqrt{X_w}\right)}}{2\sqrt{X}} - \frac{\lambda e^{-\lambda\left(\sqrt{X}-\sqrt{X_w}\right)}}{2X\sqrt{X}}X_w\right)\partial X$$

$$= \int \frac{\lambda e^{-\lambda\left(\sqrt{X}-\sqrt{X_w}\right)}}{2\sqrt{X}}\partial X - \int \frac{\lambda e^{-\lambda\left(\sqrt{X}-\sqrt{X_w}\right)}}{2X\sqrt{X}}X_w\partial X$$

$$replace, \partial X = 2\sqrt{X}\partial\sqrt{X}$$

$$= \int \frac{\lambda e^{-\lambda\left(\sqrt{X}-\sqrt{X_w}\right)}}{2\sqrt{X}}2\sqrt{X}\partial\sqrt{X} - \int \frac{\lambda e^{-\lambda\left(\sqrt{X}-\sqrt{X_w}\right)}}{2X\sqrt{X}}X_w 2\sqrt{X}\partial\sqrt{X}$$

$$= \int \lambda e^{-\lambda\left(\sqrt{X}-\sqrt{X_w}\right)}\partial\sqrt{X} - \int \frac{\lambda e^{-\lambda\left(\sqrt{X}-\sqrt{X_w}\right)}}{X}X_w\partial\sqrt{X}$$

$$= \int \lambda e^{-\lambda\sqrt{X}+\lambda\sqrt{X_w}}\partial\sqrt{X} - \int \frac{\lambda e^{-\lambda\sqrt{X}+\lambda\sqrt{X_w}}}{\sqrt{X}^2}X_w\partial\sqrt{X}$$

$$= \lambda e^{\lambda\sqrt{X_w}}\int e^{-\lambda\sqrt{X}}\partial\sqrt{X} - \lambda X_w e^{\lambda\sqrt{X_w}}\int \frac{e^{-\lambda\sqrt{X}}}{\sqrt{X}^2}\partial\sqrt{X}$$

$$= \lambda e^{\lambda\sqrt{X_w}}\frac{1}{-\lambda}e^{-\lambda\sqrt{X}} - \lambda X_w e^{\lambda\sqrt{X_w}}\left(-\frac{e^{-\lambda\sqrt{X}}}{\sqrt{X}} - \lambda\int \frac{e^{-\lambda\sqrt{X}}}{\sqrt{X}}\partial\sqrt{X}\right)$$

$$= -e^{\lambda\sqrt{X_w}}e^{-\lambda\sqrt{X}} - \lambda X_w e^{\lambda\sqrt{X_w}}\left(-\frac{\lambda e^{-\lambda\sqrt{X}}}{\lambda\sqrt{X}} - \lambda\int \frac{e^{-\lambda\sqrt{X}}}{\lambda\sqrt{X}}\partial\lambda\sqrt{X}\right)$$

$$replace; y = \lambda\sqrt{X}$$

$$so,$$

$$= -e^{y_w}e^{-y} - \lambda X_w e^{y_w}\left(-\frac{\lambda e^{-y}}{y} - \lambda\int\frac{e^{-y}}{y}\partial y\right)$$

$$= \lambda e^{y_w}\left[-\frac{e^{-y}}{\lambda} - X_w\left(-\frac{\lambda e^{-y}}{y} - \lambda\int\frac{e^{-y}}{y}\partial y\right)\right]$$

$$ei(x) = \int_x^\infty \frac{e^{-y}}{y}\partial y$$

Introducing;

So,

$$\int\frac{S(X,T)}{X}\partial X = -\lambda^2 e^{y_w}T\left(\frac{e^{-y}}{y} + ei\right) + e^{y_w}e^{-y} - X_w\lambda^2 e^{y_w}\left(\frac{e^{-y}}{y} + ei\right)$$

Integration with limits,

$$\int_{X_w}^{X_w+T}\frac{S(X,T)}{X}\partial X = -\lambda^2 e^{y_w}T\left(\frac{e^{-\lambda\sqrt{T}}}{\lambda\sqrt{T}} + ei(\lambda\sqrt{T}) - \frac{e^{-y_w}}{y_w} - ei(^{y_w})\right)$$
$$+ e^{y_w}e^{-\lambda\sqrt{T}} - 1 - X_w\lambda^2 e^{y_w}\left(\frac{e^{-\lambda\sqrt{T}}}{\lambda\sqrt{T}} + ei(\lambda\sqrt{T})\right)$$
$$+ X_w\lambda^2 e^{y_w}\left(\frac{e^{-y_w}}{y_w} + ei(y_w)\right)$$

A simplification process to further simplify the equation was done in a spreadsheet file by eliminating the term that can be neglect due to its typical value which is significantly small.

After the simplification process,

$$\int_{X_w}^{X_w+T}\frac{S(X,T)}{X}\partial X = (\lambda' R_c)^2 T\left(\frac{1}{\lambda' r_w} + e^{\lambda r_w}ei(\lambda' r_w)\right)$$

And finally we get the equation for the dimensionless pressure drop,

$$\Delta P = -\frac{1}{2}\ln X_w + \frac{\beta\phi c^o}{2}(\lambda' R_c)^2 T\left(\frac{1}{\lambda' r_w} + e^{\lambda r_w}ei(\lambda' r_w)\right)$$

Previously we obtained that the initial dimensionless pressure drop,

$$\Delta P_o = -\frac{1}{2}\ln X_w = -\frac{1}{2}\ln\left(\frac{r_w}{R_c}\right)^2 = \ln\left(\frac{R_c}{r_w}\right)$$

The formula for the impedance, J (T),

$$J(T) = \frac{\Delta P}{\Delta P_o} = \frac{-\frac{1}{2}\ln X_w + \frac{\beta\phi c^o}{2}(\lambda' R_c)^2 T\left(\frac{1}{\lambda' r_w} + e^{\lambda r_w} ei(\lambda' r_w)\right)}{-\frac{1}{2}\ln X_w}$$

$$J(T) = 1 + \frac{\frac{\beta\phi c^o}{2}(\lambda' R_c)^2}{\ln\left(\frac{R_c}{r_w}\right)}\left(\frac{1}{\lambda' r_w} + e^{\lambda r_w} ei(\lambda' r_w)\right)T$$

$$J(T) = 1 + mT$$

So :

$$m = \frac{\frac{\beta\phi c^o}{2}(\lambda' R_c)^2}{\ln\left(\frac{R_c}{r_w}\right)}\left(\frac{1}{\lambda' r_w} + e^{\lambda r_w} ei(\lambda' r_w)\right)$$

The skin factor equation,

$$J(T) = 1 + mT = \frac{\Delta P}{\Delta P_o}$$

$$\Delta P = \frac{q\mu}{2\pi hk}\left(\ln\frac{R_e}{r_w} + S\right)$$

$$\Delta P_o = \frac{q\mu}{2\pi hk}\left(\ln\frac{R_e}{r_w}\right)$$

$$J(T) = 1 + \frac{S}{\ln\frac{R_e}{r_w}} = 1 + mT$$

so,

$$S = mT\ln\frac{R_e}{r_w}$$

$$\boxed{S_f = T\frac{\beta\phi c^o}{2}(\lambda' R_c)^2\left(\frac{1}{\lambda' r_w} + e^{\lambda r_w} ei(\lambda' r_w)\right)}$$

APPENDIX D - INTERNAL FORMATION DAMAGE AT THE TRANSITION ZONE

The transition time correspond to the deposited concentration,

$$\sigma = \alpha\phi$$

So the deposition rate,

$$\frac{\delta\sigma}{\delta t} = \frac{\lambda' c^o q}{2\pi r_w}$$

$$\delta\sigma = \frac{\lambda' c^o q}{2\pi r_w}\delta t$$

$$\alpha\phi = \frac{\lambda' c^o q}{2\pi r_w} t_{tr}$$

$$t_{tr} = \frac{2\pi r_w \alpha\phi}{\lambda' c^o q}$$

Using the dimensionless time definition,

$$dT = \frac{q}{\phi\pi R_c^2} dt$$

So,

$$\frac{T_{tr}\phi\pi R_c^2}{q} = \frac{2\pi r_w \alpha\phi}{\lambda' c^o q}$$

$$T_{tr} = \frac{2 r_w \alpha}{\lambda' c^o R_c^2}$$

Replacing the above equation in the impedance equation to get the expression of impedance at transition zone,

$$J(T) = 1 + \frac{\frac{\beta\phi c^o}{2}(\lambda' R_c)^2}{\ln\left(\frac{R_c}{r_w}\right)}\left(\frac{1}{\lambda' r_w} + e^{\lambda r_w} ei(\lambda' r_w)\right)\frac{2 r_w \alpha}{\lambda' c^o R_c^2}$$

$$J(T) = 1 + \frac{\beta\phi\lambda' r_w \alpha}{\ln\left(\frac{R_c}{r_w}\right)}\left(\frac{1}{\lambda' r_w} + e^{\lambda r_w} ei(\lambda' r_w)\right)$$

The pressure drop between the injector and producer at the transition zone,

$$J(T_{tr}) = \frac{\Delta p(T_{tr})}{\Delta p_o}$$

$$\Delta p(T_{tr}) = \Delta p_o J(T_{tr})$$

$$\Delta p_o \frac{2\pi k_o k_{rwor}}{\mu q} = \ln \frac{R_c}{r_w}$$

$$\Delta p_o = \frac{\mu q}{2\pi k_o k_{rwor}} \ln \frac{R_c}{r_w}$$

replace,

$$\Delta p(T_{tr}) = \frac{\mu q}{2\pi k_o k_{rwor}} \ln \frac{R_c}{r_w} J(T_{tr})$$

APPENDIX E - EXTERNAL FILTER CAKE GROWTH

The cake thickness,

$$\pi\left[r_w^2-\left(r_w-h_c\right)^2\right]\left(1-\phi_c\right)=c^o\int_{t_{tr}}^{t}q(t)\delta t$$

Since the value of $h_c<<r_w$ so,

$$\pi\left[r_w^2-\left(r_w-h_c\right)^2\right]\left(1-\phi_c\right)=c^o\int_{t_{tr}}^{t}q(t)\delta t$$

$$\pi\left[r_w^2-r_w^2+2r_wh_c-h_c{}^2\right]\left(1-\phi_c\right)=c^o\int_{t_{tr}}^{t}q(t)\delta t$$

$$\pi\left[2r_wh_c\right]\left(1-\phi_c\right)=c^o\int_{t_{tr}}^{t}q(t)\delta t$$

$$h_c(t)=\frac{c^o}{\pi 2r_w\left(1-\phi_c\right)}\int_{t_{tr}}^{t}q(t)\delta t$$

Using the Darcy‟s law for the flow through the external cake,

$$\frac{q}{2\pi r_w}=-\frac{k_c}{\mu}\frac{\delta p}{\delta r}$$

$$\frac{\mu q}{2\pi r_wk_c}=\frac{\delta p}{\delta r}$$

Calculating the pressure drop along the cake,

$$\Delta p_c=-\int_{r_w-h_c}^{r_w}\frac{\delta p}{\delta r}dr=\frac{\mu q}{2\pi r_wk_c}h_c$$

$$\Delta p_c=\frac{\mu q}{2\pi r_wk_c}\frac{c^o}{\pi 2r_w\left(1-\phi_c\right)}\int_{t_{tr}}^{t}q(t)\delta t$$

$$\Delta p_c=\frac{\mu q}{4\pi^2r_w{}^2k_c}\frac{c^o}{\left(1-\phi_c\right)}\int_{t_{tr}}^{t}q(t)\delta t$$

Replacing the dimensionless parameters into the above equation,

$$\Delta p_c = \frac{\mu q}{4\pi^2 r_w{}^2 k_c}\frac{c^o}{(1-\phi_c)}(T-T_{tr})\phi\pi R_c^2$$

$$\Delta p_c = \frac{\mu q}{4\pi k_c}\frac{c^o}{(1-\phi_c)}(T-T_{tr})\phi\frac{R_c^2}{r_w{}^2}$$

$$\Delta P_c\frac{\mu q}{2\pi k_o k_{rwor}} = \frac{\mu q}{4\pi k_c}\frac{c^o}{(1-\phi_c)}(T-T_{tr})\phi\frac{1}{X_w}$$

$$\Delta P_c = \frac{2\pi k_o k_{rwor}}{\mu q}\frac{\mu q}{4\pi k_c}\frac{c^o}{(1-\phi_c)}(T-T_{tr})\phi\frac{1}{X_w}$$

$$\Delta P_c = \frac{k_o k_{rwor}\phi c^o}{2k_c(1-\phi_c)X_w}(T-T_{tr})$$

For times, T>Ttr, the pressure drop in the reservoir formation,

$$\Delta P(T>T_{tr}) = J(T_{tr})\Delta P_o$$

From the equation above we can obtained the impedance equation for $T>T_{tr}$, where the pressure drop between the wellbore and the reservoir is the summation between the pressure drop along the cake and along the reservoir formation,

$$\Delta P(T>T_{tr}) = J(T_{tr})\Delta P_o$$

$$\Delta P_t = \Delta P(T>T_{tr}) + \Delta P_c$$

$$\frac{\Delta P_t = J(T_{tr})\Delta P_o + \Delta P_c}{\Delta P_o}$$

$$J(T) = J(T_{tr}) + \frac{\Delta P_c}{\Delta P_o}$$

Replace the equation for impedance at transition zone and during cake formation in above equation,

$$J(T) = 1 + mT_{tr} + \frac{\frac{k_o k_{rwor} \phi c^o}{2k_c(1-\phi_c)X_w}(T - T_{tr})}{-\frac{1}{2}\ln X_w}$$

$$J(T) = 1 + mT_{tr} + \frac{k_o k_{rwor} \phi c^o}{k_c(1-\phi_c)X_w(-\ln X_w)}(T - T_{tr})$$

The slope m_c,

$$m_c = \frac{k_o k_{rwor} \phi c^o}{k_c(1-\phi_c)X_w(-\ln X_w)}$$

So the skin factor after the transition time,

$$J(T) = 1 + mT_{tr} + m_c(T - T_{tr}) = 1 + \frac{S}{\ln \frac{R_e}{r_w}}$$

so,

$$S = (mT_{tr} + m_c(T - T_{tr}))\ln \frac{R_e}{r_w}$$

E.1 CAKE EROSION LIMIT

Consider conditions of momentum balance of drag and permeate forces on the particle on cake surface

$$F_p = E_r \sqrt{3} F_{cj}$$

Where the erosion factor is E_R=0.03. So, for the cake to be eroded

$$F_p < 0.03\sqrt{3} F_{cj}$$

The permeate and cross flow forces are defined as

$$F_p = \frac{6\pi\mu a \mathrm{Q}_L}{2\pi(R-h)} = \frac{3\mu a \mathrm{Q}_L}{(R-h)}$$

and

$$F_{cf} = \frac{\omega\pi\mu a^2 \overline{u_{cf}}}{R-h}$$

We assume constant pressure drop between well and the reservoir along the well, i.e. injection rate q is constant along the well. Therefore, average cross flow rate is equal to half of overall injected rate q, and Q= q/L. Finally, formulae for forces take the form

$$F_p = \frac{3\mu a q}{L(R-h)}$$

and

$$F_{cf} = \frac{30\pi\mu a^2 Q_{cf}}{\pi(r_w-h)^3} = \frac{15\mu a^2 q}{(r_w-h)^3}$$

Finally, the condition where the cake eroded,

$$\frac{3\mu a q}{L(r_w-h)} < 0.03\sqrt{3}\frac{15\mu a^2 q}{(r_w-h)^3}$$

It allows determining the cake erosion thickness

$$\frac{1}{L} < 0.03\sqrt{3}\frac{5a}{(r_w-h)^2}$$
$$0.26aL > (r_w-h)^2$$
$$0.51\sqrt{aL} > r_w - h$$
$$h_c > r_w - 0.51\sqrt{aL}$$

Formula shows that the constant in right hand side ($0.51\sqrt{aL}$) must be less than r_w. The opposite means that the drag force sweeps any cake.

For the case of our model injection rate, the cake thickness is defined as,

$$h_c(t) = \frac{C^o}{2\pi r_w(1-\phi_c)} \int_{t_{tr}}^{t} q(t)dt$$

Replacing the cake thickness definition into the cake erosion condition

$$\frac{C^o}{2\pi r_w(1-\phi_c)} \int_{t_{tr}}^{t} q(t)dt > r_w - 0.51\sqrt{aL}$$

So the volume of total water needs to be injected for the cake erosion to happen

$$W_t > r_w - 0.51\sqrt{aL}\,\frac{2\pi r_w(1-\phi_c)}{C^o} + W_{tr}$$

Where W_t is the total water injected at time t and W_{tr} is the total water injected up until transition time.

APPENDIX F- MAXIMUM RETENTION FUNCTION

The following is a derivation of the maximum retention function for a cylinder capillary. A particle on the surface of the capillary or an internal particle cake is on the point of detaching with ε=1 in torque balance. Substitution of expressions for drag, electrostatic, lifting and gravity forces (Bedrikovetsky et al 2010) for the equilibrium condition ε=1 results in:

$$F_e + \frac{4\pi r_s^3}{3}\Delta\rho g - \chi r_s^3\sqrt{\frac{\rho\mu U^3}{\phi^3 R^3\left(1-h_c/R\right)^3}} = \frac{\sqrt{3}\omega\pi\mu r_s^2 U}{\phi R\left(1-h_c/R\right)} \qquad \text{(F-1)}$$

$$\frac{I_d}{I_n} = \sqrt{3}$$

where the lever ratio is taken as that for cylindrical particles Introducing the dimensionless unknown yield:

$$y = \sqrt{\frac{\mu r_s^2 U}{\phi R\left(1-h_c/R\right)F_e}} \qquad y = F\left(\frac{\chi\sqrt{\rho F_e}}{\mu}, \frac{4\pi r_s^3}{3F_e}\Delta\rho g\right) \qquad \text{(F-2)}$$

$$y^3 + \frac{\sqrt{3}\omega\pi\mu}{\chi\sqrt{\rho F_e}}y^2 - \frac{\left(1+\frac{4\pi r_s^3}{3F_e}\Delta\rho g\right)\mu}{\chi\sqrt{\rho F_e}} = 0 \qquad \text{(F-3)}$$

The maximum retained concentration is calculated from an expression for the internal cake thickness:

$$\sigma_{cr}(U) = \left[1-\left(\frac{\mu r_s^2 U}{\phi R F_e y^2}\right)^2\right]\left(1-\phi_c\right)\phi \qquad \text{(F-4)}$$

where y is calculated as the real positive root of the cubic polynomial equation (F-3). The erosion number depends on both velocity U and brine salinity (ionic strength) γ. This gives:

$$\varepsilon = \varepsilon(U,\gamma) = \frac{F_d(U)\,l_d / l_n + F_l(U)}{F_e(\gamma) + F_g} \qquad \text{(F-5)}$$

showing that the drag and lifting forces are functions of flow velocity, and the electrostatic particle/grain force depends on the brine salinity (ionic strength) γ. The dependency (2) can be recalculated into velocity or salinity functions for σ_{cr} using the relationship (F-5). It also allows for the recalculation of the velocity dependency (F-4) into a salinity dependency $\sigma_{cr}=\sigma_{cr(\gamma)}$.